

**The role of Age-Related Maculopathy
Susceptibility Protein 2 (ARMS2) in the
complement regulation of ARPE-19 cells**

Dissertation

To Fulfill the
Requirements for the Degree of
„Doctor of Philosophy“ (PhD)

**Submitted to the Council of the Faculty
of Biology and Pharmacy
of the Friedrich Schiller University Jena**

by Yuchen Lin
Master of Science
born on 26.10.1988 in Hanzhong, China

Reviewers:

1. Prof. Dr. Christine Skerka

Department of Infection Biology

Leibniz Institute for Natural Product Research and Infection Biology, Hans Knöll Institute

Beutenbergstrasse 11a

07745 Jena, Germany

2. Prof. Dr. Ilse D. Jacobsen

Department of Infection Biology

Leibniz Institute for Natural Product Research and Infection Biology, Hans Knöll Institute

Beutenbergstrasse 11a

07745 Jena, Germany

3. Prof. Dr. Michael Kirschfink

Institut of Immunology

Heidelberg University Hospital

Im Neuenheimer Feld 305

69120 Heidelberg, Germany

Public defense: 12.02.2018

SR Louis Pasteur, Hans Knöll Institute

Beutenbergstrasse 11a, Jena

Gutacher:

1. Prof. Dr. Gerhard K. E. Scriba (Vorsitzender)
2. Prof. Dr. Peter Zipfel
3. Prof. Dr. Berit Jungnickel
4. Prof. Dr. Bernhard Hube
5. Prof. Dr. Ilse D. Jacobsen

Table of Contents

Table of Contents	I
List of figures and tables	IV
Abbreviations	V
Summary	VII
Zusammenfassung	IX
1. Introduction	1
1.1. The human immune system	1
1.1.1 The innate and adaptive immune system	1
1.1.2 Neuroimmune system	2
1.1.3 Activation of the human complement system	3
1.1.4 Regulation of complement	5
1.1.4.1 Properdin	5
1.1.4.2 Complement factor H	6
1.1.5 Complement-mediated diseases	7
1.2 Age-related macular degeneration (AMD)	8
1.2.1 Retina	8
1.2.2 Age-related macular degeneration (AMD)	9
1.2.3 Risk factors of AMD	10
1.2.3.1 Vascular endothelial growth factor (VEGF)	12
1.2.3.2 Oxidative stress	12
1.2.3.3 Age-related maculopathy susceptibility 2 (ARMS2)	13
1.3 Aim of this study	14
2. Materials and Method	16
2.1 Materials	16
2.1.1 Chemicals and reagents	16
2.1.2 Cells and strains	16
2.1.3 Media and buffers	16
2.1.4 Purified proteins and peptides	17
2.1.5 Antibodies, sera and blood	17
2.1.6 Assay kits	18
2.1.7 Equipment and laboratory supplies	18
2.2 Methods	18

2.2.1 Blood monocytes isolation	18
2.2.2 Cell cultures and oxidative stress induction	19
2.2.3 Polymerase chain reaction (PCR)	19
2.2.4 Agarose gel electrophoresis	19
2.2.5 Confocal laser-scanning microscopy	19
2.2.6 Immunoprecipitation	20
2.2.7 Sodium dodecyl sulfate polyacrylamide gel electrophoresis (SDS-PAGE)	20
2.2.8 Silver staining	20
2.2.9 Western blot	20
2.2.10 Cloning and transformation	21
2.2.11 Recombinant protein expression	21
2.2.12 Affinity chromatography purification of proteins	21
2.2.13 Protein in-gel digestion and mass spectrometric peptide analysis by MALDI-TOF...	22
2.2.14 <i>In vitro</i> binding assays	22
2.2.15 C3b deposition	23
2.2.16 Enzyme-linked immunosorbent assay (ELISA)	23
2.2.17 Bio-layer interferometry	23
2.2.18 Pepsots peptide arrays on cellulose membrane	23
2.2.19 Cell viability assay	24
2.2.20 Statistics	24
3.Results	25
3.1 Human monocytes and iPS-derived microglia express ARMS2	25
3.1.1 Detection of <i>ARMS2</i> transcripts in human monocytes and iPS-derived microglia ...	24
3.1.2 ARMS2 protein is expressed in human monocytes and iPS-derived microglia	25
3.1.3 ARMS2 expression is enhanced under oxidative stress	26
3.1.4 Identification of endogenous ARMS2 in human THP-1 monocytes	27
3.2 AMD associated polymorphism rs10490924 in ARMS2	29
3.2.1 ARMS2 haplotype analysis in AMD patients	29
3.2.2 Monocytes derived from AMD patients with the ARMS2 risk haplotype lack the ARMS2 protein	30
3.3 Characterization of ARMS2	31
3.3.1 Expression and purification of recombinant ARMS2	31
3.3.2 ARMS2 forms homodimers	33
3.3.3 ARMS2 - properdin interactions	36

3.3.4 The ARMS2 C-terminus mediates interaction with properdin	36
3.3.5 ARMS2 binds to human ARPE-19 cells and heparan sulfate	38
3.3.6 Cloning and transformation of ARMS2 variant A69S plasmid	39
3.3.7 Expression and purification of recombinant ARMS2 A69S variant protein	39
3.3.8 Comparison of ARMS2 and ARMS2 A69S variants	41
3.4 Complement activation on ARPE-19 cells	41
3.4.1 Oxidative stress sensitizes cells to NHS	41
3.4.2 Cell surface bound ARMS2 enhances complement activation	41
3.4.3 Oxidative stress promotes complement activation which is controlled by FH	43
3.4.4 Oxidative stress and complement activation induces VEGF secretion in ARPE-19 cells	44
3.4.5 Detection of intracellular complement components in ARPE-19 cells	46
4. Discussion	49
4.1 Human iPS-derived microglia and monocytes express ARMS2	49
4.2 AMD patients carrying the ARMS2 risk haplotype lack the ARMS2 protein in monocytes	50
4.3 ARMS2 interacts with complement activator properdin and heparan sulfate	51
4.4 Oxidative stress promotes complement activation and VEGF secretion in ARPE-19 cells	53
Conclusion	57
References	58
Acknowledgements	68
Declaration of honor	69
Curriculum vitae	70
Publications, awards and scientific presentations	71

List of figures

Figure 1. Overview of human immune system	2
Figure 2. Activation of the human complement system	4
Figure 3. Structure of factor H	7
Figure 4. Structure of the human retina.....	9
Figure 5. Overview of AMD pathogenesis	10
Figure 6. Overview of chromosome 10q26 locus and gene structure of <i>ARMS2</i>	14
Figure 7. Analysis of <i>ARMS2</i> gene expression in various monocytes	26
Figure 8. <i>ARMS2</i> protein expression in human monocytes and microglia	27
Figure 9. Blood – derived monocytes express <i>ARMS2</i> upon oxidative stress	28
Figure 10. Identification of endogenous <i>ARMS2</i> in THP-1 monocytes.....	29
Figure 11. <i>ARMS2</i> genotypes in a cohort of 56 AMD patients	31
Figure 12. Detection of <i>ARMS2</i> protein in monocytes from AMD patients	32
Figure 13. Codon optimized <i>ARMS2</i> cDNA was cloned into the <i>pPICZαB</i> expression vector.....	33
Figure 14. Recombinant <i>ARMS2</i> expression and purification	33
Figure 15. Recombinant <i>ARMS2</i> forms homodimers and is glycosylated	35
Figure 16. MS analysis of <i>ARMS2</i> peptides from purified protein	34
Figure 17. <i>ARMS2</i> interacts with complement activator properdin	39
Figure 18. <i>ARMS2</i> binds to properdin	40
Figure 19. <i>ARMS2</i> binds to heparan sulfate as well as human ARPE-19 cells	41
Figure 20. <i>ARMS2</i> variant S69 expression and purification	42
Figure 21. Comparison of <i>ARMS2</i> A69 and S69 variant	44
Figure 22. Cytolysis assay	45
Figure 23. Oxidative stress and <i>ARMS2</i> enhance complement activation on cell surfaces in serum	46
Figure 24. FH blocks C3b deposition on oxidatively stressed ARPE-19 cells	46
Figure 25. Oxidative stress and complement activate VEGF secretion in ARPE-19 cells	48
Figure 26. Intracellular FH is upregulated upon oxidative stress in ARPE-19 cells	49
Figure 27. C3 expression in the human retina and ARPE-19 cells	50
Figure 28. C5 is absent in the human retina and ARPE-19 cells	50
Figure 29. Hypothetical three-dimensional structure of the <i>ARMS2</i> molecule	54
Figure 30. Complement activation on RPE cell surfaces	55
Figure 31. Factor H modulates complement activation on stressed cell surfaces	57

List of tables

Table 1. Forward and reverse primer sequences used in PCR	16
Table 2. Buffers used in this study	17
Table 3. Antibodies used in this study.....	18
Table 4. Identified endogenous <i>ARMS2</i> peptides from five immunoprecipitations	30
Table 5. Identified <i>ARMS2</i> peptides from purified protein bands	36
Table 6. Identified <i>ARMS2</i> peptides from glycosylated protein bands	37

Abbreviation

μg, mg, g	microgram, milligram, gram
ab	antibody
AMD	Age-related macular degeneration
AP	alternative complement pathway
ARMS2	Age-related maculopathy susceptibility 2
BMGY	buffered glycerol-complex medium
BMMY	buffered methanol-complex medium
BBB	blood-brain barrier
BRB	Blood-retinal barrier
BSA	bovine serum albumin
CFHRs	complement factor H-related proteins
CP	classical complement pathway
DAPI	4',6-diamidino-2-phenylindole
DMEM	Dulbecco's modified eagle medium
DPBS	Dulbecco's phosphate buffered saline
ELISA	enzyme-linked immunosorbent assay
FACS	fluorescence-activated cell sorter
FBS	fetal bovine serum
FH	complement factor H
FHL-1	complement factor h-like protein 1
GAGs	glycosaminoglycans
h	hour
H ₂ O ₂	Hydrogen peroxide
iNHS	heat-inactivated normal human serum
HS	heparan sulfate
IP	Immunoprecipitation
K _D	dissociation constant
kDa	kilo Dalton
LB	Luria-Bertani medium
LDL	low density lipoprotein
LP	lectin complement pathway
LPS	Lipopolysaccharides
LSM	laser scanning microscopy
MAA	malondialdehyde-acetaldehyde
mAB	monoclonal Antibody
MAC	membrane-attack-complex
MALDI-TOF	matrix-assisted laser desorption/ionization-time of flight
MCP	membrane cofactor protein
MDA	malondialdehyde
MFI	mean fluorescence intensity

MS	mass spectrometry
NHS	normal human serum
OD	optical density
pAB	polyclonal antibody
PBMC	peripheral blood mononuclear cell
PCR	polymerase chain reaction
PMA	phorbol myristate acetate
YPD	yeast peptone dextrose
SCR	short consensus repeat
SD	standard deviation
SDS-PAGE	sodium dodecyl sulfate polyacrylamide gel electrophoresis
RPE	retinal pigment epithelium
RPMI	Roswell Park Memorial Institute medium
TCC	terminal complement complex
VEGF	vascular endothelial growth factor
w/v	weight/volume
wt	wildtype

Summary

Age-related macular degeneration (AMD) represents the most common cause of blindness in developed countries. The disease is characterized by the formation of drusen at the macula followed by the degeneration of retinal pigment epithelium (RPE) with photoreceptors. Aging, smoking and oxidative stress are considered to contribute to AMD risk. In addition, genetic findings have revealed that variants in complement component genes such as *factor H*, *factor I* and *C3* are significantly associated with AMD, indicating that abnormal complement activation and innate immunity are also linked to the development of AMD. The complement system is a major part of innate immunity and plays an essential role in cellular homeostasis, host defense and inflammation. Dysregulated complement function or abnormal activation have been implicated in AMD and many other diseases. Although the underlying pathogenic mechanism is still unclear, recent genetic studies have reported that a polymorphism rs10490924 linked with an indel mutation del443ins54 in the *ARMS2* (age-related maculopathy susceptibility 2) gene is strongly associated with AMD. Polymorphism rs10490924 results in replacement of alanine by serine at amino acid position 69 (A69S), and the associated indel results in *ARMS2* transcript instability. However, the source of *ARMS2*, the function of the *ARMS2* protein and the biological consequences of the polymorphism are poorly understood. Thus, I aimed to characterize the subcellular distribution and function of the *ARMS2* protein, functional consequences of the AMD associated polymorphism in *ARMS2*, and the effect of complement activation on human RPE. This thesis builds on results from a previous study in the department showing *ARMS2* interaction with properdin.

In the present work, *ARMS2* gene- and protein expression were identified in human induced pluripotent stem cell-derived microglia (iPS-derived microglia) and human monocytes by PCR and laser scanning microscopy, whereas no expression was detected in murine macrophage RAW264.7. For the first time, endogenous *ARMS2* was localized in the cytoplasm of human blood-derived monocytes as determined by fluorescence microscopy and three different *ARMS2* antibodies. *ARMS2* is weakly expressed in monocytes, but synthesis increased upon oxidative stress, indicating that *ARMS2* is involved in the response to oxidative conditions. To confirm its expression, *ARMS2* was pulled down from THP-1 cell lysate by immunoprecipitation using a newly generated *ARMS2* monoclonal antibody and *ARMS2* peptides were identified by mass spectrometry. AMD patients homozygous for the risk variant (rs10490924) showed no *ARMS2* protein in their blood-derived monocytes, thus supporting the instability by the indel variation.

Recombinant *ARMS2* expressed in *Pichia pastoris* is a glycosylated protein of 17 and 34 kDa and forms homodimers. An interaction of *ARMS2* with the complement activator protein properdin was demonstrated by ELISA and biolayer interferometry, suggesting an activating role of *ARMS2* in the complement system. The responsible interaction domain in *ARMS2* for properdin was located to the sequence FFSPAGTQRRF within the C-terminus of *ARMS2*. *ARMS2* binds to apoptotic cells via interaction with heparan sulfate, but not via DNA or lipids and acts as a complement activator on these surfaces. *ARMS2* bound to ARPE-19 cells, enhanced complement activation and opsonization for phagocytosis. Recombinantly

expressed and purified under the same conditions, the ARMS2 variant A69S, showed a similar binding activity to ARMS2, indicating that the indel mutation, not this polymorphism, effects protein functions. Oxidative stress, one of the risk factors for AMD, decreased viability of ARPE-19 cells and led to increased complement activation on the surface. Notably, activated complement in oxidatively stressed ARPE-19 cells greatly enhanced vascular endothelial growth factor (VEGF) secretion, which is associated with the exudative form of AMD. Oxidative stress also upregulated intracellular synthesis of complement C3 and FH, but the contribution to complement activation is still unclear.

Taken together, this dissertation identified the endogenous expression and a new function of ARMS2. This protein is expected to be involved in the clearance of dying cells by complement mediated phagocytosis. Thus, deficiency of ARMS2, as seen with the indel variation, likely reduces clearance of dead cells in the retina and enhances drusen formation, the typical characteristics of AMD.

Zusammenfassung

Die altersbedingte Makuladegeneration (AMD) ist die häufigste Ursache von Blindheit in den Industriestaaten und ist durch die Bildung von Ablagerungen in Form von sogenannten Drusen an der Makula charakterisiert, sowie der Degeneration des retinalen Pigmentepithels (RPE) mit den Photorezeptoren. Alterung, Rauchen und oxidativer Stress erhöhen das Risiko an einer AMD zu erkranken. Gen-Variationen in Komplementkomponenten, wie *Faktor H*, *Faktor I* und *C3* sind signifikant mit dem AMD-Risiko assoziiert und zeigen eine prominente Rolle von Komplement bei der AMD. Das Komplement-System ist ein wichtiger Bestandteil des angeborenen Immunsystems und spielt eine wesentliche Rolle in der zellulären Homöostase, Wirtsverteidigung und Entzündung. Dysregulierte Komplementfunktionen wurden mit der AMD und vielen anderen Krankheiten in Verbindung gebracht. Jüngste genetische Studien haben auch gezeigt, dass ein Polymorphismus im *ARMS2*-Gen eine starke Assoziation mit AMD aufweist. Der Polymorphismus rs10490924 erzeugt einen Austausch von Alanin durch Serin an Aminosäureposition 69 (A69S) und ist gleichzeitig mit einer Indel-Mutation im untranslatierten Bereich von *ARMS2* verknüpft. Der Polymorphismus rs10490924 mit der Indel Mutation soll zu einer geringeren Stabilität des *ARMS2*-Transkriptes führen. Die in vivo Expression von *ARMS2*, die Funktion des *ARMS2* Proteins und die Konsequenzen des Polymorphismus sind noch weitestgehend unklar. Deshalb war das Ziel meiner Dissertation, die subzelluläre Verteilung des *ARMS2*-Proteins zu bestimmen, die funktionellen Konsequenzen des AMD-assoziierten Polymorphismus in *ARMS2* zu untersuchen und die Konsequenzen einer Komplementaktivierung auf humanen retinalen Pigment Epithelzellen zu charakterisieren. Die Arbeiten schließen an eine vorangehende Studie über die Interaktion von *ARMS2* mit Properdin in der Abteilung Infektionsbiologie an.

In der vorliegenden Arbeit wird gezeigt, dass *ARMS2* in induzierten, pluripotenten humanen Stammzell-abgeleiteten Mikroglia-Zellen (iPS-abgeleitete Mikroglia) sowie humanen Blut isolierten Monozyten exprimiert wird, während keine Expression in murinen Makrophagen RAW264.7 nachweisbar ist. Das endogene *ARMS2* wurde im Zytoplasma menschlicher Zellen mittels Mikroskopie mit drei verschiedenen *ARMS2* Antikörpern detektiert. Die *ARMS2* Proteinlevel sind gering, aber die Synthese von *ARMS2* steigt deutlich unter oxidativem Stress an, was darauf hinweist, dass *ARMS2* als Reaktion auf oxidative Bedingungen aktiviert wird. Die *ARMS2* Synthese in Monozyten wurde mit Hilfe der Immunpräzipitation und Massenspektrometrie von THP-1 Zellen unter Verwendung eines neuen *ARMS2* monoklonalen Antikörper nachgewiesen. Wie erwartet zeigten AMD-Patienten mit der homozygoten Risikovariante (rs10490924) kein *ARMS2*-Protein in ihren Blutmonozyten, was damit die Instabilität der *ARMS2* RNA durch die indel Mutation bestätigte .

Rekombinantes *ARMS2*-Protein ist ein glykosyliertes Protein von 17 und 34 kDa und bildet Homodimere aus. Die Interaktion von *ARMS2* mit Properdin wurde durch Bio-Layer-Interferometrie charakterisiert und bestätigte die Rolle von *ARMS2* als Aktivator des Komplementsystems. Die verantwortlichen Properdin Bindungsdomäne wurde in *ARMS2* in der Sequenz FFSPAGTQRRF im C-terminus von *ARMS2* lokalisiert. *ARMS2* bindet an apoptotische Zelle über die Interaktion mit Heparansulfat, aber nicht über DNA oder Lipide,

und erhöht die Komplement vermittelte Opsonisierung der Zellen. Die A69S ARMS2 Variante wurde ebenfalls rekombinant exprimiert und zeigte eine ähnliche Mobilität und Bindungsaktivität wie ARMS2, so dass dieser Polymorphismus alleine ohne die Indelvariation die Proteinfunktion vermutlich nicht ändert. Die Wirkung von oxidativem Stress, welches einer der Risikofaktoren für AMD ist, verringert die Lebensfähigkeit von ARPE-19-Zellen und führt zu einer erhöhten Komplementaktivierung auf der Oberfläche, die durch FH gesteuert werden kann. Zusammen erhöhen aktiviertes Komplement und oxidativer Stress deutlich die VEGF-Synthese in ARPE-19-Zellen, was die Ausbildung einer exudativen AMD begünstigen könnte. Unter oxidativem Stress wird gleichzeitig intrazelluläres Komplement C3 und FH in ARPE-19-Zellen hochreguliert dessen Rolle im Prozess der Aktivierung noch unbekannt ist.

Zusammenfassend zeigt diese Dissertation die endogene Expression von ARMS2 In Monozyten und dass dieses Protein vermutlich an der Komplement vermittelten Beseitigung von toten Zellen oder Zellmaterial durch Phagozytose beteiligt ist. Das Fehlen von ARMS2 könnte die Ablagerung von Zellmaterial in Form von Drusen erhöhen, welches ein charakteristisches Merkmal der AMD darstellt.

1. Introduction

1.1 The human immune system

The immune system is a defense system that protects host against foreign microorganisms or injury. It consists of numerous biological molecules and immune cells. Disorders of the immune system can result in various diseases. In many species, the immune system can be classified into an innate and adaptive immune system.

1.1.1 The innate and adaptive immune system

Innate immunity is the first line of host defense that is found in all species from primitive multicellular organisms to vertebrates [1]. Anatomical barriers, natural antimicrobial products, immune cells, pattern recognition receptors (PRRs), cytokines, the coagulation system and the complement system are critical innate immunity components in vertebrates (Figure 1) [1, 2]. PRRs are proteins located on the cell surface and/or in the cytoplasm that recognize a variety of microbial molecules as well as endogenous inflammatory signals derived from damaged cells [3]. The pathogens can be sensed via their carbohydrates, nucleic acids, peptides, peptidoglycans and fungal glucans by both immune cells such as mast cells, natural killer (NK) cells, macrophages, monocytes, dendritic cells (DCs), neutrophils, B cells, regulatory T cells and non-immune cells including epithelial cells, endothelial cells and fibroblasts. The cytoplasmic PRRs regulate inflammatory and apoptotic responses. The recognition of endogenous ligands is involved in the development of a variety of chronic inflammatory and autoimmune diseases [1, 3]. Cytokines are a broad of proteins including chemokines, interleukins, interferons and tumor necrosis factors produced by immune cells and non-immune cells. They act in cell signaling, inflammation and in response to infection through different cell surface receptors, subsequently active intracellular signaling cascades and regulate cell functions. Immune regulation by cytokines is crucial in maintaining immune homeostasis, promoting responses to infection, resolving inflammation, and promoting immunological memory. Cytokine responses also drive pathology in many immune-mediated diseases [4].

The innate immune response occurs soon after pathogen exposure. It is carried out by phagocytic cells such as neutrophils, macrophages, cytotoxic NK cells, and antigen-presenting cells, like DCs. Macrophages and DCs are differentiated from monocytes, a subset of circulating white blood cells [5]. Bloodstream monocytes are derived from precursors in the bone marrow, and are divided into subsets that differ in size, trafficking and innate immune receptor expression, and in their ability to differentiate following stimulation with cytokines and/or microbial molecules [6, 7]. Circulating monocytes can leave the bloodstream and migrate into tissues during inflammation. They further differentiate into macrophages and DCs induced by local growth factors, pro-inflammatory cytokine and microbial products. The recruitment of monocytes is essential for an effective control and clearance of infections and damaged cells. But recruited monocytes also contribute to the pathogenesis of inflammatory and degenerative diseases [8, 9].

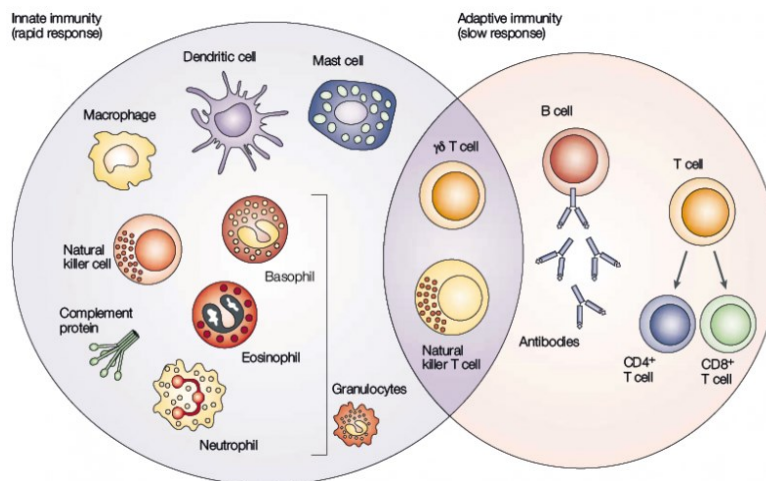


Figure 1. Overview of human immune system [2].

The immune system is a host defense system comprising innate and adaptive immune system. Innate immune defenses are rapid and random as well as target specific, while adaptive immunity is antigen-specific and requires the recognition of specific "non-self" antigens by antigen presentation processing.

In addition to innate immunity, vertebrates have developed adaptive immunity. The adaptive response is largely dependent on the capacity of the innate immune system to distinguish self from non-self. Adaptive immunity is characterized by its major cellular players including B cells and T cells. They are subtypes of lymphocytes. B cells will differentiate into plasma cells that can produce and secrete antibodies in response to immune reaction, whereas T cells are involved in cell-mediated immunity [10]. T cells perform several distinct functions in the host body, such as cytokine secretion, recognition of specific peptide antigen presented on DCs or B cells, and providing immune memory of previously encountered pathogens [11, 12].

1.1.2 Neuroimmune system

In the brain, the blood-brain barrier (BBB) is important for the maintenance of brain homeostasis. BBB protects the brain from most pathogens and prevent macromolecules, toxins and leukocytes from passing through the barrier to reach the central nervous system (CNS) [13]. However, due to high oxygen metabolism in the brain, the production of reactive oxygen species (ROS) and pro-inflammatory cytokines may alter barrier structures. The increased permeability of the barriers activates glial cells such as microglia. Microglia are bone marrow-derived macrophage-like cells that constitute the resident mononuclear immune cells of the nervous system [14]. They play important roles in immune surveillance and maintaining homeostasis, and act as patrolling cells. Microglia are constantly surveying their environment for damaged neurons or infectious agents with extreme sensitivity in healthy brain [15]. When a neuronal damage is detected by microglia, they initiate specific programs that result in the transformation of ramified microglia into activated microglia.

Activated microglia become amoeboid shape and move to injured site and become phagocytes, clearing cellular debris by phagocytosis [16]. Blood-brain barrier disruption stimulates immediate activation of microglia, switching their behavior from patrolling to promoting protection of the damage area [17]. Activated microglia produce cytotoxic mediators such as tumor necrosis factor- α (TNF- α), nitric oxide, interleukin-1 β (IL-1 β), and ROS [15]. These mediators are critical for the functions of microglia and their production is usually decreased once their task is complete. But in chronic neuroinflammation, extended period of microglia activation leads to the overproduction of mediators, which in turn damage the brain barriers [15]. When the blood-brain barrier is impaired, peripheral immune cells, including monocytes, neutrophils, T cells and B cells, can enter the CNS and infiltrate into the injury site. Once infiltrated, the immune cells play a key role in modulating the progression of primary brain injury development.

1.1.3 Activation of the human complement system

The complement system is a major part of innate immunity to defend against infection and to clear altered host cells such as apoptotic particles and cellular debris. Also, it plays a key role in host homeostasis, inflammation and modifying the adaptive immune response. Complement is composed of soluble proteins, membrane expressed receptors and regulators which operate in plasma, in tissues, on cell surfaces, and even within the cells [18]. Local production of complement proteins by many types of tissue-resident cells and immune cells can enhance the functions of innate and adaptive immunity in health and disease.

The activation of complement is divided into four steps: initiation of complement activation, C3 convertase activation and amplification, C5 convertase activation, and terminal complement pathway activation or the assembly of the membrane-attack-complex (MAC, also known as terminal complement complex, TCC) [19]. Complement can be initiated by three pathways, the alternative pathway (AP) is spontaneously and continuously activated on biological surfaces, the classical pathway (CP) is triggered by antigen-antibody interaction (immune complexes) and the lectin pathway (LP) is activated by the binding of mannan-binding lectin to certain sugars [20]. The central component of complement system is C3, the activation of three pathways leads to cleavage of C3 into the functional fragments C3a and C3b by C3 convertase. The convertase for the AP is formed by C3b and factor Bb, whereas the convertase for the CP and LP is composed of C4b and C2b [20]. Both convertases cleave C3 into C3a and C3b. C3b can bind to the cell surface via its own thioester bond or interaction with surface molecules that serve as platforms for C3b recruitment. C3b binds to C3 convertase to form another complex - C5 convertase which cleaves C5 into a potent anaphylatoxin C5a and a bioactive fragment C5b [21]. C5b recruits complement components C6, C7, C8 and C9 which polymerize to form the MAC C5b-9. The complex can form a pore in the target membrane inducing calcium influx and pathogen lysis. Host cells are protected from lysis by expression of CD59, which prevents the insertion of MAC, and by clusterin and vitronectin, which bind to C8 and prevent the insertion in the membrane [22, 23]. The anaphylatoxins, C3a and C5a are constantly released during complement activation. They play a critical role in supporting inflammation and activation of cells that express anaphylatoxin receptors C3aR and C5aR, such as the induction of chemotaxis of microglia, naïve T cell activation and the regulation of cytokine expression of monocytes/macrophage

[24, 25, 26].

Apart from C3 convertase, it has been demonstrated that C3 cleavage also occurs within human T cells mediated by cathepsin L into C3a and C3b. In resting T cells, this C3a binds to the intracellular C3a receptor and thereby mediates T cell activation [27]. It is clear now that intracellular C3 activation is ubiquitous in human cells to produce complement components. The liver is responsible for the synthesis of plasma complement proteins, but most complement components are unlikely to reach the brain due to the BBB. In these immune-privileged organs, including the brain and the eye, local production is the main source of complement [28]. The local complement functions to clear invading microbes in the brain. In age related diseases, such as Alzheimer's disease, abnormal complement activation and a local, chronic inflammatory response leads to attraction and activation of glial cells. The activated cells produce neurotoxic substances including pro-inflammatory cytokines and oxygen radicals which contribute to the disease [29]. Thus, local synthesis of complement proteins by glial cells and neurons plays critical roles in pathogen defense and neuroinflammation of the brain and the eye.

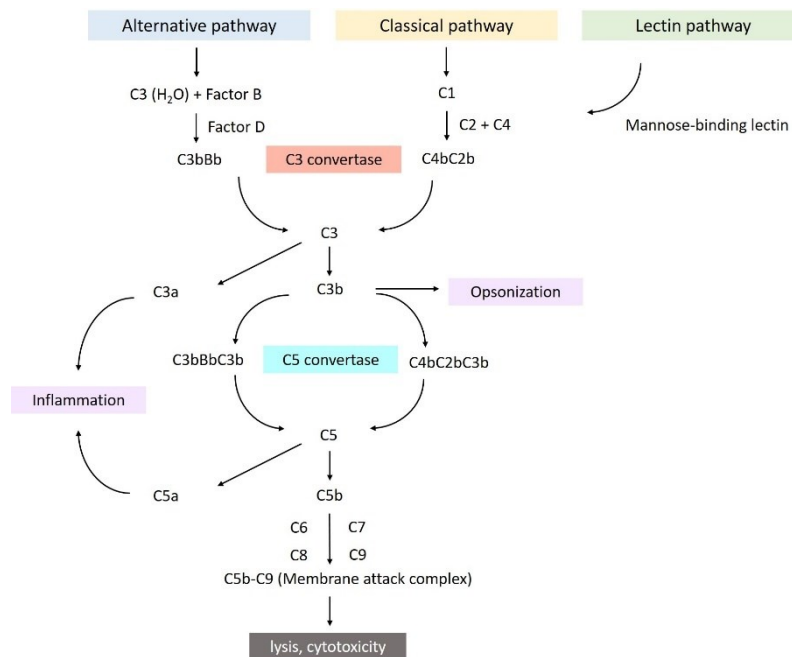


Figure 2. Activation of the human complement system.

The complement system is initiated by three pathways, the alternative pathway (AP), the classical pathway (CP) and the lectin pathway (LP). AP is permanently activated at low level by hydrolysis of C3 into C3(H₂O) and induces alternative convertase C3bBb. The CP and LP are triggered by the interaction of recognition molecules on a target structure, both induce formation of the classical C3 convertase C4bC2a. Complement activation leads to opsonization and phagocytosis by C3b deposition, bacterial lysis by C5b-9 membrane attack complex, and inflammation by anaphylatoxins C3a and C5a release and recruitment of immune cells.

In healthy individuals, the AP is permanently active at low levels to survey for presence of

pathogens. The activation also occurs by membrane alterations and by decreased expression of complement regulators on the membrane of apoptotic cells [20]. It is constantly generated and tightly regulated to eliminate dying cells without further activation of other innate or adaptive immunity during normal cellular homeostasis. Healthy host cells are resistant to persistent low-grade complement activation and protected against complement attack by negative regulation of the AP C3 convertase mediated by decay acceleration factor (DAF), complement receptor 1 (CR1), C4b-binding protein, membrane cofactor protein (MCP) and factor H. Complement is fully activated in cases of pathogen infection. Once activated, complement cascade generates effector compounds that are delivered to the surface. During the infection, pathogens are attacked by three complement pathways triggered by recognition molecules including C1q, MBL and properdin. The recognition events induce the activation of the cascades and generate the CP and AP C3 convertases. The key role of complement in pathogen elimination is opsonization, which is characterized by the depositions of complement fragments such as C3b, iC3b and C4b on pathogen surfaces. Opsonization results in the recognition, phagocytosis and destruction of the pathogens by phagocytes which express specific receptors for C3 fragments. Ultimately, it leads to activation of the adaptive immune response [21]. The consequence is the elimination of pathogens. Furthermore, the complement also plays a major role in clearance of dying cells to maintain homeostasis. The inactive fragment of C3, iC3b, interacts with complement receptor 3 (CR3) on monocytes, macrophages and DCs and participates in the removal of apoptotic cells and induces anti-inflammatory response. C1q, part of the C1q-complex in classical pathway, recognizes a various of ligands that expressed on the surface of apoptotic cells which allows C3b deposition and inhibits macrophage inflammation [21]. However, mutations in the regulators result in deficient complement control and inappropriate complement activation products accumulation on host cell surfaces, which leads to complement attack and cell damage. Inefficient clearance of apoptotic cells increases debris, thus contribute to autoimmune diseases.

1.1.4 Regulation of complement

The C3 amplification loop is the center of all three complement pathways (Figure 2). This amplification loop is the balance between amplification enhancement and downregulation acting on C3 convertase formation. The downregulation cycle generates iC3b as inactive product. The complement system contains a couple of inactive components that are linked and activated in a cascade manner. Thus, progression of the cascade and the action of the effectors need to be strictly controlled at each level by multiple complement regulators and inhibitors. Such regulators and inhibitors discriminate between self and non-self surfaces, such as cells, tissues and pathogens, operate at every level of the cascade and therefore, are central to control complement activation. Lack of complement inhibitor induces alternative C3 convertase activation.

1.1.4.1 Properdin

During complement activation, the convertases are assembled on target surfaces and initiate the complement amplification loop. However, the AP C3 convertase C3bBb is a short-lived complex with a half-live time of about 90 s [30]. Therefore, a stabilization of this complex is

required to assure efficient activation. Properdin, a plasma component released by various cell types, such as activated neutrophils, T cells and monocytes, stabilizes the AP C3 convertase 5-to-10 fold by association with the convertase more precise [30, 31]. Properdin forms cyclic dimers, trimers and tetramers by head-to-tail association of the 53 kDa protein [32]. Functional studies demonstrated that the oligomerization is essential for interaction with the C3bBb convertase since the oligomerization results in tighter interaction with C3b and is required for efficient stabilization of convertase [33]. Properdin binds C3bBb, as well as the pro-convertase C3Bb and C3b to activate complement, but the stabilization is most effective with C3bBb. Additionally, properdin is able to bind to pathogens, activated or damaged (apoptotic and necrotic) host cells to recruit C3b onto the surface and to induce the AP activation and phagocytosis [34]. The surface interaction was mediated by GAGs (glycosaminoglycans) which are important constituent of the cell membrane. GAGs play a critical role in complement regulation and participate in the protection of host tissues from complement damage by promoting inactivation of tissue-bound C3b [30]. Thus, properdin is not only a stabilizer of the C3 convertase, but also a pattern recognition molecule providing a platform for C3 convertase assembly.

1.1.4.2 Complement factor H

Accelerated dissociation of the AP C3 convertase and inactivation of C3b are critical steps to maintain complement homeostasis and to prevent non-specific damage to self-cellular components when complement is activated. If C3b is generated on host cells, it must be inactivated by regulatory proteins. To regulate complement activation, several inhibitors, primarily against AP, exist in the fluid phase and on host cells. Factor H is a soluble inhibitor of the C3 convertase, while membrane cofactor protein (MCP), decay acceleration factor (DAF) and complement receptor 1 (CR1) work as membrane inhibitors [19]. FH is an abundant (~500 µg/ml) 155 kDa plasma linear protein that belongs to the factor H protein family [35]. This glycoprotein is composed of 20 short consensus repeat (SCR) domains and regulates the alternative pathway. FH competes with factor B for binding to C3b and induces C3bBb complex dissociation and also serves as a cofactor to factor I which degrades C3b to inactive iC3b [19].

The N-terminal domains of FH, SCR 1-4, bind to C3b and contain the primary complement regulatory activity. SCR 1-4 of FH mediates cofactor and decay acceleration activities to regulate complement in the fluid phase and on surfaces. Decay-accelerating activity is characterized by the dissociation of Bb from the C3 convertase. SCR 19-20 FH harbors a second major binding site for C3b (Figure 3). SCR 19 binds to deposited C3b while SCR20 recognizes the self-surface. Flexible peptide linkers between the SCRs allow the FH protein chain to fold back on itself. This enables FH to bind a single C3b molecule with both the N- and C-terminus, thereby increasing the avidity of the interaction [35]. Furthermore, two binding sites in SCR7 and SCR 19-20 allow FH to recognize negatively charged heparan sulfate (HS), malondialdehyde (MDA) and C-reactive protein (CRP) on the membrane [36-39] (Figure 3). HS is a complex linear sulfated polysaccharide of the GAGs family that is present on host cell surface and in the extracellular matrix. HS attaches to particular core proteins to form HS proteoglycans which have essential roles in signaling and tissue homeostasis [40]. HS can accelerate the rate of conversion of C3b to iC3b by FH and FI, and this conversion is sulfation

dependent [41]. CRP is a regulator of innate immune system and exists as pentamer composed of 5 identical units in plasma. However, oxidative stress, low pH and bioactive lipids from activated or damaged cells can dissociate CRP into its subunits [42, 43]. This monomeric form of CRP induces pro-inflammatory responses which are inhibited by FH on ARPE-19 cells [44]. This inhibition is due to the interaction between FH and monomeric CRP, but not pentameric CRP. FH reduces oxidative stress by increased binding to oxidized phospholipids, thus preventing them from inflammatory activities [45].

Besides FH, there are FHL-1 (Factor H-like protein 1) and five factor H-related (CFHR) proteins that belong to FH protein family. FHL-1 arises from the alternative splicing of the *factor H* gene [46]. It is identical to FH for the first seven SCRs before terminating with a unique four amino acid C-terminus (Figure 3). It has been reported that FHL-1 is the main regulatory protein in Bruch's membrane of the retina due to the ability to diffuse across the membrane, but full sized glycosylated FH cannot [47]. The factor H/CFHR family also comprises a group of highly related proteins that includes five CFHR proteins. The five *CFHR* genes are located downstream of the *factor H* gene at chromosome 1q32, and each *CFHR* gene codes for a plasma protein containing between five and nine SCRs that are very similar to SCRs in FH. Each member of this group binds to the central complement component C3b and regulates complement activation. While the functions of the family are not fully understood [48, 49].

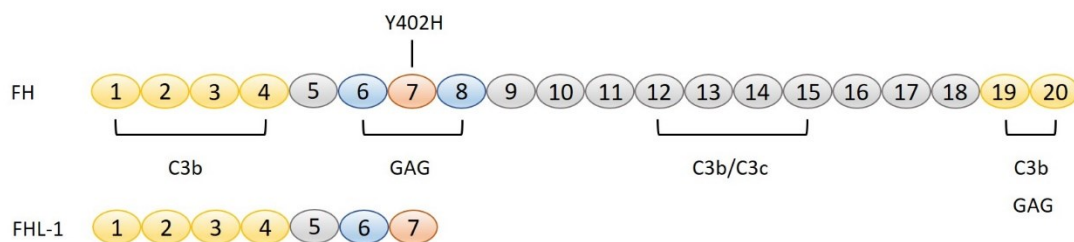


Figure 3. Structure of factor H.

Domains of complement FH and FHL-1. C3 binding sites are highlighted in yellow and GAG binding domains in blue. FHL-1 protein is represented below according to their sequence similarity to FH.

1.1.5 Complement-mediated diseases

The importance of the complement system is reflected in many severe and life-threatening complement-mediated diseases. Both deficiency and overactivation of complement system are associated with increased susceptibility to infections or non-infectious diseases including chronic inflammatory, autoimmune diseases and cancer [21]. For example, impaired clearance of apoptotic cells, induced by lack of C1q complement activation due to deficiency of C1q, C1r, C1s, or C2 or C4 are associated with systemic lupus erythematosus (SLE) [50]. Complement overactivation due to uncontrolled C3 and/or C5 convertase activation is associated with or lead to C3 glomerulopathy (C3G), characterized by C3 deposits and intra-glomerular inflammation [51]. Furthermore, complement is considered as an immune surveillance system because modified self surfaces like on tumor cells activate complement, become opsonized and subsequently phagocytosed. However, tumor cells can develop

inhibitory mechanisms to block the complement cascade, thus preventing complement-mediated cytotoxicity [20]. Recent studies showed that complement activation leads to chronic inflammation and an immunosuppressive microenvironment. This induces angiogenesis and activates cancer-related signaling pathways. Meanwhile, cancer cells also secrete complement proteins that stimulate tumor growth upon activation via direct autocrine effect through C3aR and C5aR signaling [52].

As a complement inhibitor, mutations or single-nucleotide polymorphisms (SNP) in the *factor H* gene that affect the function of the protein lead to an imbalance in complement regulation and specific diseases [53]. The major condition associated with the deficiency of FH is atypical hemolytic uremic syndrome (aHUS). Atypical HUS is caused by chronic, uncontrolled activation of the AP on the surface of endothelial cells in microvesicles and leads to renal failure [54]. AHUS-associated mutations are predominantly found in the C-terminal SCR19 and 20 of FH, the region responsible for cell surface association of FH and for mediating protecting the endothelium from complement damage [35]. One polymorphism in FH is also associated with age-related macular degeneration (AMD) and substantially enhances the risk to develop AMD [55]. Thus, genetic variations *in factor H* can affect different functions of the protein leading to distinct pathologies.

1.2 Age-related macular degeneration (AMD)

1.2.1 Retina

The human retina is the inner layer of the eye and part of the human brain. It is a high organized and specialized neural network where light is converted into electrical impulses. The retina is an immune privileged space, composed of layers of neural cells (photoreceptor cells, bipolar cells and ganglion cells) and retinal pigment epithelial cells (RPE) (Figure 4) [55]. Nutrition is supplied to the retina by ophthalmic arteries which are separated from the retina by a basal membrane, so called Bruch's membrane [56]. Transport across retinal blood vessels is controlled by the inner blood-retinal barrier (BRB) which consists of retinal vascular endothelium and retinal pigment epithelium tight junctions [57]. The high organized monolayer of RPE, has several roles in supporting the metabolically active photoreceptor layer. These include light absorption, the phagocytosis of photoreceptor outer segments (POS) membranes, controlling ion homeostasis, supplying a variety of nutrients and signaling molecules such as vascular endothelial growth factor A (VEGF-A) and maintaining the integrity of the outer BRB through tight junctions [58]. Meanwhile, the combination of light and oxygen brings oxidative stress to RPE. In addition, the RPE acts as a gateway for monocyte trafficking to the retina following direct or distant injury [59]. Thus, the integrity and functions of the RPE are essential for the homeostasis in the retina. Posterior to the RPE, the Bruch's membrane forms together with the RPE the outer BRB which prevents the entrance of macromolecules and immune cells from the underlying choroid into the photoreceptor layer. The choroid contains a dense network of blood vessels which supplies oxygen and nutrients to the RPE, outer retina and optic nerve. The choroid consists of tissue-resident melanocytes, fibroblasts, macrophages, mast cells and DCs and enables the transport of molecules to the metabolically demanding RPE [60]. The conversion of light

signal into electrical impulses occurs in light sensory cells (cone and rod photoreceptors) in the retina. The cones enable us to distinguish different colors. Rod cells are more sensitive than cones, but have little role in color vision. Optimal vision requires a high-functioning central retina, in particular the macula [56].

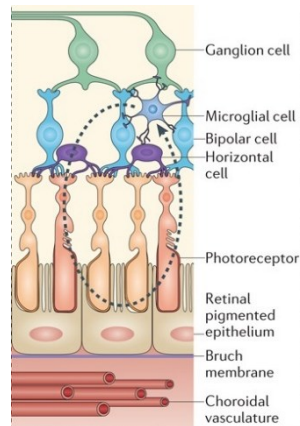


Figure 4. Structure of the human retina [55].

The retina is composed of several layers: ganglion cell layer, resident retinal microglia, bipolar cells, photoreceptor layer, the retinal pigment epithelium, the Bruch' membrane and a choroidal vascular network.

The macula is made up of millions of photoreceptor cells and responsible for the visual acuity. It is near the center of the human retina [57]. There are fovea and foveola regions within the macula containing high density of cone photoreceptors. Thus, the damage of the macula results in central vision loss.

1.2.2 Age-related macular degeneration (AMD)

Diseases of the retina and choroidal neovascularization such as AMD are the most common causes of severe visual loss in developed countries [61]. AMD is a slow, processive and degenerative disease and the major cause of central vision loss in elder individuals over 55 years of age, with as many as 30 million people affected worldwide [62, 63]. AMD is associated with the formation of drusen in the retina and subsequent loss of photoreceptors. Drusen are visualized as whitish yellow extracellular deposits that accumulated between RPE and Bruch's membrane, or sometimes between RPE and photoreceptors [64]. Many different molecules have been identified in drusen, including complement components, glycoconjugates, vitronectin, apolipoprotein, and lipids [65]. Macrophages have been detected in regressing drusen, suggesting that macrophages are recruited to eliminate the AMD lesions. The RPE is a major source of drusen components, and extracellular and serum-derived factors are also highly abundant.

The pathology of AMD is characterized by degeneration involving the outer portion of the retina, retinal pigment epithelium, Bruch's membrane, and less prominently, the choriocapillaris. AMD can be distinguished into early, intermediate and advanced forms that are associated with marked changes in normal retinal anatomy. Pathological changes during early stage AMD involve basal deposits in Bruch's membrane which cannot be determined by clinical evaluation [66]. It often begins slowly and may remain asymptomatic. Patients' first

symptoms are reduced visual acuity, non-specific blurred vision, and later also distorted vision. AMD can progress to the advanced form which will lead to central vision loss. Clinically, the advanced form can be further categorized as dry (atrophic) or wet (exudative) form. In the dry form of this disease, drusen are formed between the RPE and Bruch's membrane, with photoreceptor loss or choriocapillaris attenuation and extensive RPE atrophy. Wet AMD shows the presence of choroidal neovascularization extending through Bruch's membrane and the RPE into the subretinal space [56].

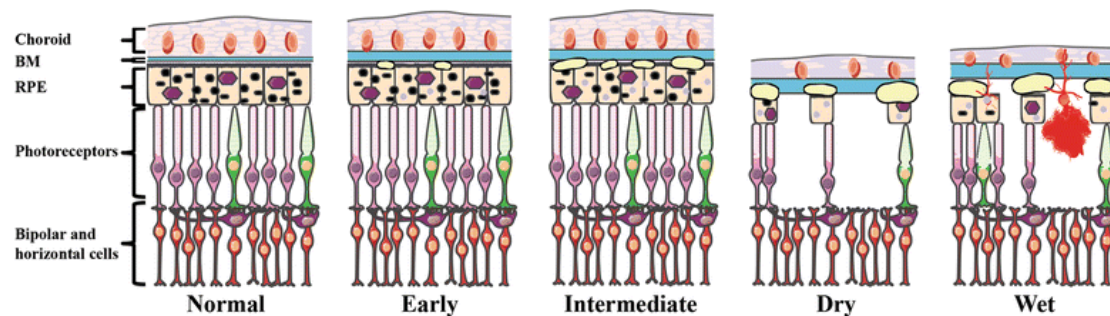


Figure 5. Overview of AMD pathogenesis [65].

Early or intermediate dry AMD is associated with an accumulation of subretinal drusen and microglia, and a thickened Bruch's membrane. Geographic atrophy is the advanced form of dry AMD which is characterized by photoreceptor degeneration, while neovascular AMD is characterized by the invasion of abnormal choroidal blood vessels and accompanying macrophages in the retina [65].

1.2.3 Risk factors of AMD

AMD is a multifactorial disease with demographic, environmental, and genetic risk factors contributing to disease development. The pathogenesis is still unclear. Age is the strongest risk factor for AMD. Smoking is also a highly significant environmental factor [65]. Over the past decade, a large number of studies identified an uncontrolled activation of the complement cascade which contributes to the development and progression of AMD. This is supported by the fact that complement activation products such as C1q, C3 and C5 were identified in drusen [64, 67, 68, 69]. Moreover, the generation of anaphylatoxins C3a and C5a promotes leukocytes recruitment and choroidal neovascularization [70]. Genetic analyses identified genetic factors involved in AMD [66, 71]. More recently, numerous polymorphisms within the *factor H* gene and their correlation with susceptibility to AMD were described [66]. A single nucleotide polymorphism (SNP) rs1061170 that results in a coding change of tyrosine (Y) to histidine (H) in SCR 7 (amino acid position 402) of FH, increases AMD risk dramatically [66]. As a major AMD susceptibility gene, the Y402H polymorphism in *factor H* has been found to alter the protein's specificity for the binding to GAGs and heparan sulfate (HS), but did not affect FH protein expression or complement regulatory function [72-77]. The interaction between FH and HS on the Bruch's membrane is particularly important for complement control due to the absence of membrane-bound complement inhibitors on the membrane [73]. Detailed analysis of the mechanism revealed that FH H402 variant also binds

substantially less to MDA and oxidized phospholipids expressed on RPE compared to normal FH protein [37, 78]. The presence of MDA on the surface of RPE cells acts as a binding site for FH, to inhibit complement activation and inflammation [77, 78]. Therefore, the Y402H polymorphism in the *factor H* gene contributes to pro-inflammatory cytokine production that promote activation of macrophage and microglia [69, 79]. In vivo, the decreased ability of FH H402 to localize to Bruch's membrane can result in impaired regulation of the complement AP and the production of pro-inflammatory mediators [40, 69, 73]. FH is also described to remove endogenous low-density lipoproteins (LDL) from human Bruch's membrane [80]. Thus, low binding of FH H402 to the oxidized lipids may increase sub-RPE deposit formation and accumulation. Recently, FH Y402 was found to contribute to mononuclear phagocytes accumulation at the inflammatory site by inhibiting their elimination mediated by CD47. FH H402 increased subretinal phagocytes accumulation and limited microglia elimination, thereby influences subretinal inflammation in AMD [81]. Patients with early signs of AMD and carrying the FH H402 variant differed substantially according their retinal function when compared with non-risk carriers [82]. However, the rs1061170 has been identified as the major genetic factor for developing AMD in Caucasians though the allele is low in frequent in Chinese and Japanese populations [83]. Overall, these observations suggest that the FH risk variant H402 results in increased complement activation and reduction in the immune antioxidant defense, the retention of activated microglia cells in the retinal space, thereby enhancing the local chronic pro-inflammatory status, and contributing to AMD pathology.

Other genetic variants in the *factor H/CFHR* gene cluster also modify the AMD risk, including a relatively common homozygous deletion of an 84-kb genomic fragment in chromosome 1 that encompasses *CFHR1* and *CFHR3* genes [84, 85, 86]. This deletion is protective for AMD. *CFHR1* and *CFHR3* can compete with FH for binding to complement C3. Although *CFHR1* controls the activity of the C5 convertase and membrane insertion of MAC, deficiency of *CFHR1* and *CFHR3* likely enhances local regulation of FH [87]. Recently, a *CFHR2* polymorphism (rs3790414) was suggested as a risk factor for neovascular AMD in a cohort [88]. *CFHR2* does not compete with factor H, and inhibits the AP C3 convertase and terminal complex assembly [89]. In addition, some variants in other complement component genes are associated with the risk of AMD, including *complement component 2 (C2)*, *C3*, *factor B* and *factor I* genes [67, 68, 90, 91].

Microglia activation is associated with retinal degeneration and photoreceptor apoptosis [92]. In the normal retina, resident microglia mainly populate the plexiform layer and continuously scan their environment, phagocytose cell debris and secrete a variety of supporting factors. In cases of abnormal or degenerative processes in RPE, the photoreceptor layer or the ganglion cell layer microglia rapidly become activated. Microglia trigger inflammasome activation in RPE cells. Resident microglia and/or recruited blood-derived precursors migrate to the lesion sites, where they transform into amoeboid phagocytes. These effector cells may be protective or detrimental depending on their immunological phenotype and the local cytokine production [93].

1.2.3.1 Vascular endothelial growth factor (VEGF)

In exudative AMD, abnormal blood vessels grow in choriocapillaris through Bruch's

membrane (choroidal neovascularization). These new blood vessels are fragile and ultimately leading to blood and protein leakage below the macula. VEGF plays a critical role in retinal and subretinal/choroidal neovascularization. The VEGF family in humans consists of several proteins: VEGF-A, VEGF-B, VEGF-C, VEGF-D, and placental growth factor (PlGF). VEGF-A is the major factor that stimulates vasculogenesis and angiogenesis [94]. This molecule is a homo-dimeric glycoprotein which is expressed by all vascularized tissues. There are several isoforms of VEGF-A produced from *VEGFA* gene by alternative splicing, and they show various expression patterns with contrasting characteristics [95]. In the eye, VEGF-A is the most abundant and an important factor of ocular homeostasis. Inhibition of VEGF confirmed that VEGF is the main growth factor in the retina leading to the increased angiogenesis within the eyeballs [61]. Angiogenesis is the physiological process that consists of the sprouting, migration and remodeling of existing blood vessels and plays important roles in many physiological processes [61]. Angiogenesis is regulated by the factors that stimulate and inhibit the formation of new blood vessels. Abundant factors are involved in this process, including the VEGF-VEGFR system. However, angiogenesis also occurs in several pathological conditions like cancer. Under normal conditions, RPE cells secrete VEGF to support choriocapillaris. During retinal hypoxia, VEGF is also produced by endothelial cells, Müller cells, and other ocular tissues and binds to their specific receptors on endothelial cells [60]. This in turn leads to neovascularization with subsequent breakdown of the blood-retina barrier and macula.

It has been reported that C3a and C5a can upregulate RPE/choroid production of VEGF [70], and the exposure of choroidal endothelial cells to serum also increased VEGF expression [96]. VEGF in turn stimulates proliferation of abnormal blood vessels in the retina. These results suggest that complement activation may promote an angiogenic effect via VEGF production in the retina, thus contribute to the development of AMD.

Currently, the only therapeutic approach to reduce the risk of progression to the advanced atrophic form of AMD is the use of food supplements (vitamin E, vitamin C, zinc, and beta-carotene or lutein). Injection of a monoclonal antibody against all forms of VEGF-A into the vitreous (jelly-like substance that fills the space back of the eye) has become the treatment for patients with active neovascular AMD. For the dry form of AMD, there is no therapy available so far [67].

1.2.3.2 Oxidative stress

Cells respond to environmental stressors in various ways including activation of survival pathways and programmed cell death [97]. There are many different types of stress and cell responses, such as heat shock response, the DNA damage response, the response to toxins and oxidative stress. The cells' essential purposes in response to extracellular stress are promoting the survival of cells and recovering from the environmental conditions. The survival pathways can be activated by different signals such as growth factor and extracellular molecules. However, if the stimulus is unresolved, then cells activate death signaling pathways to eliminate damaged cells.

Cell survival requires appropriate proportions of molecular oxygen and also various antioxidants [97]. The human body produces oxygen free radicals and other reactive oxygen

species (ROS) as byproducts from numerous physiological and biochemical processes of aerobic metabolism. ROS are among the most potent and ubiquitous threats faced by cells. ROS include reactive species like superoxide, hydrogen peroxide (H₂O₂), hydroxyl radical and peroxy radical [98]. At the same time, antioxidants, such as glutathione, arginine, citrulline, selenium, zinc, vitamin A, vitamin C and vitamin E regulate ROS generation and inhibit the oxidation of other molecules. Antioxidants are supported by antioxidant enzymes in removing free radicals [97]. Normally, there is an equilibrium between ROS production and antioxidant defense system [98]. However, ROS level can be increased dramatically due to infection and some environmental stress such as chronic exposure to UV light and toxins. If this balance is disturbed, oxidative stress occurs and generates free radicals that attack for example neuronal cells and interfere with their activities. Overproduction of free radicals cause oxidative damage to a range of biomolecules including lipids, proteins and DNA. Sustained stress results in apoptotic or necrotic cell death, eventually leads to many chronic diseases, such as atherosclerosis, cancer, diabetics, rheumatoid arthritis, stroke, cardiovascular diseases and degenerative diseases, like Alzheimer diseases and Parkinson's diseases [97]. In the eye, there are high-oxygen demands and ocular UV radiation of the retina. The disrupted oxygen supply to the retina due to retinal vasculature change with aging is a critical factor of oxidative stress. Furthermore, overexposure to blue light induced higher ROS production in human corneal epithelial cells, and leads to the structure alterations and disruption of BRB in vivo [99, 100]. In particular, RPE damage/dysfunction and the generation of the pro-inflammatory MDA by lipid peroxidation of membrane phospholipids also leads to RPE susceptible to complement [101, 102, 103]. They are thought to contribute to retinal disease. Although the pathogenesis of AMD is still unknown, oxidative stress plays a critical role in this disease.

1.2.3.3 Age-related maculopathy susceptibility 2 (ARMS2)

A number of additional AMD-associated genetic variants have been reported. Besides the *factor H/CFHR* locus, genetic variations at a second locus on chromosome 10q26 are also associated with AMD [104]. Both neovascular AMD and geographic atrophy have similar risk allele distribution. Three nearby genes are located in this locus, *pleckstrin homology domain containing, family A, member 1 (PLEKHA1)*, *age-related maculopathy susceptibility 2 (ARMS2)*, and *high-temperature requirement factor A1 (HTRA1)*, all of which, especially the latter two genes, are highly associated with AMD [105, 106]. The AMD associated polymorphism rs11200638 in the promoter region of *HTRA1* results in increased expression levels of *HTRA1* mRNA and protein in the human retinas [107, 108]. Although the upregulated *HTRA1* has not been fully verified in AMD, its effects on animal models were observed [109]. *HTRA1* overexpression induced choroidal neovascularization in mice, suggesting *HTRA1* is involved in pathogenesis of AMD [110, 111]. The *ARMS2* gene exists in primates, but is not conserved in other vertebrates. Genetic studies revealed a complex insertion-deletion (indel) in the 3' UTR of *ARMS2* as the AMD susceptibility allele (Figure 6) [112]. The indel variant deletes the polyadenylation signal and inserts a 54-bp AU-rich element known to mediate rapid mRNA turnover, resulting in an unstable *ARMS2* transcript and protein expression loss in placenta [105]. The indel mutation is also in strong linkage disequilibrium (LD) with a non-synonymous single nucleotide polymorphism rs10490924

(A69S) in exon1 of the *ARMS2* gene [104]. Individuals being homozygous for the risk alleles of both *factor H* and *ARMS2* have a ~50-fold increased risk for AMD [113]. However, retinas collected from Caucasian subjects, –homozygous or heterozygous carriers of the indel variation did not significantly differ in transcript levels of *ARMS2* [109, 114]. A polymorphism rs2736911 at amino acid position 38 in the *ARMS2* gene (R38X) results in a stop signal and subsequently a truncated protein which is however considered as a non-risk and protective variant [113, 115]. This suggests that the stability of *ARMS2* mRNA is regulated via distinct mechanisms in the retina and other tissues, and that the loss of gene message due to haploinsufficiency is not related to AMD pathogenesis.

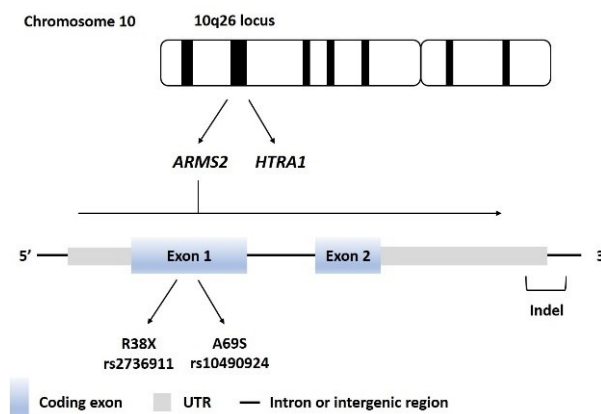


Figure 6. Overview of chromosome 10q26 locus and gene structure of *ARMS2* with three polymorphisms, rs2736911, rs10490924 and the del443ins54.

Exons are shown as blue boxes and untranslated regions as grey boxes. Polymorphism rs2736911 in *ARMS2* which leads to a nonsense exchange R38X was reported to be inversely associated with AMD. A combinative deletion/insertion (indel) polymorphism has been identified in *ARMS2* 3' UTR and flanking region. The association of indel with AMD is equal to that of polymorphism rs10490924 (A69S) since these variants are in strong linkage disequilibrium (modified from G.Wang [115]).

Kanda et al. reported that the *ARMS2* protein localizes to the mitochondrial outer membrane when expressed in mammalian cells, indicating that the *ARMS2* protein has functions in mitochondria, especially as mitochondria are critical for optimal ocular function [116, 117]. However, several studies could not confirm the mitochondrial location, instead subcellular *ARMS2* localization was identified in the cytosol [118, 119, 120]. Recently, silencing of *ARMS2* expression by siRNA in RPE cells was shown to result in a dramatic decrease in phagocytosis of POS (photoreceptor outer segments) [121]. As clearance of POS is one of the most important functions of the RPE, absent *ARMS2* functions would explain drusen formation and development of AMD [57]. However, the exact role of *ARMS2* requires further investigation.

1.3 Aim of this study

AMD is a multifactorial disease and a prevalent cause of vision loss in developed countries.

Recent genetic meta-analyses revealed the high association of a polymorphism (rs10490924) in the *ARMS2* gene with AMD. Preliminary data about ARMS2 protein functions showed an involvement of ARMS2 in complement activation. Immobilized ARMS2 interacts specifically with the complement activator properdin. This again suggested that an inappropriate complement activation is linked to the pathogenesis of AMD. However, at present, the expression and the biological functions of ARMS2 in AMD are poorly understood. Therefore, this study aimed to investigate the expression and function of ARMS2. Since the complement system plays a crucial role in the development of AMD, this study wanted to determine complement regulation on the retinal pigment epithelial cells, the most effected cells in AMD and responsible for photoreceptor loss. This study specifically aimed to:

Determine the expression of endogenous ARMS2 in human cells.

Express and purify recombinant ARMS2.

Characterize the function of ARMS2.

Investigate complement regulation on ARPE-19 cells.

2. Materials and Methods

2.1 Materials

2.1.1 Chemicals and reagents

All chemicals were obtained from Carl Roth (Karlsruhe, Germany), Merck (Darmstadt, Germany) or Sigma-Aldrich (Taufkirchen, Germany) if not mentioned separately.

Oligo nucleotide primers for PCR (Table 1) were synthesized from Life Technologies (Darmstadt, Germany).

Table 1

Forward and reverse primer sequences used in PCR.

Amplification	Forward (5'-3')	Reverse (5'-3')	Product
cDNA ARMS2	TCGGTGGTTCTGTGTCCTTCATT	TCGGTGGTTCTGTGTCCTTCATT	239 bp
Genomic ARMS2 (exon 1)	TGTCACCACATTATGTCCC	GGCACCCTCCAGAATTT	391 bp
Genomic ARMS2 (indel)	TGTCACTGCATCCCTCCTGTCAT	AAGCTTCTTACCCTGACTTCCAGC	598 bp indel - 209 bp indel +
cDNA actin	ACCAACTGGGACGACAT	CTAGAAGCATTGCGGTG	900 bp

2.1.2 Cells and strains

Cell experiments were performed using human blood-derived monocytes, human monocytic cell line THP-1 (ATCC® TIB-202TM), or human retinal pigment epithelial cell line ARPE-19 (ATCC® CRL-2302TM). Human microglial cell line iPsdM (induced pluripotent stem cell-derived microglial precursor cells) was kindly provided by Prof. Harald Neumann (Institute of Reconstructive Neurobiology, University of Bonn, Bonn, Germany). Retina samples were obtained from the Center of Ophthalmology Eye Bank, University of Cologne (Cologne, Germany). All research conducted followed the tenets of the Declaration of Helsinki. The local ethics committee of the University of Cologne has approved the study under No. 14-247 and the Institutional Review Board of the Charité Berlin, Germany under study protocol No. EA2/004/2014.

Escherichia coli DH5 α competent cells were purchased from Life Technologies. ARMS2 gene was cloned into pPICZ α B vector (Life Technologies, Darmstadt, Germany) and transformed in *Pichia pastoris* strain X33 (Life Technologies) by Dr. Sven Micklisch (Department of Infection Biology, HKI, Jena, Germany).

2.1.3 Media and buffers

RPMI (Roswell Park Memorial Institute medium) 1640, DMEM (Dulbecco's modified eagle medium) and DMEM/F12 (Dulbecco's modified eagle medium/nutrient mixture F12) used for

eukaryotic cells were purchased from Lonza (Verviers, Belgium). Media were supplemented with 10% fetal bovine serum (FBS, Gibco, Darmstadt, Germany), 1% L-Glutamine (Lonza) and 50 µg/ml Gentamicin (Lonza). DPBS (Dulbecco's phosphate buffered saline) was from Lonza. Ficoll-Paque PLUS and Percoll used for blood monocytes isolation were purchased from GE Healthcare (Freiburg, Germany).

Table 2**Buffers used in this study.**

buffer	recipes
Low salt LB medium (Luria-Bertani)	1% tryptone, 0.5% yeast extract, 0.5% NaCl, pH 7.0 in 1 liter of distilled water. Autoclave for 20 min at 15 lb/sq. in.
LB agar	1% tryptone, 0.5% yeast extract, 0.5% NaCl and 2% agar pH 7.0 in 1 liter of distilled water. Autoclave for 20 min at 15 lb/sq. in.
YPD agar (Yeast extract peptone dextrose medium)	1% yeast extract, 2% peptone, 2% dextrose, 2% agar in 1 liter of distilled water. Autoclave for 20 min at 15 lb/sq. in.
BMGY medium (buffered glycerol-complex medium)	1% yeast extract, 2% peptone, 100 mM potassium phosphate pH 6.0, 1.34% yeast nitrogen base, 4 x 10 ⁻⁵ % biotin, 1% glycerol in 1 liter distilled water. Autoclave for 20 min at 15 lb/sq. in.
BMMY medium (buffered methanol-complex medium)	1% yeast extract, 2% peptone, 100 mM potassium phosphate pH 6.0, 1.34% yeast nitrogen base, 4 x 10 ⁻⁵ % biotin, and 10% methanol in 1 liter distilled water. Autoclave for 20 min at 15 lb/sq. in.
RIPA lysis buffer	25 mM Tris-HCl pH 7.6, 150 mM NaCl, 1% (v/v) Nonidet P-40 (NP-40), 1% (w/v) sodium deoxycholate, 1% (w/v) SDS containing 1 mM PMSF (phenylmethylsulfonyl fluorid, Roth). Filter sterilize.
TBS-T buffer	2.4 g Tris base, 8.8 g NaCl, 1 ml Tween 20 in 1 liter distilled water, pH 7.6.

2.1.4 Purified proteins and peptides

Purified human C3, C3b, C5, FH and properdin proteins were purchased from Complement Technology (Tyler Texas, USA). Recombinant ARMS2 and ARMS2 variant S69 proteins were expressed and purified from *P. pastoris* as previously described by Sven *et al.* [119]. Three ARMS2 peptides were synthesized with 95% purity from Jerini Peptides Technologies (JPT, Berlin, Germany). Peptide 1 includes amino acid 1 to 40, peptide 2 amino acid 41 to 70 and peptide 3 amino acid 71 to 107. In addition, 24 small peptides of ARMS2 C-terminus (each of 13 amino acids with 10 amino acids overlap) were synthesized and spotted onto a cellulose membrane (JPT).

2.1.5 Antibodies, sera and blood

The rabbit anti-ARMS2_{jena} antiserum was generated by immunization of rabbit with purified recombinant ARMS2 from CovaLab (Cambridge, UK). Generated antiserum was purified with HiTrap Protein A HP 1 ml column (GE Healthcare). The mouse anti-ARMS2_{mAB} was generated by Dr. Diana Pauly (Institute of Human Genetics, University of Regensburg, Regensburg, Germany) via ARMS2 C-terminus peptide 3 as mentioned above. The antibodies used in this study were shown in Table 2. Secondary HRP-conjugated antibodies for ELISA or western blot were purchased from Dako (Hamburg, Germany) (Table 2). Fluorescent secondary antibodies (Table 2) for flow cytometry or laser scanning microscopy were purchased from Life Technologies (Darmstadt, Germany).

Table 3**Antibodies used in this study.**

Primary antibodies		Secondary antibodies
name	source	name
ARMS2 _{jena} antiserum	rabbit (polyclonal)	HRP-conjugated goat anti-mouse
ARMS2 _{mAB} antibody	mouse (monoclonal)	HRP-conjugated swine anti-rabbit
C3 antiserum (Complement Technology)	goat (polyclonal)	HRP-conjugated rabbit anti-goat
C5 antiserum (Complement Technology)	goat (polyclonal)	Alexa 647®-conjugated goat anti-rabbit
FH antiserum (Complement Technology)	goat (polyclonal)	Alexa 488®-conjugated goat anti-mouse
properdin antiserum (Complement Technology)	goat (polyclonal)	
C3d antiserum (CalBioChem, Darmstadt, Germany)	rabbit (polyclonal)	
penta histidine antibody (QiaGen, Hilden, Germany)	mouse (monoclonal)	
beta actin antibody (BioLegend, London, UK)	mouse (monoclonal)	

Normal human serum (NHS) was obtained from healthy donors from Department of Infection biology, HKI (Jena, Germany). Sera of 5 donors were pooled, aliquoted and stored at -80 °C. To inactivate complement, NHS was heated at 56 °C for 30 min (iNHS).

Wet form of AMD patients' blood was collected from Berlin by Saskia Jacob and Catharina Busch (Department of Ophthalmology, Charité - University hospital Berlin, Berlin, Germany). Fresh blood was donated by healthy donors from Department of Infection biology, HKI (Jena, Germany).

2.1.6 Assay kits

VEGF measurement was performed using human VEGF standard TMB ELISA development kit (Peprotech, Hamburg, Germany). Cell viability was quantified using cell cytotoxicity assay kit from Abcam (Cambridge, UK). QIAprep spin miniprep kit for plasmid isolation was purchased from Qiagen. Invisorb spin DNA extraction kit for DNA purification was from Stratec biomedical (Birkenfeld, Germany).

2.1.7 Equipment and laboratory supplies

The laser scanning microscope LSM 710 (Carl Zeiss, Jena, Germany) was used to obtain images. Flow cytometry was performed by BD LSR II (Becton Dickinson, Heidelberg, Germany). Yeast cells were cultivated using a rotary shaker (Innova 44, New Brunswick Scientific, Eppendorf, Germany). Centrifugation of protein, cells and samples was done using table top centrifuges from Eppendorf (5424, Hamburg, Germany) or a large-scale centrifuge

(3-18KS) from Sigma (Osterode am Harz, Germany). FPLC Äkta system for protein purification was from GE Healthcare Life Sciences. ELISA reader used was Safire2 from Tecan (Zürich, Switzerland). Vortex Genie 2 (Scientific Industries, Merck, Dresden, Germany) and the magnet shaker Unimax 2010 (Heidolph, Merck, Dresden, Germany) were used. Western blot membrane was developed in Fusion FX (Vilber, Eberhardzell, Germany). Biolayer interferometry was performed by Blitz system from Pall ForteBio (Fremont). Thermomixer comfort was used for incubation of reaction tubes (Eppendorf). Round bottom tubes for flow cytometry analysis were purchased from BD. High binding ELISA plates were purchased from Sarstedt (Nümbrecht, Germany). Cell culture flasks, plates and pipettes were purchased from Nunc (Mannheim, Germany) and falcon tubes from Greiner (Frickenhausen, Germany). Reaction tubes were purchased from Eppendorf. BD Vacutainer (Sodium Heparin) blood collection tubes were purchased from BD.

2.2 Methods

2.2.1 Blood monocytes isolation

Human blood monocytes were isolated with Ficoll-Paque PLUS according to the manufacturer's protocol. Briefly, human fresh blood was drawn and collected using a vacutainer containing sodium heparin. 30 ml fresh blood was overlaid carefully on 15 ml Ficoll-Paque PLUS and centrifuged at 1,600 rpm without break for 20 min at room temperature. After centrifugation, the plasma layer was slowly removed and the white ring of PBMCs (peripheral blood mononuclear cells) were collected. PBMCs were washed with DPBS and centrifuged at 900 rpm with low acceleration break at room temperature. Then, the PBMCs pellet was resuspended in 25 ml of IMDM (1 x Iscove's modified dulbecco's medium, Gibco) and the suspension was overlaid carefully on top of 25 ml 46% Percoll (23 ml of Percoll mixed with 27 ml of IMDM). After centrifugation at 1,600 rpm without break for 20 min at room temperature, the white ring of monocytes enriched layer was collected and washed with DPBS. The pellet was resuspended into 3 ml of DPBS and counted using CASY TCC cell counter (OLS OMNI Life Science, Bremen, Germany).

2.2.2 Cell cultures and oxidative stress induction

ARPE-19 cells were cultured in DMEM/F12 medium and maintained in a humidified atmosphere incubator at 37 °C containing 5% CO₂. After 80% - 90% confluency in T75 cm² flasks, cells were trypsinized using 0.25%/0.02% (w/v) trypsin/EDTA solution (Biochrom, Berlin, Germany) and split in ratio 1:4 in 15 ml warm medium. RAW247.6 cells were cultivated in DMEM medium and passaged twice per week using trypsin/EDTA solution. THP-1 cells were cultured in RPMI medium in suspension under the same conditions. For the induction of cell differentiation, 1 x 10⁶ per ml THP-1 cells were seeded with 20 ng/ml PMA (Phorbol 12-myristat 13-acetat, Sigma-Aldrich GmbH, Dreisenhofen) for 24h. For cell viability assay or cytokine analysis, ARPE-19 cells were seeded into 24-well plate or 96-well plate at a density of 1 x 10⁵ or 4 x 10⁴ cells per well and grown in media for 24 h. For oxidative stress induction, stable ARPE-19 cell monolayers were treated with different concentrations of H₂O₂ (0.1-2 mM) in serum-free medium for 1 h, after treatment, cells were washed with serum-free medium carefully and incubated with serum-free medium, or medium containing

NHS/iNHS for 24 h before analysis.

To induce ARMS2 expression, blood monocytes were isolated from fresh blood and cultured in RPMI medium for 2 h until they adhere to the plate surface, and then incubated for 1 h with H₂O₂ (0.001-1 mM) in medium, for another 20 h in normal medium before analysis.

2.2.3 RNA isolation RT-PCR and polymerase chain reaction (PCR)

Total RNA was isolated from blood cells using the PAX gene blood RNA kit (QiaGen) according to the manufacturer's instructions. The concentration of RNA was measured by a nanodrop spectrophotometer. 20 ng RNA was reverse transcribed into cDNA using QuantiTect® Reverse Transcription Kit (QiaGen). 100 ng cDNA was amplified using Phusion PCR Kit (New England Biolabs) in 50 µl PCR reaction containing 100 pM of each primer, 0.4 µl of 10 mM dNTPs, 10 µl 5 x HF Buffer and 0.5 µl Phusion polymerase. Thermocycling conditions for PCR reactions were: an initial denaturation step at 98 °C for 1 min, 30 cycles of 30 s at 98 °C, 30 s at 60 °C and 30 s at 72 °C, and final extension at 72 °C for 5 min. PCR products were separated by agarose gel electrophoresis and analyzed.

2.2.4 Agarose gel electrophoresis

Agarose gel electrophoresis was used to determine DNA fragments and plasmid. Samples were mixed with 6 x orange DNA loading dye (Thermo fisher, Schwerte, Germany), and then separated with 100 bp DNA ladder (NEB) by 1% TAE agarose gel containing 3 µl SYBR® safe DNA gel stain (Invitrogen) in TAE running buffer (0.04 M tris-acetate, 1 mM EDTA (Titriplex III), pH 8.0). DNA bands were visualized under UV light using gel imaging system (Syngene, Cambridge, UK).

2.2.5 Confocal laser-scanning microscopy

Monocytes or ARPE-19 cells were seeded onto glass coverslips (Roth) (1 x 10⁵ cells/well) and grown for 2 h or 24 h. Cells were fixed in 4% paraformaldehyde (Roth) for 15 min and permeabilized in 0.3% Triton X-100 (Roth) for 10 min. After washing, cells were preincubated with FcR Blocking Reagent (20 µl per 10⁷ cells, Miltenyi Biotec, Teterow, Germany) for 10 min on ice and then incubated with primary antibody (1:200) in DPBS for 1 h, washed three times with DPBS, and visualized with Alexa-488 or 647 conjugated secondary antibody (Life Technologies) (1:400) for 1 h. 4', 6'-Diamidino-2-Phenylindole, Dilactate (DAPI, Life Technologies) was added (1:1000) for cellular DNA staining. The slides were washed, dried and all images were recorded using Zeiss LSM710 confocal microscope equipped with a 63 x oil objective.

2.2.6 Immunoprecipitation

To pull down endogenous ARMS2 from human cells, immunoprecipitation was performed. 50 µl Protein G magnetic beads (NEB, New England BioLabs, Frankfurt) were resuspended in binding buffer (20 mM sodium phosphate buffer, pH7.0) and incubated with 10 µg α-ARMS2_{mAB} antibody for 1 h at 4 °C and washed with DPBS. 1 x 10⁷ THP-1 cells were lysed using 1 ml RIPA lysis buffer containing 1 mM PMSF for 30 min on ice and centrifuged at 12,000 rpm for 10 min at 4 °C. The supernatant was added subsequently to the antibody-immobilized beads and incubated on a rotating shaker at 4 °C overnight. Later on,

the supernatant was removed and beads were washed three times followed by adding 30 μ l of elution buffer (0.1 M glycine, pH 2.7). The eluted fraction was collected to proceed to SDS-PAGE and western blot analyses.

2.2.7 Sodium dodecyl sulfate polyacrylamide gel electrophoresis (SDS-PAGE)

Samples were mixed with 4 x reducing buffer (50 mM Tris-HCl pH 6.8, 1.6% (w/v) SDS, 7% (v/v) glycerol, 8 M UREA, 4% (v/v) β -mercaptoethanol, 0.016% (w/v) bromophenol blue, pH 6.8) and boiled for 10 min at 95 °C or mixed with 4 x non-reducing buffer (50 mM Tris-HCl pH 6.8, 1.6% (w/v) SDS, 7% (v/v) glycerol, 0.016% (w/v) bromophenol blue). Proteins and PageRuler™ prestained protein ladder (Life Technologies) were separated using vertical gel electrophoresis chambers (Bio-Rad Laboratories, München, Germany). 4% stacking gels (0.5 M Tris-HCl pH 6.8, 1% SDS, acrylamide/bis acrylamide (37.5:1), 100 mg/ml APS (ammonium persulfate), 0.1% TEMED (tetramethylethylenediamine) in distilled water) and 10% running gels (1.5 M Tris-HCl pH 8.8, 1% SDS, acrylamide/bis acrylamide (37.5:1), 100 mg/ml APS, 0.1% TEMED in distilled water) were used. 10 x SDS running buffer stock (30.3 g Tris, 144 g glycine, 10 g SDS in 1 liter distilled water) was diluted 100 ml into 900 ml distilled water to make 1 x running buffer and used. Electrophoresis was done at a constant voltage of 150 V for 1 h until the dye front reached the bottom of the gel.

2.2.8 Silver staining

After electrophoresis, gels were fixed in fixing buffer (15% (v/v) ethanol, 12% (v/v) acetic acid) for 30 min, rinsed for 10 min in washing buffer (15% (v/v) ethanol). After sensitisation in buffer A (0.2 g/l sodium thiosulfate) for 1 min and washed with distilled water, gels were incubated with buffer B (2 g/l silver nitrate) for 20 min. Gels were then washed with distilled water and developed in buffer C (0.75 ml/l formaldehyde (37%), 30 g/l sodium carbonate, 10 mg/l sodium thiosulfate) until the bands appeared. The reaction was stopped using fixing buffer. Gels were incubated with drying buffer (5% (v/v) glycerol, 10% (v/v) ethanol) and dried with DryEase® Mini-gel Drying System (Invitrogen).

2.2.9 Western blot

After electrophoresis, proteins were transferred onto a 0.22 μ m PVDF membrane (GE healthcare) in blotting buffer (25 mM Tris pH 8.5, 0.2 M glycine, 20 % methanol) using semi-dry transfer method in Trans-Blot® Turbo™ Transfer System (Bio-Rad Laboratories). Blotting was performed at 12 V for 30 min. After incubation in blocking buffer (TBS-T buffer with 3% nonfat dry milk, 1% BSA and 0.1% tween 20) for 1 h at room temperature, membranes were incubated with appropriate primary antibody (1:1000 in blocking buffer) for 1 h. The membrane was washed three times with TBS-T buffer followed by incubation with corresponding secondary antibody (1:2000 in blocking buffer) for 1 h at room temperature. After washing, chemiluminescence signals were visualized using 100 μ l/cm² chemiluminate-HRP PicoDetect (AppliChem, Darmstadt, Germany) by Fusion FX system.

2.2.10 Cloning and transformation

The variant A69S DNA was synthesized from Invitrogen. DNA as well as the expression vector *pPICZ α B* (Invitrogen) were digested with restriction enzymes *EcoR I* and *Xba I* (NEB) for 4 h at

37 °C. The digested DNA and vector were purified using Invisorb spin DNA extraction kit, and ligated using T4 DNA ligase (NEB) at 20 °C overnight. The ligated vector was transformed into competent *E. coli* cells by heat shock [122]. Positive colonies were analyzed, and the sequencing of plasmid was done by Monika von der Heide (Department of Infection Biology, HKI, Jena, Germany) using an ABI-Prism 3100 Genetic Analyzer (Applied Biosystems). Thereafter, one positive transformant was grown in LB medium at 37 °C overnight and plasmid was isolated using QIAprep spin miniprep kit following the manufacturer's instruction. Purified plasmid was linearized with *Sac I* (NEB) at 37 °C for 4 h and digested plasmid was purified as described above. Then, plasmid was transformed into competent *P. pastoris* X33 cells by electroporation according to the manufacturer's instructions (Invitrogen). The transformation reaction was spread on YPD plate containing 100 µg/ml zeocin and incubated at 30 °C for 3 days. Grown colonies were picked and tested for desired protein expression.

2.2.11 Recombinant protein expression

ARMS2 and ARMS2 variant A69S were recombinantly expressed as myc and 6 x histidine-tagged proteins according to the manufacturer's instructions. Briefly, expression strains were grown on YPD agar plates supplemented with 100 µg/ml zeocin and incubated for 3 days at 30 °C. Using a single colony, inoculated 25 ml of BMGY in a 250 ml baffled flask. Cells were grown at 30 °C until culture reached the OD₆₀₀ = 2-6. Then, cells were harvested by centrifugation (4,700 rpm, 10 min, RT) and resuspended in 200 ml BMMY medium. Protein expression was done at 30 °C in the shaker incubator and induced by adding methanol to a final concentration of 0.5% (v/v) every 12 h. After 3 days, the cell pellet was collected and analyzed by SDS-PAGE and western blot.

2.2.12 Affinity chromatography purification of proteins

The recombinant ARMS2 A69 and ARMS2 variant S69 proteins were purified by nickel chelate affinity chromatography from cell lysates. Briefly, cell pellets were lysed in binding buffer (10 mM Na₂HPO₄, 10 mM NaH₂PO₄, 10 mM imidazol, 1 M NaCl, 2% NP-40 (v/v), 20% glycerol (v/v), pH 7.0) together with glass beads (Roth) by FastPrep® -24 (MP Biomedicals) at 2 x 50 for 60 s. Protease activity was inhibited by addition of complete EDTA-free protease inhibitor (Roche, Mannheim, Germany). After centrifugation (12,000 rpm, 1 h, 4 °C) and filtration (22 µm cellulose acetate filter, Sartorius Stedim Biotech, Germany), the supernatant of cell extract was loaded to 1 ml HisTrap HP column (GE Healthcare) at 4 °C overnight and then washed with 10 column volumes of washing buffer (95% binding buffer combined with 5% elution buffer). Bound protein was eluted from column using elution buffer (10 mM Na₂HPO₄, 10 mM NaH₂PO₄, 500 mM imidazol, 500 mM NaCl, pH 7.0). Eluted fractions were tested by western blot and then concentrated by 5,000 MWCO centrifugal filter device (Sartorius Stedim Biotech, Göttingen, Germany) in storage buffer (10 mM Na₂HPO₄, 10 mM NaH₂PO₄, 500 mM NaCl, pH 7.0). Protein concentration was measured using a spectrophotometer (Nanodrop® ND-1000) and then stored at -20 °C.

2.2.13 Protein in-gel digestion and mass spectrometric peptide analysis by MALDI-TOF

The purified recombinant ARMS2 or immunoprecipitated endogenous ARMS2 from THP-1

monocytes were separated using SDS-PAGE and stained with coomassie blue (Thermo Scientific). The differentially expressed protein bands observed in the polyacrylamide gel were excised from the gel and washed repeatedly with distilled water and 50 mM NH_4HCO_3 /acetonitrile 1+1 (v/v) for 15 min. The gel pieces were then shrunk in acetonitrile and dried down by the vacuum centrifuge. After that the gel pieces were soaked in solution containing 10 mM DTT in 50 mM NH_4HCO_3 for 45 min at 56 °C followed by alkylation by treatment with 50 mM iodoacetamide in 50 mM NH_4HCO_3 for 30 min in dark. After the treatment, gel pieces were washed with 50 mM NH_4HCO_3 /acetonitrile. Thereafter the gel pieces were treated with trypsin (Promega, Mannheim, Germany) digestion buffer (20 ng/ μl trypsin in 25 mM NH_4HCO_3) at 37 °C overnight. The peptides were extracted by adding acetonitrile/trifluoroacetic acid 1+1 (v/v) to the gel plugs and incubation for 30 min at room temperature. 1 μl peptide digest extracted from the gel piece was premixed with same volume of the matrix α -CHCA solution and spotted onto a matrix-assisted laser desorption ionization (MALDI) plate. The peptide mass was analyzed using MALDI TOF-mass spectrometer (UltrafleXtreme, Bruker Daltonics, Bremen, Germany) in the reflector mode with appropriate m/z range and laser intensity. Current NCBI nr database using MASCOT search with a peptide mass tolerance of 100 ppm was used to search the data generated.

2.2.14 *In vitro* binding assays

Flow cytometry was done using a BD LSRII flow cytometer (BD Biosciences) and data were analyzed using the FACSDiva and FlowJo software (Tree Star). Incubation and washing steps were performed in DPBS supplemented with 1% BSA. For the binding to heparan, 1 million heparan beads were suspended in 200 μl DPBS and incubated with 1 μg protein for 1 h at 4 °C, beads were centrifuged for 5 min at 8,000 rpm and washed with DPBS. Then, the beads were incubated with polyclonal antiserum α -ARMS2_{Jena} (1:200) in DPBS for 1 h at 4 °C. After washing, Alexa 647 conjugated-goat anti-rabbit (Life Technologies) (1:400) were added to the beads and incubated for 1 h at 4 °C. The beads were washed and resuspend in 1 ml DPBS to measure the fluorescence.

To investigate the binding of proteins to ARPE-19 cells, cells were trypsinized and 1 million cells were incubated with protein for 1 h at 4 °C. After washing, primary antibody (1:200) was added followed by Alexa conjugated secondary antibody (1:400) incubation for 1 h at 4 °C to detect bound protein.

2.2.15 C3b deposition

The complement alternative pathway activation assay was performed by incubation of ARPE-19 cells with NHS in AP MgEGTA buffer (20 mM HEPES, 144 mM NaCl, 7 mM MgCl_2 , 10 mM EGTA, pH 7.4) at 37 °C for 30 min. C3b deposition was determined by flow cytometry using rabbit anti-C3d antibody (1:200) for 1 h at 4 °C and secondary Alexa 647-conjugated goat anti-rabbit antibody (1:400) for 1 h at 4 °C. The influence of ARMS2 or FH on C3b deposition was evaluated after preincubation of cells with each protein.

2.2.16 Enzyme-linked immunosorbent assay (ELISA)

High binding microtiter plate was immobilized with 5 $\mu\text{g}/\text{ml}$ desired proteins in DPBS at 4 °C overnight. After washing unbound protein and blocking with DPBS containing 1% BSA for 1 h

at 37 °C, different dilutions of bound ligand was added to wells for 1 h. The plate was sequentially washed and incubated with appropriated primary antibody (1:1000 in DPBS), followed by the incubation of corresponding HRP-conjugated secondary antibody (1:2000 in DPBS) for 1 h. The reaction was developed with TMB substrate reagent (BioTrend Chemikalien, Cologne, Germany) and the absorbance was measured at 450 nm using ELISA reader. Experiments were performed in triplicate.

To investigate VEGF secretion, ARPE-19 cells were treated with H₂O₂ (0.1-2 mM) for 1 h followed by exposure to serum-free medium or medium containing NHS/iNHS for 24 h. The conditioned medium was collected, centrifuged at 1,000 rpm for 5 min to remove detached cells. ELISA analysis was performed from the supernatants for VEGF production using the commercial kit (PeproTech) according to the manufacturer's instructions. Briefly, supernatants were added to 0.5 µg/ml immobilized capture antibody in order to catch the cytokine. Bound VEGF was detected by 0.125 µg/ml detection antibody and subsequently with 0.05 µg/ml streptavidin-HRP. The absorbance was measured at 450 nm using ELISA reader. Experiments were performed in triplicate.

2.2.17 Bio-layer interferometry

To measure the interaction affinity between properdin and ARMS2, biolayer interferometry was performed. Purified human properdin was preincubated with 2 mM sulfo-N-hydroxysuccinimide long chain-biotin (Pierce) dissolved in distilled water for 30 min at 37 °C. Excess non-reacted biotin was removed by size exclusion chromatography using desalting columns (Pierce). The interferometry experiment was started with a 30 s baseline step. The biotinylated properdin then was immobilized on streptavidin (SA)-coated biosensor tips for 180 s, various concentrations of ARMS2 were used in the association step. Association and dissociation phases were recorded for 240 s and 240 s, respectively. All sensor traces were analyzed as a global set of multiple dissociation curves. Reference sensor trace was used to correct for nonspecific binding.

2.2.18 Pepsots peptide arrays on cellulose membrane

To localize the binding domain in ARMS2 which mediates the interaction with properdin, 24 ARMS2 peptides of 13 amino acids with 10 amino acids overlap were synthesized and bound onto a cellulose membrane by the C-terminus and have an acetylated N-terminus. Purified properdin was labelled with red fluorescent Alexa Fluor 647 using the molecular probes Alexa Fluor® labelling kit (Life Technologies). The membrane was blocked in blocking buffer (1 % BSA and 3 % nonfat dry milk in DPBS) for 1 h and incubated with 5 µg Alexa Fluor 647-conjugated properdin at 4 °C overnight. After washing three times, the fluorescent signals were excited using Fusion FX system under standard APC/Cy5® filters. Incubated membrane which can be used again was washed three times with TBS-T buffer for 10 min and regenerated following the manufacturer's protocol. After washing with methanol twice, the membrane was air dried and kept at -20 °C.

2.2.19 Cell viability assay

To determine the susceptibility of ARPE-19 cells to serum-free media, NHS, iNHS or H₂O₂, cell

viability was quantified 24 h after the treatment using cell cytotoxicity assay kit (colorimetric). ARPE-19 cells (4×10^4 /well) were seeded into a 96-well microtiter plate and cultivated in medium for 24 h at 37 °C to reach a confluent monolayer. After the treatment, cells were washed and cultivated in serum-free medium or medium containing NHS/iNHS. Then 1/5 volume of cytotoxicity assay solution was added into each well and incubated in a 37 °C incubator protecting from light for 3 h. For control experiments, cells were cultivated in normal medium. Absorbance at 570 nm and 605 nm was measured by ELISA reader. The ratio of OD_{570} to OD_{605} was used to determine the cell viability in each well. Experiments were performed in triplicate.

2.2.20 Statistics

Data are presented as mean \pm SD where indicated. Comparison of two conditions was performed with Student's two tailed *t*-test using GraphPad Prism 5. Differences with $p < 0.05$ were considered significant, and statistical significance is shown as *, $p < 0.05$; **, $p < 0.01$; ***, $p < 0.001$.

3. Results

3.1 Human monocytes and iPS-derived microglia express ARMS2

3.1.1 Detection of ARMS2 transcripts in human monocytes and iPS-derived microglia

Choroidal monocytes/macrophages infiltrate the human retinal space in both early and late AMD [123, 124]. However, the contribution of these cells in drusen pathogenesis or progression is still unknown. As ARMS2 expression was previously described in the retina, placenta and whole blood [105, 109, 114], we asked whether monocytes express ARMS2. First, we analyzed ARMS2 expression in human monocytic cell line THP-1. Briefly, RNA was extracted from cells, and transcribed into cDNA. Using ARMS2 primers, a specific PCR amplicon was generated from uninduced or PMA-induced (400 ng, 24 h) THP-1 cells as well as human blood-derived primary monocytes (Figure 7). DNA sequencing was done with the support of Monika von der Heide (Department of Infection Biology, HKI) and subsequent sequence analysis confirmed ARMS2 amplification. Thus, ARMS2 gene transcription was confirmed in human THP-1 and blood-derived monocytes.

The retina contains at least three types of immune cells: microglia, perivascular macrophages and dendritic cells (DCs) [57]. Microglia have several important functions in immune surveillance and neuronal homeostasis, they are capable to communicate with other glial cells and neurons, which regulate their activation status and their capacity for phagocytosis of cellular debris [11]. We asked whether microglia, the resident immune cells of the brain and the retina, express the ARMS2 gene. Human microglia are unavailable as cells line so far, nor can they be extracted from tissue. Thus, we used induced human pluripotent stem cell derived microglia (iPSdM), which were kindly provided by Prof. Dr. Harald Neumann (Institute of Reconstructive Neurobiology, University of Bonn, Bonn, Germany). Using the same specific primers as before, ARMS2 was also amplified from cDNA isolated from both unstimulated and LPS-stimulated (5 ng/ml, 24 h) iPSdM. In contrast, macrophages of murine origin lacked any ARMS2 signal (Figure 7).

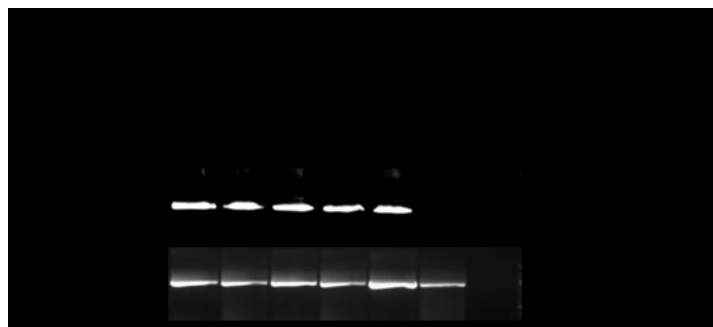


Figure 7. Analysis of *ARMS2* gene expression in various monocytes.

ARMS2 is expressed in human monocytes and microglia, but not in RAW 264.7 cells. RNA was extracted from uninduced or PMA-induced THP-1 monocytes, unstimulated or LPS-stimulated iPSdM, blood-derived human monocytes and murine macrophages RAW 264.7 cells, transferred into cDNA and analysis of *ARMS2* transcripts were investigated by PCR using specific primers and agarose gel electrophoresis (RNA isolation and PCR were done with the support of Monika von der Heide from Department of Infection Biology).

3.1.2 *ARMS2* protein is expressed in human monocytes and iPS-derived microglia

To verify *ARMS2* protein presence in human cells, laser scanning microscopy (LSM) was performed using α -*ARMS2*_{Jena} antiserum. After fixation and permeabilization, uninduced or PMA-induced THP-1 monocytes and unstimulated or LPS-stimulated iPSdM were stained for *ARMS2* and assayed by LSM (Figure 8A). *ARMS2* was observed in these cells but not in RAW264.7 (Figure 8A). In addition, primary monocytes were isolated from fresh blood and *ARMS2* protein was detected in a similar experiment. *ARMS2* signals were also captured in the cytoplasm of blood monocytes (Figure 8B). Taken together, *ARMS2* is transcribed and expressed in human monocytes and iPSdM.

3.1.3 *ARMS2* expression is enhanced under oxidative stress

Oxidative stress is linked to many chronic inflammatory diseases, especially AMD [102]. As the *ARMS2* signal in monocytes was very weak, we asked whether *ARMS2* expression is regulated under oxidative stress. Therefore, human blood monocytes were isolated from fresh blood and 1×10^6 cells were exposed to H_2O_2 (0.1-1 mM) in serum-free medium for 1 h. After careful washing with medium, monocytes were incubated in complete medium overnight. Then cells were lysed in RIPA buffer and the lysates were investigated for *ARMS2* expression by western blot analysis using α -*ARMS2*_{Jena} antiserum. Endogenous *ARMS2* was detected as about 13 and 26 kDa protein bands, indicating a monomeric and homo-dimeric form of *ARMS2* (Figure 9). Interestingly, *ARMS2* expression was detected upon weak oxidative stress but not in untreated cells. The *ARMS2* signals increased with higher concentrations of H_2O_2 (Figure 9, lane 5).

A

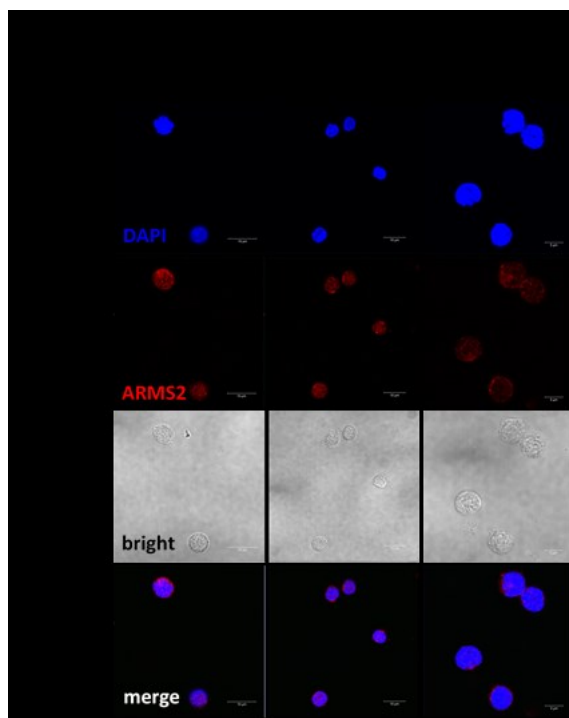
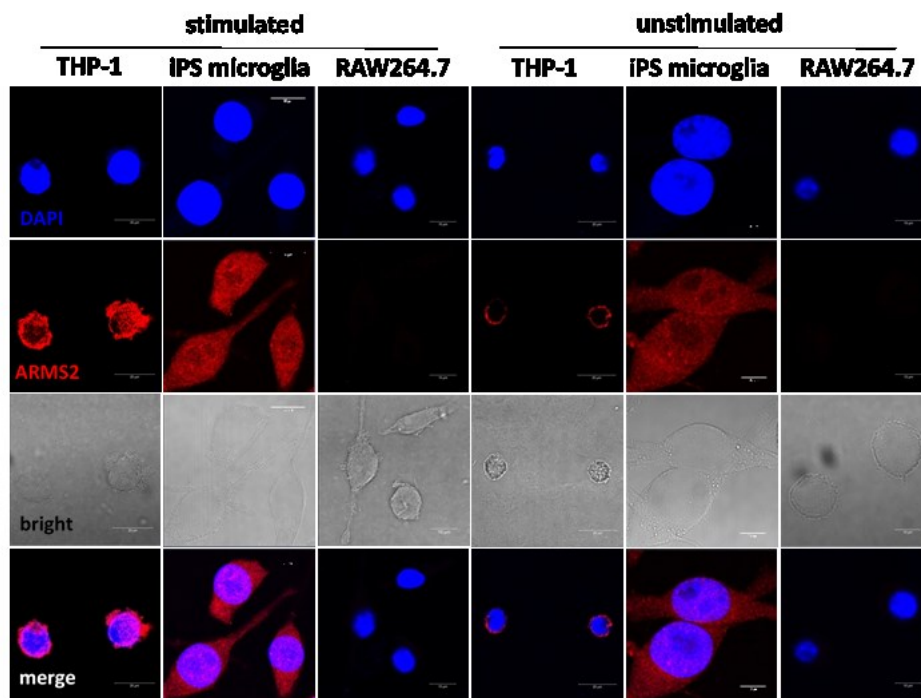


Figure 8. ARMS2 protein expression in human monocytes and microglia.

(A) ARMS2 is expressed in both uninduced or PMA-induced THP-1 monocytes, and unstimulated or LPS-stimulated iPSdM, but not in RAW264.7 cells. Cells were permeabilized, stained and visualized by LSM using α -ARMS2_{Jena} antiserum (red). (B) ARMS2 is present in blood-derived human monocytes. Cells were isolated from fresh blood of three different donors and stained using α -ARMS2_{Jena} antiserum (red). DAPI was used to stain the nuclei (blue). (Scale bar, 10 μ m).

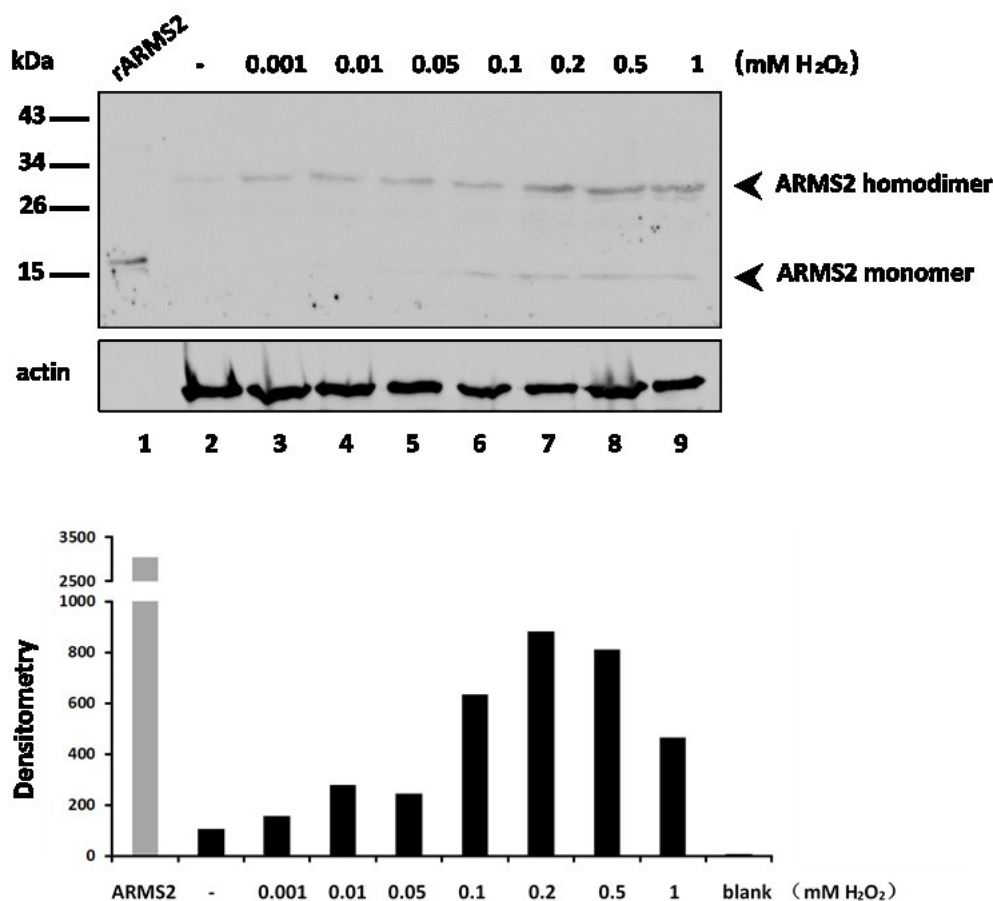


Figure 9. Blood – derived monocytes express ARMS2 upon oxidative stress.

The ARMS2 signals appeared in two protein bands of about 13 and 26 kDa upon cell treatment with H₂O₂. Monocytes were isolated from fresh blood and incubated with H₂O₂ (0.001-1 mM) in serum-free medium for 1 h. Cells were incubated for another 20 h in normal medium, then lysed in lysis buffer and detected by western blot analysis using α -ARMS2_{Jena} antiserum. Purified recombinant ARMS2 was separated in lane 1 for comparison. Densitometric analysis of 13 kDa bands is shown in the graph below.

3.1.4 Identification of endogenous ARMS2 in human THP-1 monocytes

Having shown that ARMS2 was expressed in human monocytes, we next aimed to confirm endogenous ARMS2 protein expression by immunoprecipitation combined with mass spectrometry. A monoclonal antibody α -ARMS2_{mAB} was generated in collaboration with Dr. Diana Pauly (Department of Ophthalmology, University Hospital Regensburg, Regensburg, Germany). The monoclonal α -ARMS2_{mAB} antibody detected endogenous ARMS2 with higher intensity than the polyclonal α -ARMS2_{Jena} antiserum as seen by parallel staining of THP-1 cells with the antibodies and detection by microscopy (Figure 10A). To pull down ARMS2 from THP-1 monocytes, α -ARMS2_{mAB} was bound to protein G magnetic beads. 1×10^7 THP-1 cells were lysed by RIPA lysis buffer containing 10 mM PMSF and subsequently centrifuged. The antibody-coupled beads were incubated in the cell lysate overnight at 4 °C, washed and antibody bound proteins were eluted from the beads. After separation via

SDS-PAGE and staining with coomassie blue, single bands were excised from the gel (indicated by black bars in Figure 10B-10D) according to the size of recombinant ARMS2 bands. The peptides were extracted from the gel pieces and analyzed using MALDI TOF-mass spectrometry. Five independent experiments were performed and the defined peptides were summarized in Table 2. The analysis revealed that endogenous ARMS2 peptides were precipitated from the cell lysate of THP-1 cells.

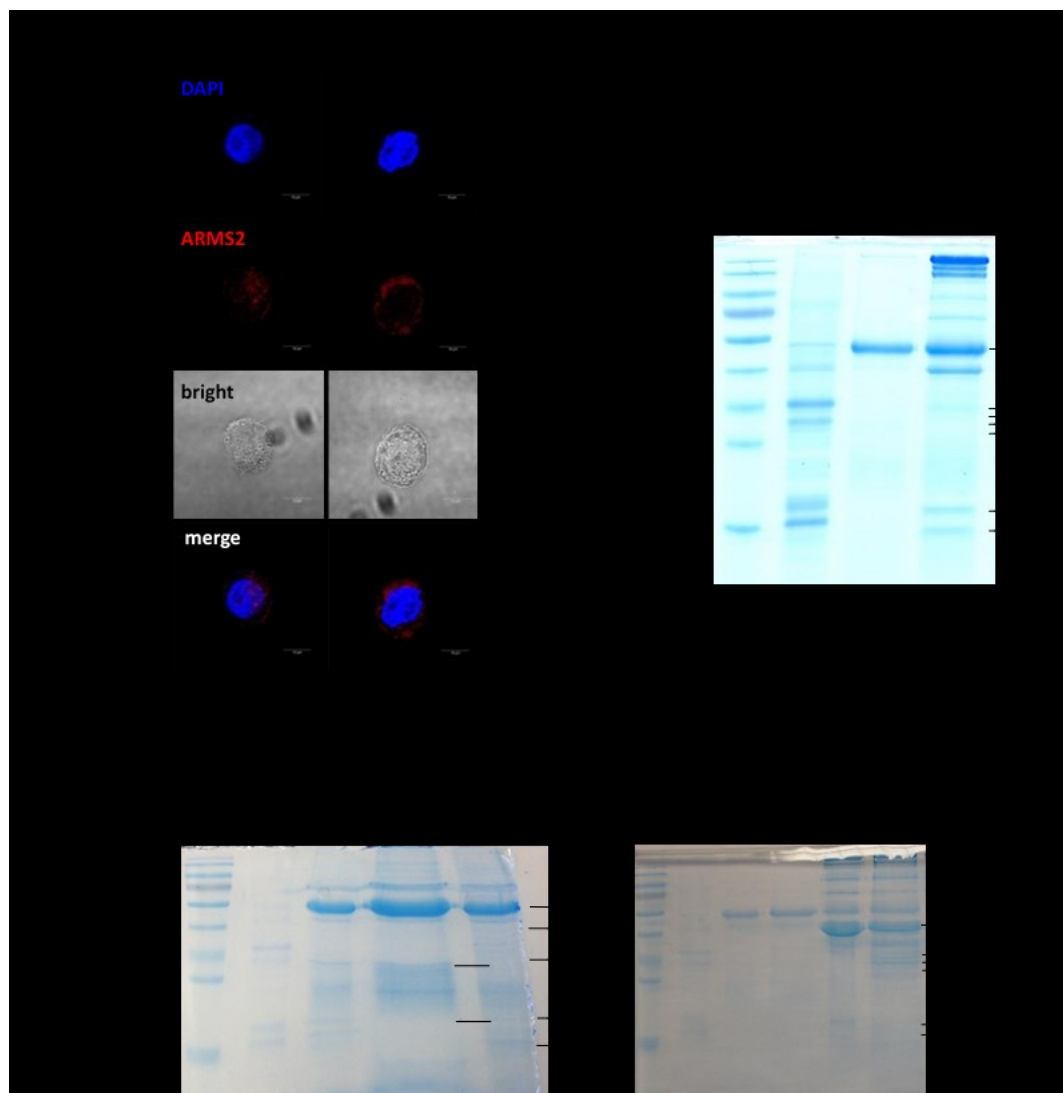


Figure 10. Identification of endogenous ARMS2 in THP-1 monocytes.

(A) The monoclonal α -ARMS2_{mAB} antibody detected endogenous ARMS2 with higher intensity than the α -ARMS2_{Jena} antiserum. THP-1 monocytes were permeabilized and stained with either α -ARMS2_{mAB} or α -ARMS2_{Jena} of ARMS2 (red). DAPI stained the nuclei (blue). (Scale bar, 10 μ m). (B) + (C) ARMS2 immunoprecipitation from THP-1 (1×10^7) cell lysate. α -ARMS2_{mAB} was immobilized to beads, and incubated with cell lysate. Eluted proteins were separated by SDS-PAGE, stained with coomassie blue and single bands (indicated by black bars) were excised and investigated by mass spectrometry. (D) ARMS2 immunoprecipitation from deglycosylated THP-1 cell lysate. 1×10^7 THP-1 cells were lysed and incubated with N-Glycosidase F (PNGase F, Roche) for 3 h at 37 °C before incubation with antibody-coupled beads. Eluted proteins were separated by SDS-PAGE, stained with

coomassie blue and single bands were excised and investigated by mass spectrometry.

Table 4

Identified endogenous ARMS2 peptides from five immunoprecipitations.

Range	Mono(expected)	m/z meas.	Mr calc.	Δ m/z [ppm]	Range	Sequence	Modifications
[1- 16]	1791	1791,793	1790,906	-66,842	[1- 16]	MLRLYPGPMVTEAEGK	
[1- 16]	1791	1791,825	1790,906	-49,355	[1- 16]	MLRLYPGPMVTEAEGK	
[4- 16]	1407	1407,798	1406,675	81,812	[4- 16]	LYPGPMVTEAEGK	Oxidation:6
[17- 38]	2220	2221,043	2220,146	-49,881	[17- 38]	GGPEMASLSSSVVPSFISTLR	
[39- 54]	1516	1516,751	1515,705	25,265	[39- 54]	ESVLDPGVGGEGASDK	
[57- 70]	1485	1485,677	1484,802	-88,987	[57- 70]	SKLSLSHSMIPAAK	Oxidation:9
[59- 70]	1254	1254,721	1253,68	26,776	[59- 70]	LSLSHSMIPAAK	
[59- 70]	1254	1254,74	1253,68	41,711	[59- 70]	LSLSHSMIPAAK	
[59- 70]	1254	1254,723	1253,68	28,592	[59- 70]	LSLSHSMIPAAK	
[59- 70]	1254	1254,738	1253,68	40,537	[59- 70]	LSLSHSMIPAAK	
[59- 70]	1270	1270,742	1269,675	47,341	[59- 70]	LSLSHSMIPAAK	Oxidation:7
[71- 88]	2044	2045,027	2044,02	20,079	[71- 88]	IHTELCLPAFFSPAGTQR	Carbamidomethyl:6
[71- 88]	2044	2045,054	2044,02	13,046	[71- 88]	IHTELCLPAFFSPAGTQR	Carbamidomethyl:6

3.2 AMD associated polymorphism rs10490924 in ARMS2

3.2.1 ARMS2 haplotype analysis in AMD patients

The ARMS2 risk variant is defined by the polymorphism rs10490924, which is linked to an indel mutation (del443ins54) in the 3' untranslated region of the ARMS2 gene. The polymorphism rs10490924 leads to an amino acid exchange at position 69, while the ARMS2 indel mutation is considered to lead to ARMS2 mRNA instability. In addition, the polymorphism rs2736911, which generates a stop codon at amino acid position 38, is associated with AMD in a Chinese group but not in the Caucasian population. The polymorphism rs10490924 in ARMS2 gene is highly associated with both forms of AMD leading to geographic atrophy or neo-vascularization. To find out whether rs10490924 in combination with the indel mutation leads to ARMS2 protein deficiency, 56 patients with neovascular AMD were screened for the ARMS2 polymorphisms in collaboration with Prof. Dr. Antonia Jousen (Charité-University hospital Berlin, Berlin). Blood samples were collected from the patients and genomic DNA was isolated. Two different PCR reactions were performed to determine the polymorphisms rs2736911, rs10490924 and del443ins54 in ARMS2 gene. According to the polymorphisms, different groups of genotypes were defined (homozygous without rs10490924 and del443ins54 (type I/I), heterozygous for rs10490924 and del443ins54 (type I/II), homozygous for rs10490924 and del443ins54 (type II/II), heterozygous for polymorphism rs2736911 (type I/III or II/III) and homozygous for rs2736911 (type III/III) (Figure 11A). 4 patients of the cohort did not carry the ARMS2 polymorphism rs2736911, rs10490924 or del443ins54 (7%), 24 patients were heterozygous for rs10490924

and del443ins54 (43%) and 12 patients were homozygous for rs10490924 and del443ins54 (21%). 15 patients (27%) were heterozygous for rs2736911 (I/III or II/III). Notably, no haplotypes of rs10490924 plus rs10490924 and del443ins54 were identified, and only 1 patient presented homozygous for rs2736911 (type III/III, 2%) (Figure 11B).

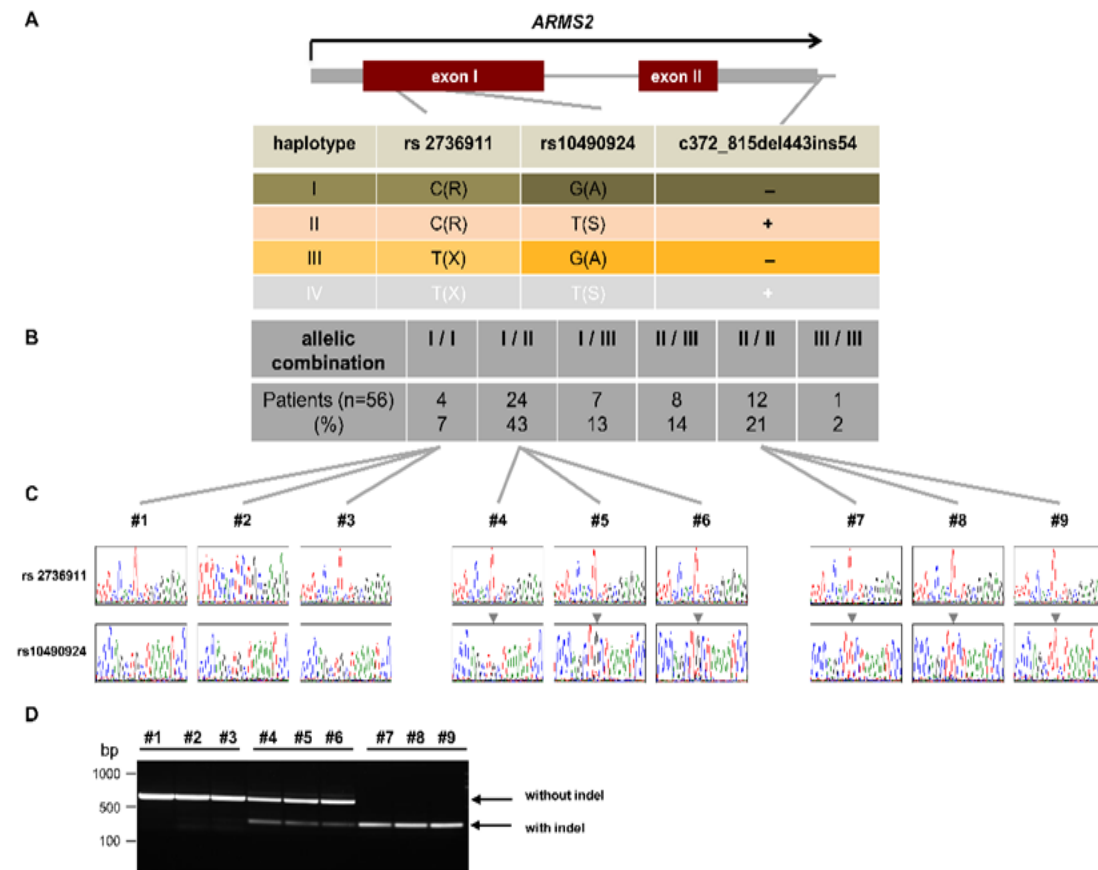


Figure 11. *ARMS2* genotypes in a cohort of 56 AMD patients.

The *ARMS2* polymorphisms rs2736911, rs10490924 and indel in a cohort of 56 patients with neovascular AMD. (A) + (B) In this cohort, 4 AMD patients did not carry the risk variants (I/I), 24 patients were heterozygous for rs10490924 and indel (I/II) and 12 patients were homozygous for rs10490924 and indel (II/II). 15 patients were heterozygous for rs2736911 and only one patient was homozygous for rs2736911. (C) Sequencing reports of the different variants from patients 1 to 9. (D) Transcription of *ARMS2* is indicated. cDNA was generated from isolated DNA of blood cells of AMD patients and *ARMS2* was amplified. *ARMS2* sequence was confirmed by sequencing. (RNA isolation, PCR and sequencing were done with the support of Monika von der Heide from Department of Infection Biology).

3.2.2 Monocytes derived from AMD patients with the *ARMS2* risk haplotype lack the *ARMS2* protein

The risk variant (polymorphism rs10490924 with indel) was described to result in *ARMS2* deficiency in human placenta [104]. Having determined the *ARMS2* genotype in 56 AMD

patients, the ARMS2 expression level in monocytes of selected patients was determined. Therefore, monocytes from patients carrying specific *ARMS2* haplotypes were isolated and stained with α -ARMS2_{Jena} antiserum to look for the presence of ARMS2 by microscopy. Genotypes were compared as follows: type I/I harbors two non-risk alleles of *ARMS2*, type I/II has one *ARMS2* risk allele (rs10490924 with del443ins54) and one non-risk allele, and type III has two alleles of the *ARMS2* risk variants (rs10490924 with del443ins54). The ARMS2 protein was identified in the cytoplasm of monocytes containing one or two alleles of the *ARMS2* non-risk variant (i.e., type I/I or I/II). In contrast, monocytes derived from the patients with two risk alleles (II/II) showed no ARMS2 protein staining. Also, monocytes derived from a single patient who is homozygous with an *ARMS2* stop mutation (rs2736911, genotype III/III) lacked the ARMS2 signal (Figure 12). These findings demonstrate an ARMS2 deficiency in homozygous carriers of the risk haplotype.

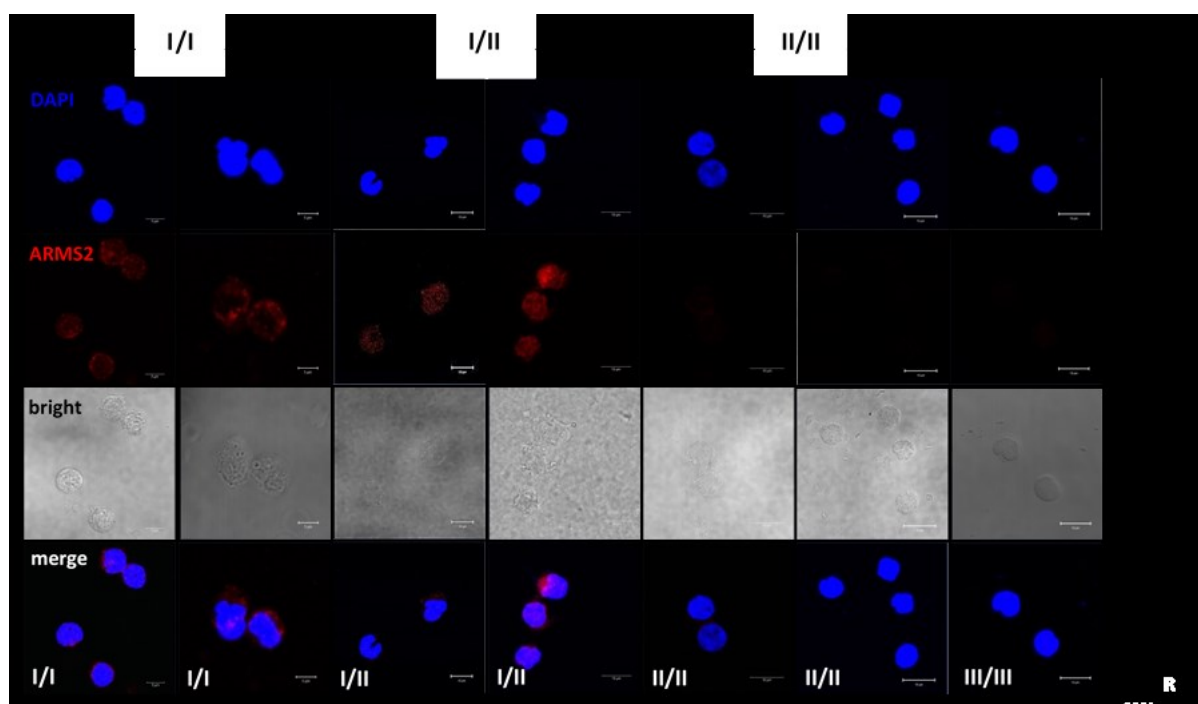


Figure 12. Detection of ARMS2 protein in monocytes from AMD patients.

ARMS2 is present in monocytes with one or two copies of the non-risk *ARMS2* variant (red), but is absent in cells with the homozygous rs10490924 (II/II) or rs2736991 (III/III) risk alleles. Monocytes were isolated from blood monocytes derived from wet AMD patients. Fluorescence staining of ARMS2 in monocytes was performed using α -ARMS2_{Jena} antiserum. DAPI was used to stain the nuclei (blue). (Scale bar, 10 μ m).

3.3 Characterization of ARMS2

3.3.1 Expression and purification of recombinant ARMS2

In order to investigate the biological functions of ARMS2, the protein was recombinantly expressed as a histidine-tagged protein using *P. pastoris* expression system. The expression

vector *pPICZ α B* contained codon usage optimized full length cDNA of the *ARMS2* gene coupled to a myc and 6 x histidine coding tag for purification as described [119]. Moreover, an Asp-Asp-Asp-Asp-Lys protease cleavage sequence was inserted to cut off the tag (Figure 13). Recombinant protein expression levels were analyzed by western blot using anti-penta histidine antibody at different time points (Figure 14A). As the protein was not detected in the supernatant of yeast cells, cell pellets were collected and lysed in binding buffer after 3 days. Purification of the protein was performed using nickel chelate chromatography. Recombinant *ARMS2* protein was bound to a nickel column overnight at 4 °C, after washing, protein was eluted. Detection of the *ARMS2* protein in the elute fractions (fraction E2 and E3) by western blot (Figure 14B) confirmed efficient protein purification.



Figure 13. Codon optimized *ARMS2* cDNA was cloned into the *pPICZ α B* expression vector.

Map and features of *pPICZ α B* expression vector. *ARMS2* gene was cloned into the *pPICZ α B* expression vector and expressed in the *P. pastoris* expression system. The optimized *ARMS2* cDNA contained a protease cleavage site (grey), a myc tag (blue) and 6 x histidine tag (green) for purification.

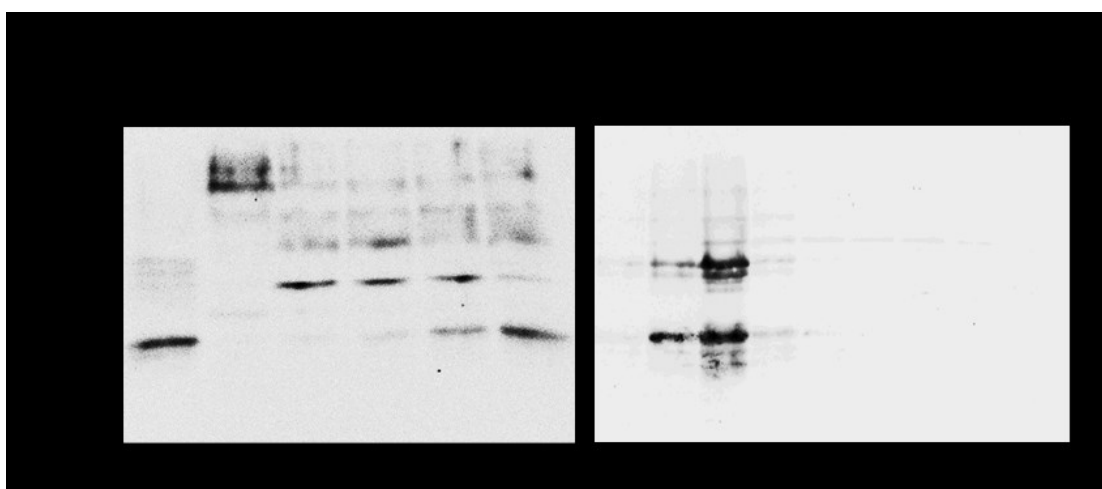
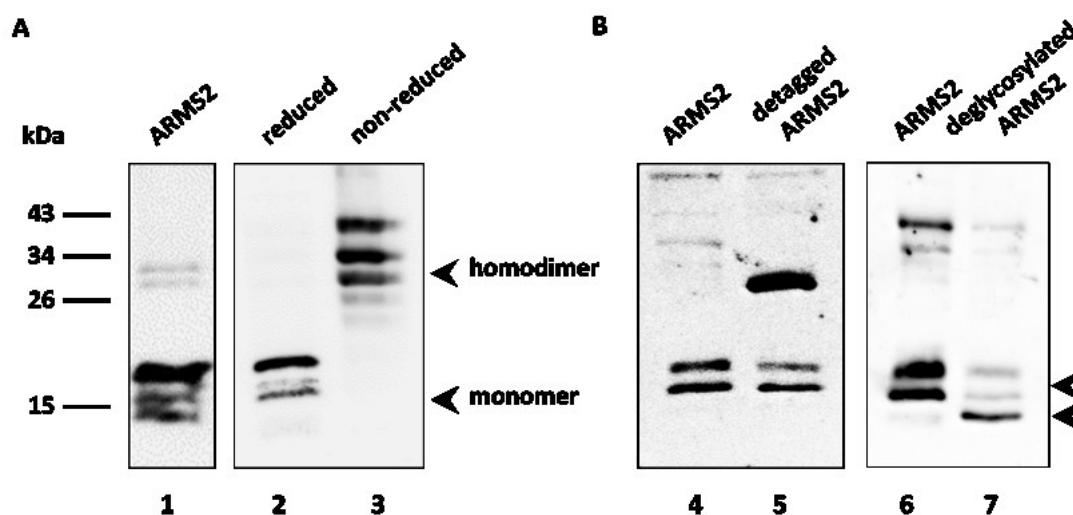


Figure 14. Recombinant ARMS2 expression and purification.

(A) Analysis of recombinant ARMS2 expression in *P. pastoris* over time by western blot analysis. ARMS2 expression showed highest level (lane 6) after 3 days. After 3 days of expression in *P. pastoris*, cell pellets were collected and lysed in binding buffer for protein purification. (B) After purification, the protein is detected in the elutes (lanes 2, 3 and 4) but not in wash fractions (lane 9). Recombinant ARMS2 protein was coupled to the HisTrap HP column. Several elute and wash fractions were obtained, separated by SDS-PAGE and analyzed by western blotting using anti-penta histidine antibody.

3.3.2 ARMS2 forms homodimers

Interestingly, separated ARMS2 by SDS-PAGE under non-reducing conditions appeared as a 34 kDa band, but 17 and 34 kDa under reducing conditions when detected with either anti-penta histidine antibody or α -ARMS2_{Jena} (Figure 15A). This result suggested that ARMS2 forms homodimers. To characterize the protein bands in more detail, recombinant ARMS2 was again separated by SDS-PAGE and stained with coomassie blue. Protein bands were excised from the gel, digested with trypsin into peptides and analyzed by mass spectrometry (MS). The MS revealed that all peptides derived from the 17 and 34 kDa bands covered regions of ARMS2 (more than 90%) (Figure 16, Table 3). These results confirmed that ARMS2 was present in both the 17 and 34 kDa bands and thus likely forms homodimers. Next, we tested whether the multiple bands reflected differently glycosylated bands of ARMS2. To this end, the recombinant protein was incubated with PNGase F for 3 h at 37 °C. After digestion, ARMS2 was identified as 15 and 30 kDa bands (Figure 15B) and ARMS2 was confirmed by mass spectrometry (Table 4). Also after the treatment of ARMS2 with Enterokinase to cleave off the histidine tag from ARMS2, the protein appeared as 17 and 30 kDa bands (Figure 14B). Taken together, recombinant ARMS2 was found to form homodimers and becomes glycosylated in *P. pastoris*.

**Figure 15. Recombinant ARMS2 forms homodimers and is glycosylated.**

(A) Under reducing conditions, ARMS2 showed mobilities of 17 and 34 kDa (lane 1 and 2). While

ARMS2 appeared as 34 kDa when separated using non-reducing conditions (lane 3), likely representing an ARMS2 homodimer. ARMS2 was separated under reducing or non-reducing conditions by SDS-PAGE and detected by western blot using α -ARMS2_{Jena}. (B) Recombinant histidine-tagged ARMS2 was incubated with enzymes to remove glycosylation (lane 5) or the complete histidine tag (lane 7) from the protein and treated proteins were separated by SDS-PAGE and detected by western blot using α -ARMS2_{Jena} (black arrows to the left indicate the homodimer and monomer of ARMS2).

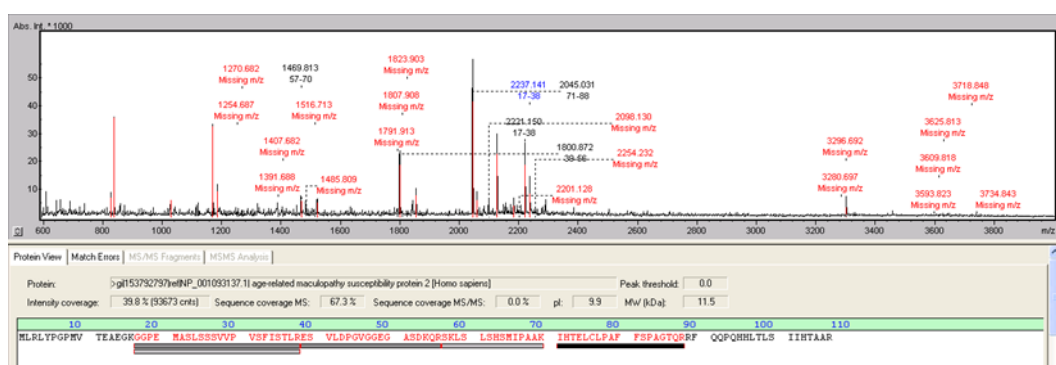


Figure 16. MS analysis of ARMS2 peptides from purified protein.

MALDI-TOF mass spectra of peptides from recombinant ARMS2. Purified ARMS2 was separated using SDS-PAGE and stained with coomassie blue. The protein was in-gel digested by trypsin and extracted from the gel. All generated peptides from 2 bands were analyzed by mass spectrometry.

3.3.3 ARMS2 - properdin interactions

We showed that ARMS2 binds to the only one complement activator properdin [119]. To confirm ARMS2-properdin interaction, ARMS2 (5 μ g/ml) was immobilized on a microtiter plate overnight at 4 °C and increasing amounts of properdin were added for 1 h. After washing, bound properdin was identified using goat anti-properdin (1:1000). Properdin bound to ARMS2 and this binding was dose-dependent (Figure 17A). To further confirm and characterize the specificity of the ARMS2-properdin interaction, the interaction affinity was investigated by biolayer interferometry using the Blitz system. Biotinylated properdin (20 μ g/ml) was immobilized on the biosensors and the real-time binding of various dilutions of ARMS2 were determined. In this set up, the equilibrium dissociation constant of ARMS2 bound to immobilized properdin is $K_D = 0.5 \pm 0.07 \times 10^{-6}$ M. Dissociation kinetics are shown in Figure 17B.

Oxidants can damage DNA and lipids [97]. As ARMS2 is upregulated in monocytes upon oxidative stress, we asked if ARMS2 plays a role in protecting cells against oxidative stress. Therefore, the interaction between ARMS2 and human DNA or LDL (low density lipoprotein) was tested. DNA and LDL (5 μ g/ml) were immobilized onto the surface of a microtiter plate overnight at 4 °C and ARMS2 (200 nM) was added. Bound ARMS2 protein was detected by ELISA using α -ARMS2_{Jena}. ARMS2 did not bind to DNA or LDL (Figure 17C, 17D).

Table 5

Identified ARMS2 peptides from purified protein bands.

Peptides from 17 kDa band (sequence coverage 97.2%)							
Range	Mono(expected)	m/z meas.	Mr calc.	Δ m/z [ppm]	Range	Sequence	Modifications
[4- 16]	1391	1391.7241	1390.6803	26.29	4 - 16	R.LYPGPMVTEAEGK.G	
[4- 16]	1407	1407.7246	1406.6752	29.96	4 - 16	R.LYPGPMVTEAEGK.G	Oxidation: 6;
[17- 38]	2220	2221.1964	2220.1460	19.40	17 - 38	K.GGPEMASLSSSVVPVSFISTLR.E	
[17- 38]	2236	2237.1994	2236.1409	22.90	17 - 38	K.GGPEMASLSSSVVPVSFISTLR.E	Oxidation: 5;
[39- 54]	1516	1516.7705	1515.7053	38.19	39 - 54	R.ESVLDPGVGGEGASDK.Q	
[39- 56]	1800	1800.9115	1799.8650	21.80	39 - 56	R.ESVLDPGVGGEGASDKQR.S	
[57- 70]	1469	1469.8525	1468.8072	25.90	57 - 70	R.SKLSLSHMIPAAK.I	
[59- 70]	1254	1254.7235	1253.6802	28.75	59 - 70	K.LSLSHMIPAAK.I	
[71- 88]	2044	2045.0599	2044.0200	15.94	71 - 88	K.IHTELCLPAFFSPAGTQR.R	Carbamidomethyl: 6;
[89-107]	2253	2254.2580	2253.2243	11.72	89 - 107	R.RFQQPQHHLTLSIIHTAAR.-	
[90-107]	2097	2098.1694	2097.1232	18.56	90 - 107	R.FQQPQHHLTLSIIHTAAR.-	

Peptides from 34 kDa band (sequence coverage 92.5%)							
Range	Mono(expected)	m/z meas.	Mr calc.	Δ m/z [ppm]	Range	Sequence	Modifications
[1- 16]	1791	1676.8768	1675.8603	5.45	2 - 16	M.LRLYPGPMVTEAEGK.G	Oxidation: 8;
[4- 16]	1391	1391.6848	1390.6803	-1.96	4 - 16	R.LYPGPMVTEAEGK.G	
[17- 38]	2220	2221.1150	2220.1460	-17.24	17 - 38	K.GGPEMASLSSSVVPVSFISTLR.E	
[17- 38]	2236	2237.1124	2236.1409	-16.02	17 - 38	K.GGPEMASLSSSVVPVSFISTLR.E	Oxidation: 5;
[39- 54]	1516	1516.7141	1515.7053	1.02	39 - 54	R.ESVLDPGVGGEGASDK.Q	
[39- 56]	1800	1800.8477	1799.8650	-13.64	39 - 56	R.ESVLDPGVGGEGASDKQR.S	
[59- 70]	1254	1254.6790	1253.6802	-6.77	59 - 70	K.LSLSHMIPAAK.I	
[59- 70]	1270	1270.6721	1269.6751	-8.13	59 - 70	K.LSLSHMIPAAK.I	Oxidation: 7;
[71- 88]	2044	2044.9963	2044.0200	-15.15	71 - 88	K.IHTELCLPAFFSPAGTQR.R	Carbamidomethyl: 6;
[90-107]	2097	2098.0979	2097.1232	-15.52	90 - 107	R.FQQPQHHLTLSIIHTAAR.-	

Table 6

Identified ARMS2 peptides from deglycosylated ARMS2 protein bands.

Peptides from 15 kDa band (sequence coverage 96.3%)							
Range	Mono(expected)	m/z meas.	Mr calc.	Δ m/z [ppm]	Range	Sequence	Modifications
[2- 16]	1676	1676.8768	1675.8603	5.45	2 - 16	M.LRYPGPMVTEAEGK.G	Oxidation: 8;
[4- 16]	1391	1391.6848	1390.6803	-1.96	4 - 16	R.LYPGPMVTEAEGK.G	
[17- 38]	2220	2221.1150	2220.1460	-17.24	17 - 38	K.GGPEMASLSSSVVPVSFISTLR.E	
[17- 38]	2236	2237.1124	2236.1409	-16.02	17 - 38	K.GGPEMASLSSSVVPVSFISTLR.E	Oxidation: 5;
[39- 54]	1516	1516.7141	1515.7053	1.02	39 - 54	R.ESVLDPGVGGEGASDK.Q	
[39- 56]	1800	1800.8477	1799.8650	-13.64	39 - 56	R.ESVLDPGVGGEGASDKQR.S	
[57- 70]	1485	1485.8093	1484.8021	-0.03	57 - 70	R.SKLSLSHSMIPAAK.I	Oxidation: 9;
[59- 70]	1254	1254.5985	1253.6802	-70.91	59 - 70	K.LSLSHSMIPAAK.I	
[59- 70]	1254	1254.6790	1253.6802	-6.77	59 - 70	K.LSLSHSMIPAAK.I	
[59- 70]	1270	1270.6721	1269.6751	-8.13	59 - 70	K.LSLSHSMIPAAK.I	Oxidation: 7;
[71- 88]	2044	2044.9963	2044.0200	-15.16	71 - 88	K.IHTELCLPAFFSPAGTQR.R	Carbamidomethyl: 6;
[71- 88]	2044	2044.9933	2044.0200	-16.63	71 - 88	K.IHTELCLPAFFSPAGTQR.R	Carbamidomethyl: 6;
[90-107]	2097	2098.0979	2097.1232	-15.52	90 - 107	R.FQQPQHHLTSLIIHTAAR.-	
[90-107]	2097	2098.0980	2097.1232	-15.48	90 - 107	R.FQQPQHHLTSLIIHTAAR.-	
[90-107]	2097	2098.1049	2097.1232	-12.17	90 - 107	R.FQQPQHHLTSLIIHTAAR.-	
[90-107]	2097	2098.1050	2097.1232	-12.14	90 - 107	R.FQQPQHHLTSLIIHTAAR.-	

Peptides from 30 kDa band (sequence coverage 97.2%)							
Range	Mono(expected)	m/z meas.	Mr calc.	Δ m/z [ppm]	Range	Sequence	Modifications
[4- 16]	1391	1391.7241	1390.6803	26.29	4 - 16	R.LYPGPMVTEAEGK.G	
[4- 16]	1407	1407.7246	1406.6752	29.96	4 - 16	R.LYPGPMVTEAEGK.G	Oxidation: 6;
[17- 38]	2220	2221.1964	2220.1460	19.40	17 - 38	K.GGPEMASLSSSVVPVSFISTLR.E	
[17- 38]	2220	2221.1963	2220.1460	19.36	17 - 38	K.GGPEMASLSSSVVPVSFISTLR.E	
[17- 38]	2236	2237.1994	2236.1409	22.90	17 - 38	K.GGPEMASLSSSVVPVSFISTLR.E	Oxidation: 5;
[39- 54]	1516	1516.7705	1515.7053	38.19	39 - 54	R.ESVLDPGVGGEGASDK.Q	
[39- 56]	1800	1800.9115	1799.8650	21.80	39 - 56	R.ESVLDPGVGGEGASDKQR.S	
[57- 70]	1469	1469.8525	1468.8072	25.90	57 - 70	R.SKLSLSHSMIPAAK.I	
[59- 70]	1254	1254.7235	1253.6802	28.75	59 - 70	K.LSLSHSMIPAAK.I	
[71- 88]	2044	2045.0599	2044.0200	15.93	71 - 88	K.IHTELCLPAFFSPAGTQR.R	Carbamidomethyl: 6;
[89-107]	2253	2254.2580	2253.2243	11.72	89 - 107	R.RFQQPQHHLTSLIIHTAAR.-	
[90-107]	2097	2098.1694	2097.1232	18.56	90 - 107	R.FQQPQHHLTSLIIHTAAR.-	

3.3.4 The ARMS2 C-terminus mediates interaction with properdin

Having shown the strong interaction between ARMS2 and properdin, the binding domain in ARMS2 which interacts with properdin was investigated in detail. Three ARMS2 peptides encompassing all amino acids of ARMS2 were synthesized. Peptide 3 but not peptide 1 or 2 of ARMS2 showed binding to properdin (Figure 18A). Since peptide 3 which represents the C-terminus of ARMS2 revealed binding to properdin, this peptide was analyzed in more detail. To this end, 24 peptides (each of 13 amino acids with 10 amino acids overlap) covering the ARMS2 C-terminus were spotted onto a cellulose membrane. These solid phase-bound peptides were used for binding studies directly on the membrane. The membrane was blocked in blocking buffer (1% BSA and 3% nonfat milk in TBS-T buffer) for 1 h, then incubated with Alexa Fluor 647-conjugated properdin (5 μ g) overnight at 4°C. Later on, after washing for three times, the fluorescent signals were captured with 635 laser lines by Fusion FX system (Figure 18B). The interaction domain for properdin was located to spots 8-10 which represented the amino acids 80-90 (FFSPAGTQRRF) of ARMS2. All other peptides showed little or no binding signal.

3.3.5 ARMS2 binds to human ARPE-19 cells and heparan sulfate

To further study the role of ARMS2, binding of ARMS2 to cell surfaces was determined *in vitro*. ARPE-19 cells were grown until a monolayer was formed and then detached by trypsin/EDTA. Recombinant ARMS2 (1 μ g) was incubated with the cells for 1 h on ice. After washing, bound proteins were detected by flow cytometry using α -ARMS2_{Jena} antiserum. ARMS2 bound to ARPE-19 cells (Figure 19A). To identify the cellular ARMS2 ligand, surface binding to exposed glycosaminoglycans (GAGs) was assayed and ARMS2 binding was analyzed to heparan coated beads. ARMS2 (1 μ g) was added to beads (1 million) and binding of ARMS2 was followed with α -ARMS2_{Jena} antiserum. ARMS2 specifically bound to heparan sulfate (Figure 19B), in contrast to a control protein with a histidine-tag.

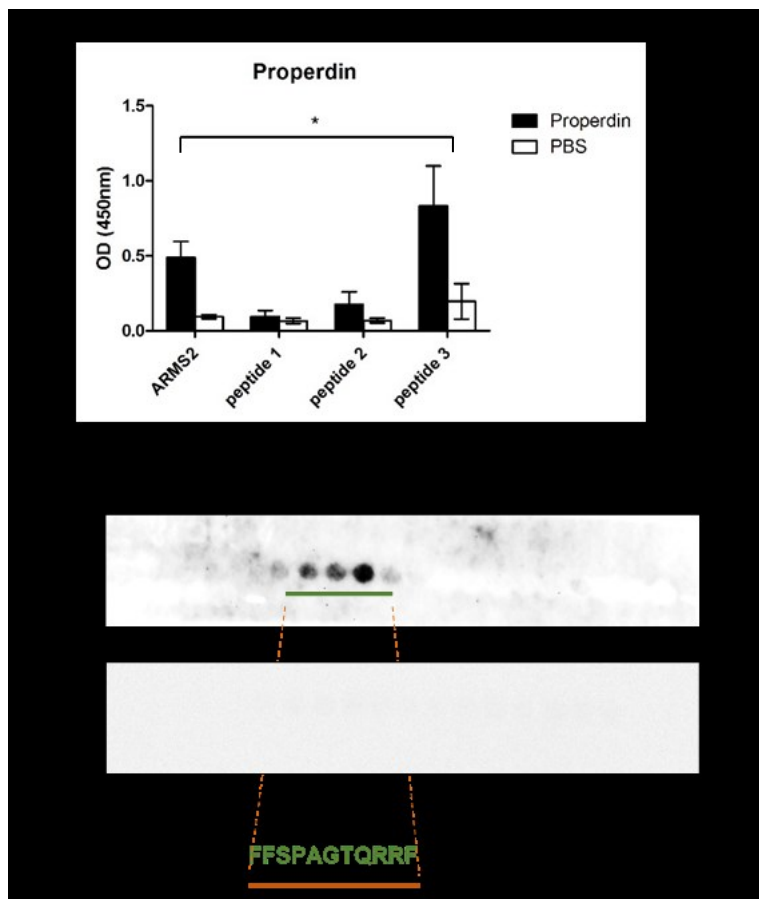


Figure 17. ARMS2 interacts with complement activator properdin but does not bind to LDL or DNA.

(A) ARMS2 binds to immobilized properdin. Error bars represent mean \pm SD of 3 independent experiments performed in triplicate. *, $p < 0.05$. (B) Dissociation constant of the interaction between ARMS2 and properdin is $K_D = 0.5 \pm 0.07 \times 10^{-6}$ M determined by biolayer interferometry. (C) + (D) ARMS2 does not interact with LDL or DNA. In contrast, FH binds to LDL, FHR4B and properdin bind to DNA. Error bars represent mean \pm SD of 3 independent experiments performed in triplicate.

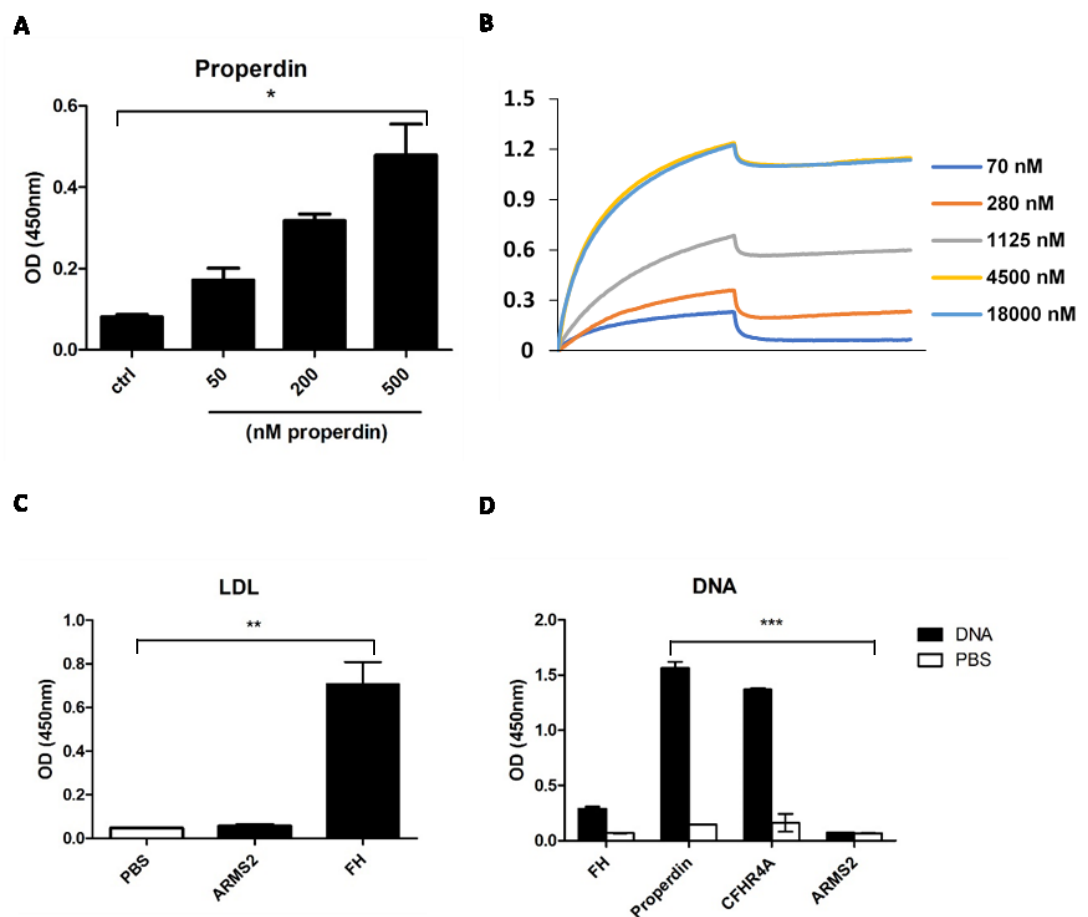


Figure 18. ARMS2 binding to properdin.

ARMS2 binds via its C-terminus to properdin. (A) ARMS2 peptide 3 (aa 71-107) but not peptide 1 (aa 1-40) or 2 (aa 41-70), binds to properdin. Properdin binding was evaluated to three peptides of ARMS2 immobilized on the ELISA plate. Bars represent mean \pm SD of 3 independent experiments performed in triplicate. *, $p < 0.05$ (B) Pepsot analysis of properdin binding to ARMS2. The interaction domain of ARMS2 to properdin is located to spots 8-10 representing ARMS2 aa 80-90. ARMS2 overlapping peptide were spotted to a membrane and incubated with properdin. The dark spots indicate properdin binding. The properdin binding region in the ARMS2 sequence is underlined. Upper blot: properdin binding. Lower blot: control development of the membrane with 488 laser lines.

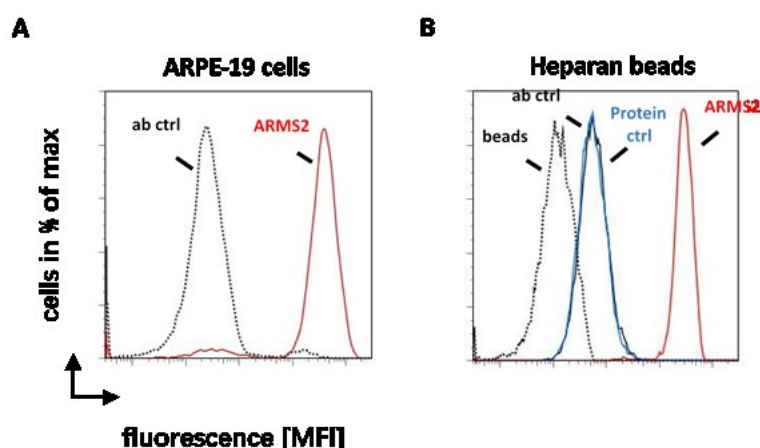


Figure 19. ARMS2 binds to heparan sulfate as well as human ARPE-19 cells.

(A) ARMS2 (red) binds to ARPE-19 cells. Background binding of the antibody to the cells is shown in grey. (B) ARMS2 (red) binds to heparan coated beads. Histidine-tagged FH fragment (blue) did not bind to the beads, confirming specificity of ARMS2 binding.

3.3.6 Cloning and transformation of ARMS2 variant A69S plasmid

The ARMS2 risk polymorphism rs10490924 (A69S) is linked to an indel mutation which leads to the instability of ARMS2 mRNA. However, it is still unclear whether the A69S polymorphism alone affects the ARMS2 protein functions. In order to investigate whether the amino acid exchange modulates the function of ARMS2, recombinant ARMS2 variant S69 protein was expressed. Initially, the cDNA with the polymorphism A69S was synthesized and inserted into expression vector *pPICZαB*. The plasmid was transformed and amplified in *E. coli DH5α* cells. Colonies were identified by plasmid isolation, restriction enzyme digestion and agarose electrophoresis. Each colony contained the inserted cDNA as determined by the presence of a ~470 bp fragment after digestion (Figure 20A) and sequenced by Monika von der Heide (Department of Infection Biology, HKI). A positive transformant was grown in LB medium overnight and the plasmid was subsequently isolated from the cells. The purified plasmid was linearized and transformed into competent *P. pastoris X33* cells by electroporation. Grown colonies were tested for ARMS2 S69 protein expression and the positive colony was utilized for further large-scale protein expression (lane 4, Figure 20B).

3.3.7 Expression and purification of recombinant ARMS2 variant A69S protein

Similar to the wild type ARMS2 A69 protein, the recombinant ARMS2 S69 protein was expressed as a histidine fusion protein in *P. pastoris*. Four ARMS2 S69 expression colonies were grown in culture medium, lysed and ARMS2 protein levels were detected by western blot analysis (Figure 20C). The ARMS2 S69 was present in all 4 colonies and detected as 17 kDa band. The ARMS2 protein was purified from the cells following the same procedure as described above for the wild type ARMS2 protein. The elution fraction E3 showed the ARMS2 S69 protein as 16 and 17 kDa protein bands (Figure 20D).

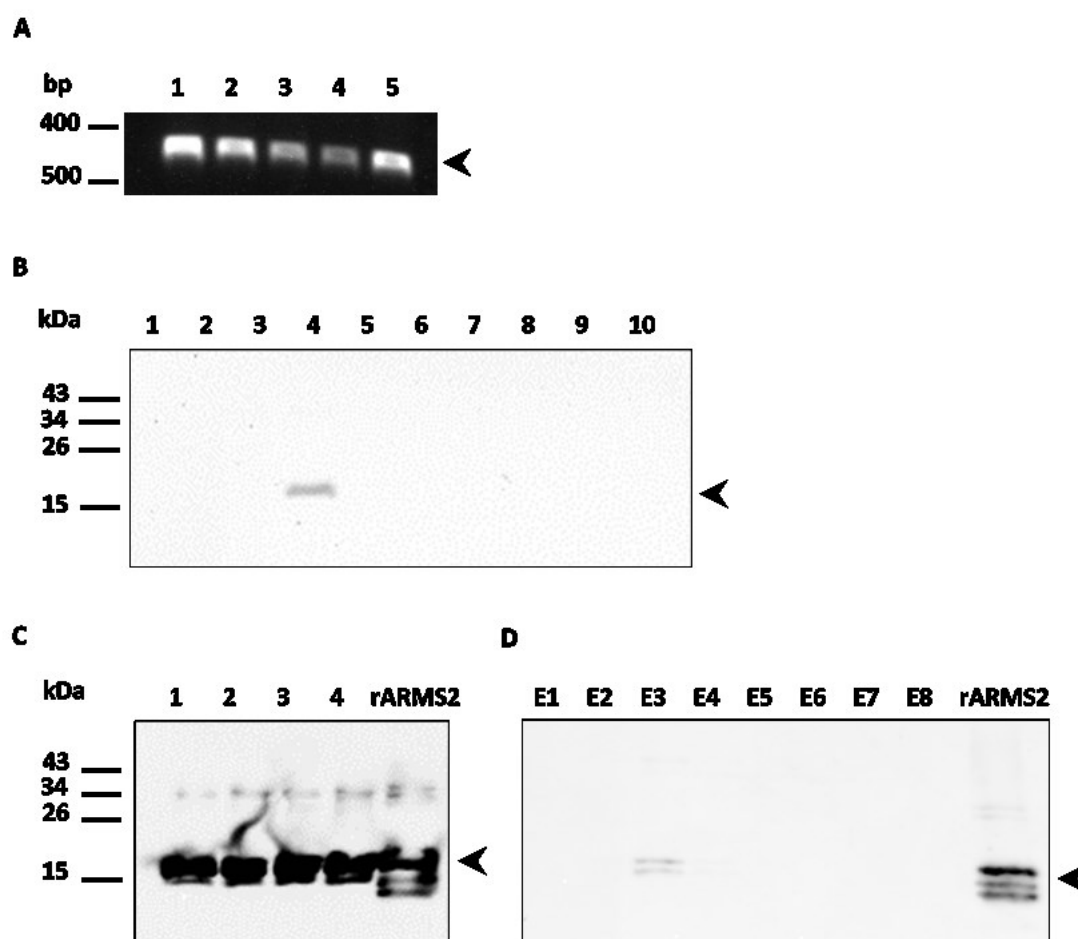


Figure 20. ARMS2 variant S69 expression and purification.

(A) Analysis of *ARMS2* variant A69S gene in *E. coli*. *ARMS2* variant A69S gene was cloned into *pPICZaB* vector and transformed into *E. coli* cells. Plasmids were isolated from five transformed colonies and *ARMS2* inserts were identified by agarose gel electrophoresis. (B) *ARMS2* protein is identified as 17 kDa protein band by western blot analysis. Grown colonies were evaluated for *ARMS2* S69 protein expression. (C) *ARMS2* S69 proteins expression in *P. pastoris*. Recombinant *ARMS2* S69 protein was expressed in *P. pastoris* for 3 days and the extracts of the cells were detected by western blot analysis with anti-penta histidine. (D) Purified *ARMS2* S69 protein and recombinant *ARMS2* wild type A69 protein show similar mobility in western blot analysis.

3.3.8 Comparison of ARMS2 and ARMS2 A69S proteins

To analyze potential functional changes of the ARMS2 A69S variant, we compared ARMS2 S69 with wild type ARMS2 A69 according their expression and function. Recombinant ARMS2 S69 showed similar mobilities as ARMS2 A69 of 17 and 34 kDa under reducing conditions in silver staining gel (Figure 21A), which indicated dimerization of also ARMS2 S69 protein. Next, we proceeded to evaluate the binding of the ARMS2 variant to properdin by ELISA and biolayer interferometry. Therefore, ARMS2 A69 and S69 (each 5 µg/ml) were coated on a microtiter plate and properdin (200 nM) was added. Bound protein was detected with anti-properdin (1:2000). ARMS2 S69 also showed an interaction with properdin and the real-time interaction affinity constant was $K_D=0.7 \times 10^{-7}$ M as measured by biolayer interferometry (Figure 21B, 21C). Moreover, ARMS2 S69 also bound to ARPE-19 cells and heparan coated beads (Figure 21D, 21E). Taken together, ARMS2 A69 and S69 showed similar expression profiles, dimerization, stability and binding activities.

3.4 Complement activation on ARPE-19 cells

3.4.1 Oxidative stress sensitizes cells to NHS

To determine cell death under increasing concentrations of oxidative stress or NHS, the cell viability was assayed by cell titer blue assay. By measuring visible light absorbance upon reduction of resazurin to resorufin, the metabolic activity of the cells was evaluated 24 h after treatment. ARPE-19 cell monolayers were treated with different concentrations of H₂O₂ (0.1-2mM) for 1 h. Subsequently, cells were washed in medium and incubated in serum-free medium or NHS (1% - 20%) before analysis. The absorptions at 570 nm and 605 nm were measured and the ratio change was set directly proportional to the number of living cells. The cell viability was significantly decreased in the presence of H₂O₂ ($p \leq 0.01$) (Figure 22A). The impact of NHS on ARPE-19 cells was determined by the same methods. Low dilution (less than 20%) of serum showed a high level of cell viability (more than 70%) suggesting mild toxicity to the cells. Heat inactivation of NHS (iNHS) significantly attenuated the injury induced by complement activity (Figure 22B). However, treatment of cells with H₂O₂ together with NHS significantly reduced cell viability (***, $p < 0.001$) (Figure 22C). Thus, exposure of oxidative stress and NHS to cells impairs cell survival.

3.4.2 Cell surface bound ARMS2 enhances complement activation

As complement is involved in the pathogenesis of AMD, and properdin is the only known complement activator, we consequently asked if ARMS2 plays a role in complement activation. ARMS2 (5 µg/ml) was attached to ARPE-19 cells, incubated in NHS (20%) for 30 min at 37 °C and surface C3b was stained using rabbit anti-C3d (1:400) by flow cytometry. ARMS2 enhanced C3b opsonization of ARPE-19 cells (Figure 23B), confirming complement activation via ARMS2 on the cell surface.

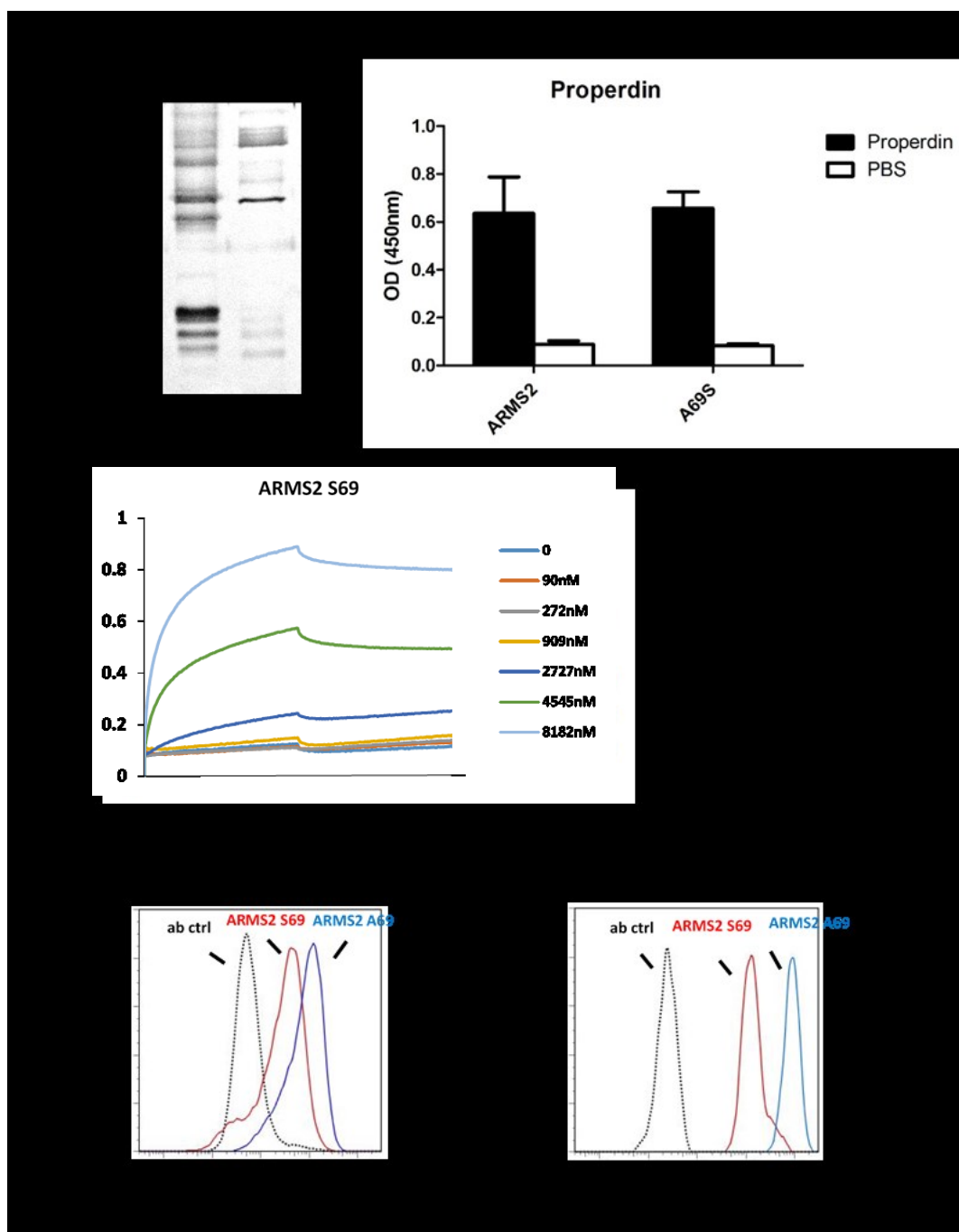


Figure 21. Comparison of ARMS2 A69 and S69 variants.

(A) ARMS2 S69 has a similar mobility like wild type ARMS2 A69 as determined by silver staining. (B) ARMS2 S69 and A69 showed similar binding to properdin. ARMS2 S69 and A69 were immobilized onto the surface of a microtiter plate and purified human properdin (200 nM) was added. Bars represent mean \pm SD of 3 independent experiments performed in triplicate. (C) The interaction affinity constant of ARMS2 S69 to properdin was 0.7×10^{-7} M as measured by biolayer interferometry. (D) + (E) Both ARMS2 S69 and A69 bound to ARPE-19 cells and heparan beads. ARMS2 S69 and A69 (each of 1 μ g) were incubated with ARPE-19 cells or heparan beads, and bound ARMS2 proteins were detected by flow cytometry using α -ARMS2_{Jena} antiserum. The experiments in D and E were performed under identical conditions for side-by-side comparison.

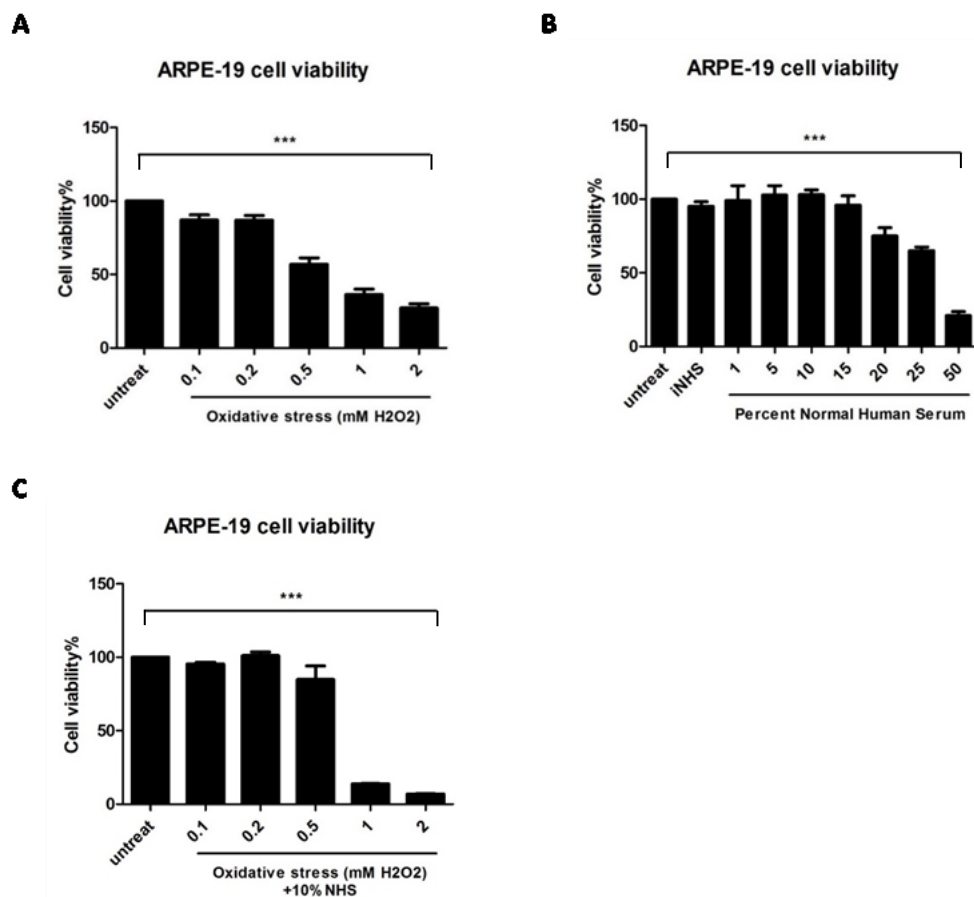


Figure 22. Cell viability assay.

(A) Cell viability was substantially decreased upon exposure to H₂O₂ (0.5 – 2mM). ARPE-19 cells were treated with varying doses of H₂O₂ for 1 h and incubated in serum-free medium for 24h. Cell viability was measured to quantify cell death. (B) In 50 % NHS, cell viability also decreased, suggesting mild toxicity of low levels of NHS (less than 20 %) to cells. (C) Treatment of cells with H₂O₂ together with NHS significantly reduced cell viability. Bars represent mean \pm SD of 3 independent experiments performed in triplicate. Stars indicate significance to control (***, $p < 0.001$).

3.4.3 Oxidative stress promotes complement activation which is controlled by FH

Next, we asked whether oxidative stress affects the ability of ARPE-19 cells to regulate complement activation after exposure to NHS as source of complement. C3b deposition was followed by flow cytometry. Exposure of the cells to NHS (20%) for 1 h caused C3b deposition on the cell surfaces and C3b deposition increased when cells were treated with H₂O₂ (1 mM) prior to exposure to NHS (20%) (Figure 23A).

FH is one of the most abundant plasma proteins and a major regulator of complement activation. An important regulatory activity of FH is its decay acceleration activity of the C3 convertase, thereby promoting the dissociation of factor Bb from C3b. We asked whether FH regulates complement on oxidatively stressed cell surfaces. Stressed cells with H₂O₂ (1 mM)

were incubated with FH (20 $\mu\text{g}/\text{ml}$) followed by exposure to NHS (20%) and C3b deposition was measured by flow cytometry. Addition of FH to NHS reduced surface C3b levels after oxidative stress (Figure 24B). In contrast, FH did not modulate complement activation on untreated cells (Figure 24A).

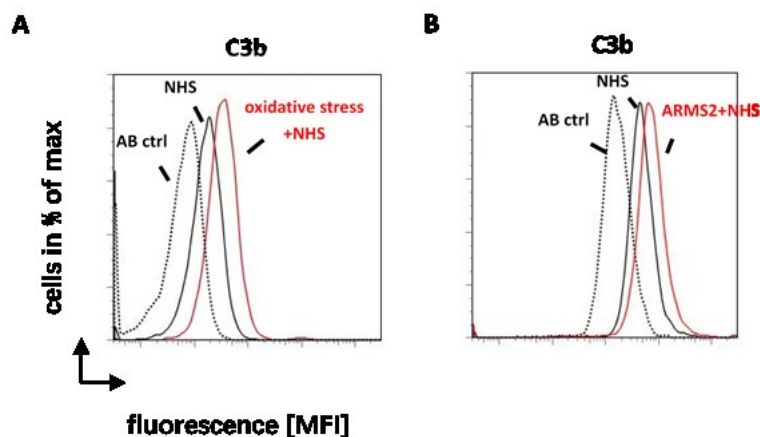


Figure 23. Oxidative stress and ARMS2 enhance complement activation on cell surfaces in serum.

(A) Cells which were treated with H_2O_2 showed a higher level of C3b deposition than untreated cells. ARPE-19 cells were treated with H_2O_2 (1 mM) for 1 h to induce oxidative stress followed by incubation with NHS (20%) for 1 h at 37 $^\circ\text{C}$. Surface bound C3b was detected by flow cytometry. (B) C3b deposition on ARMS2 coated ARPE-19 cells increased upon incubation in 20% NHS. ARPE-19 cells were incubated with ARMS2 (5 $\mu\text{g}/\text{ml}$) for 1 h followed by incubation with NHS for 30 min at 37 $^\circ\text{C}$. Surface bound C3b was detected by flow cytometry.

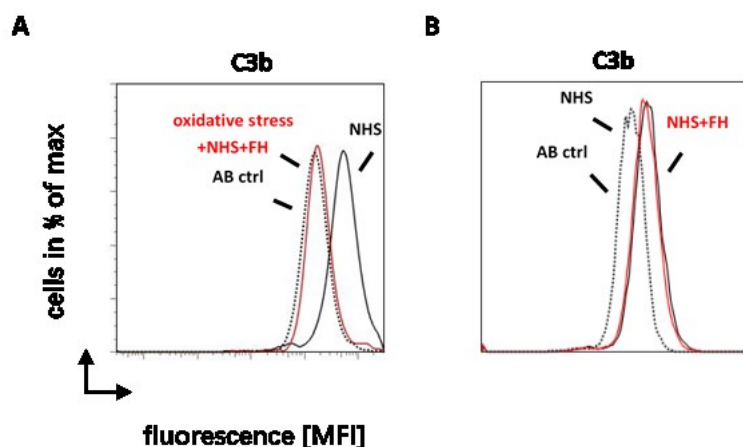


Figure 24. FH blocks C3b deposition on oxidatively stressed ARPE-19 cells.

(A) FH (20 $\mu\text{g}/\text{ml}$) controlled complement activation on stressed cell surface. Cells were treated with H_2O_2 (1 mM) for 1 h and incubated with FH (20 $\mu\text{g}/\text{ml}$) and NHS (20%) for 1 h at 37 $^\circ\text{C}$. (B) FH (20 $\mu\text{g}/\text{ml}$) did not inhibit C3b deposition on control cells. Cells were incubated with FH (20 $\mu\text{g}/\text{ml}$) and NHS (20%) for 1 h at 37 $^\circ\text{C}$. Surface bound C3b was detected by flow cytometry.

3.4.4 Oxidative stress and complement activation induces VEGF secretion in ARPE-19 cells

The wet form of AMD is characterized by choroidal neovascularization, which affects the macula, leading to photoreceptor damage and central vision loss [56]. Since uncontrolled VEGF contributes to AMD, and the RPE layer has been identified as an important site of VEGF production, we asked which stimulation of RPE might initiate the expression of VEGF. As the retina is one of the highest oxygen-consuming tissues in human body, I determined the effect of oxidative stress and complement activation on VEGF secretion. Following treatment with increasing concentrations of H₂O₂ or NHS of ARPE-19 cells, VEGF levels were measured in the supernatants of the cells by ELISA after 24 h. The analysis revealed a small increase by 0.5 mM H₂O₂ or 10% NHS when applied individually to the cells (Figure 25A). However, co-stimulation of 1 mM H₂O₂ combined with NHS resulted in a 3-fold increase in VEGF release (Figure 25A, 25B). Furthermore, high amounts of oxidative stress (1-2 mM) alone also resulted in slight VEGF production (Figure 25C). To understand whether the release of VEGF is mediated by complement activation, the cells were incubated with 5 µg/ml ARMS2 for 1 h before adding 10% NHS. ELISA analysis showed significant increased VEGF levels by 2-fold in treated cells compared to untreated cells (Figure 25D). Exposing the cells to inactive NHS did not cause any further increase of VEGF release (Figure 25D). These results demonstrated that complement activation on ARPE-19 cells induces VEGF secretion by more than 3-fold which in turn might disrupt the function of the cells.

3.4.5 Detection of intracellular complement components expression in ARPE-19 cells

A typical hallmark of AMD is the accumulation of drusen on the basal membrane in the retina [64]. The protein composition of drusen includes apolipoproteins and many complement proteins. However, the source of the proteins in drusen is still unclear. Previous report showed that FH and C3 are present in the human retina [28]. We asked whether FH expression is regulated in ARPE-19 cells and whether enhanced complement activation by oxidative stress has an effect on FH production. Therefore, ARPE-19 cells were treated as described above and lysed and samples were separated in 10% SDS gels. Western blot membranes were labelled with goat anti-FH or mouse anti-β actin and corresponding secondary antibodies. FH is expressed in RPE as demonstrated by the appearance of a ~155 kDa band, in contrast to the FH splicing protein FHL-1 which was not detected (Figure 26). When cells were treated with H₂O₂, FH protein levels increased. Mobilities of purified FH and FHL-1 proteins are shown (Figure 26).

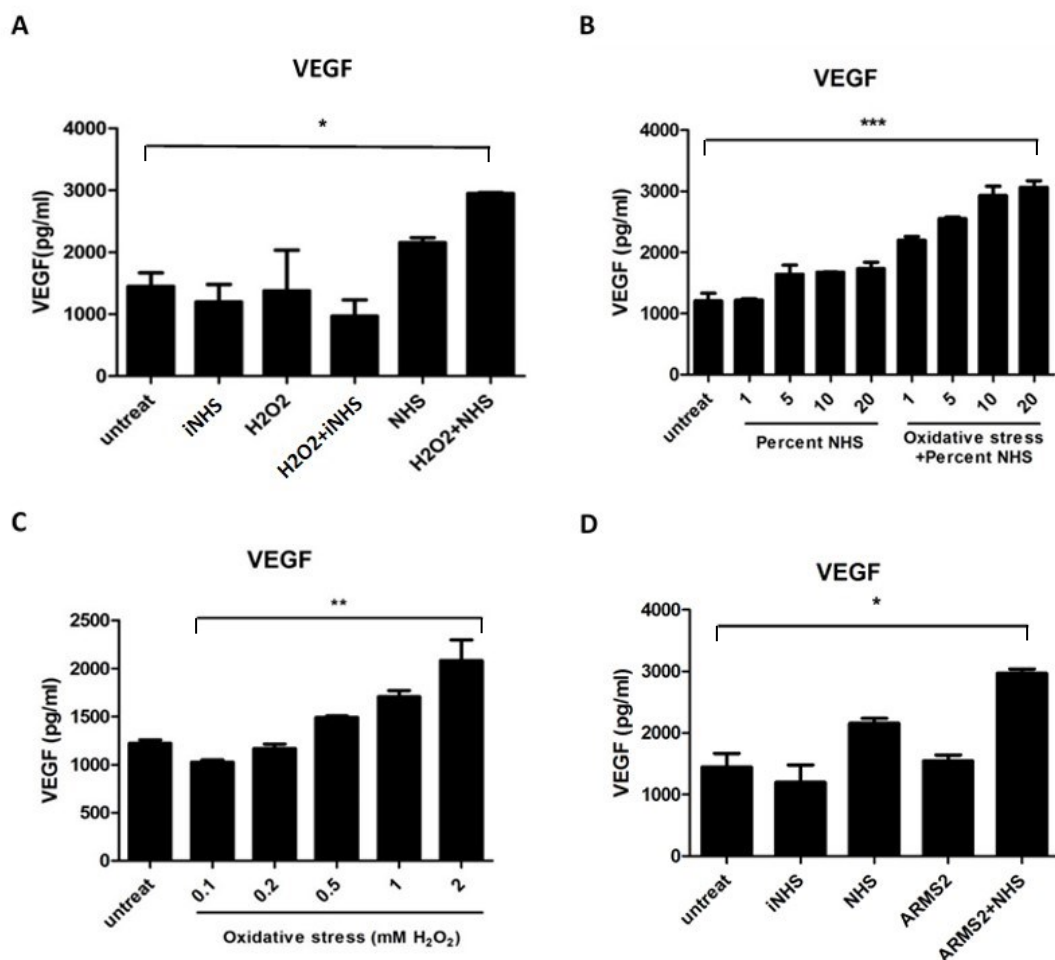


Figure 25. Oxidative stress and complement increase VEGF secretion in ARPE-19 cell.

(A) + (B) +(C) H₂O₂ (0.5 mM) or NHS (10%) alone added to the cells slightly increased VEGF secretion in ARPE-19 cells. In contrast, addition of both induced higher VEGF levels. ARPE-19 cells were treated with oxidative stress or NHS and the supernatants were analyzed by ELISA after 24 h for VEGF production. (D) Complement activation induces VEGF release from ARPE-19 cells which is enhanced by ARMS2. The cells were incubated with 5 µg/ml ARMS2 for 1 h before adding 10% NHS. Bars represent mean ± SD of 3 independent experiments performed in triplicate. Stars on top indicate significant differences to control (*p<0.05, ** <0.01, ***p<0.001).

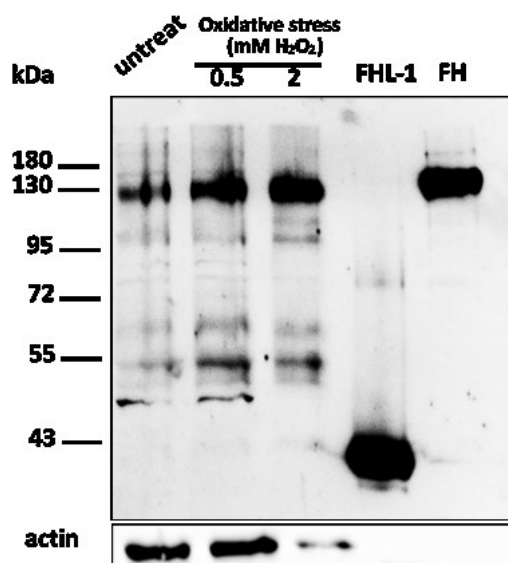


Figure 26. Intracellular FH is upregulated upon oxidative stress in ARPE-19 cells.

FH was detected in the ARPE-19 cell lysates using FH antiserum. ARPE-19 cells were treated with H_2O_2 (0.5 and 2 mM) for 1 h and analyzed 24 h after treatment by western blot analysis.

To identify whether ARPE-19 cells also express complement C3, cells were lysed and C3 expression was assayed by western blot using C3 antiserum. Similarly, human retina tissue was homogenized, lysed and centrifuged at 500 g to remove cell debris. The supernatant was used for further detection. The tissue and cell samples were separated by SDS-PAGE under non-reducing conditions. C3 was identified as a ~ 114 kDa α and ~ 75 kDa β chains in the human retina and ARPE-19 cells (Figure 27A). These data confirm C3 expression in the human retina and RPE cells. In addition, upon oxidative stress, C3 synthesis was upregulated in ARPE-19 cells. In parallel, intracellular cleavage of C3 was observed in ARPE-19 cells. The C3 cleavage product C3b increased in response to exposure of the cells to 0.5 mM oxidative stress as seen by the appearance of the C3 α' band. C3 chains are indicated on the right (Figure 27B).

In contrast to C3, no specific bands were detected in extracts from the human retina or in ARPE-19 cells using C5 antiserum in western blot analysis. Thus, C5 is very low expressed or not present in the human retina (Figure 28).

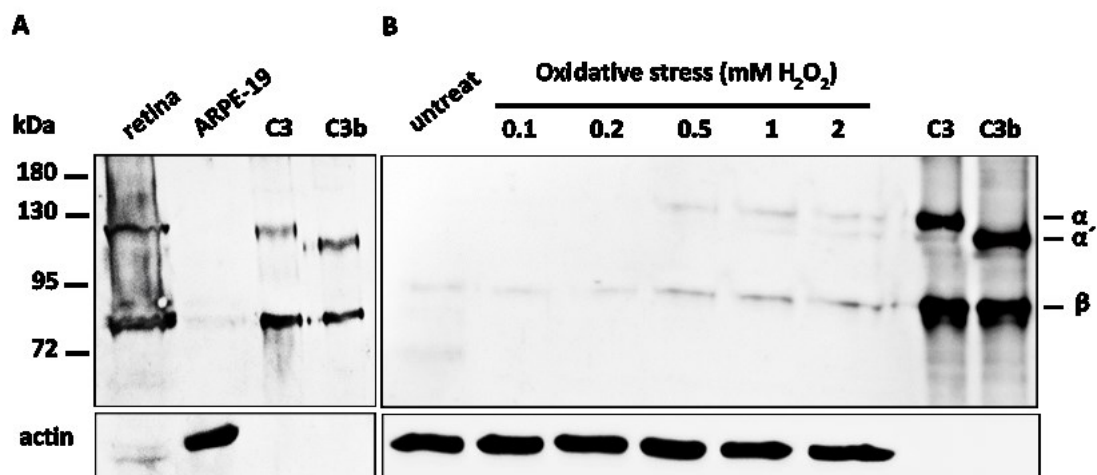


Figure 27. C3 expression in human retina and ARPE-19 cells.

(A) The human retina and ARPE-19 cells express C3. The tissue and cells were lysed and samples were separated by SDS-PAGE. Intracellular C3 was detected by western blot using C3 antiserum. (B) Intracellular C3 is upregulated and cleaved within 24 h after exposure of ARPE-19 cells to oxidative stress. Cells were treated with H₂O₂ for 1 h and incubated in serum-free medium for 24 h. Beta-actin staining serves as loading control.

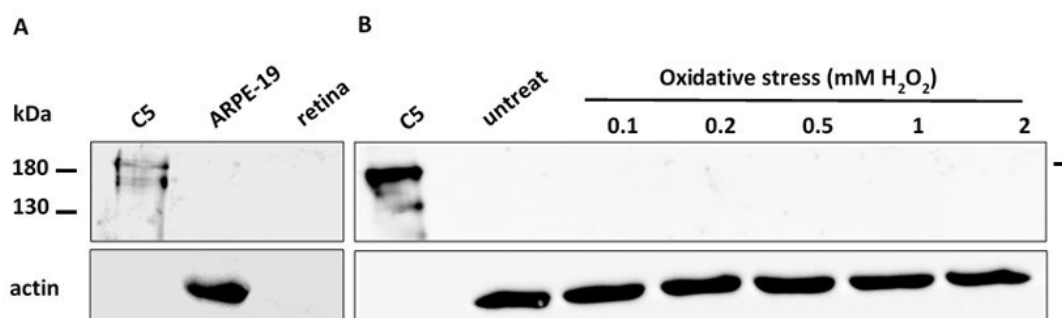


Figure 28. C5 staining of ARPE-19 cells.

C5 is absent in retina tissue and ARPE-19 cells. The human retina and ARPE-19 cells were lysed and separated by SDS-PAGE. Intracellular C5 was analyzed using goat anti-C5 antiserum. Beta-actin staining serves as loading control in ARPE-19 cells.

Overall, human retina and RPE cells express complement FH and C3, but not C5. The expression of FH and C3 was regulated upon oxidative stress. C3 was cleaved intracellularly into C3a and C3b in response to oxidative stress.

4. Discussion

Age-related macular degeneration (AMD) is a degenerative disorder of the central retina and the leading cause of blindness in developed countries. AMD is classified as dry (atrophic) form or wet (exudative) form. The dry form is characterized by drusen formation on the macula, degeneration of the RPE and photoreceptor death. The more severe wet form is characterized by the presence of choroidal neovascularization [56]. The underlying pathogenesis of this disease is still unknown, but a few risk factors have been identified. The most consistent risk factors are aging and smoking [63]. A number of findings also suggest that oxidative stress plays an important role in the development of AMD [125]. Additionally, the complement system has been considered to contribute to AMD risk since several complement components are observed in drusen [64, 68]. More recently, genetic studies have repeatedly shown a strong association of a polymorphism in the complement factor H gene, encoding an inhibitor of the complement alternative pathway activation, with the advanced form of AMD [126, 127, 128]. A second major independent susceptibility factor is identified for both dry and wet AMD with a polymorphism in *ARMS2*, located at chromosome 10q26 [129]. So far, the influence of *ARMS2* risk variants, the expression of this gene and the mechanism of how the *ARMS2* polymorphism contributes to the development of AMD are poorly understood. Therefore, the aim of this study was to investigate whether *ARMS2* is biologically involved in AMD and whether it also affects complement regulation. To this end, the work presented here shows the identification of endogenous *ARMS2*, the function of recombinant *ARMS2* and how complement activation is regulated on ARPE-19 cells.

4.1 Human iPS-derived microglia and monocytes express *ARMS2*

Although there is growing genetic evidence indicating that *ARMS2* variants are strongly associated with AMD, to date, the *ARMS2* protein expression has not been fully elucidated. Prior studies have demonstrated the *ARMS2* gene only exists in primates, which is consistent with macula evolution [130]. Thus, it is important to get insights into *ARMS2* expression and protein distribution to shed some light on its biological function. In our study, we identified both *ARMS2* transcripts and proteins in human microglia derived from induced pluripotent stem cells (iPS-derived microglia) and human monocytes using PCR and LSM microscopy, respectively (Figure 7, 8). The expression results are in agreement with *ARMS2* expression in microglia and monocytes in the human retina [120]. Kanda et al. reported that *ARMS2* mRNA can be detected in human retina and ARPE-19 cells, and moreover, exogenous *ARMS2* protein which is expressed in transfected mammalian cells localizes in the mitochondrial outer membrane [116]. However, the subcellular localization of exogenous *ARMS2* in transfected cells is disputed since others have described endogenous *ARMS2* to be distributed in the cytosol, while another group found *ARMS2* in the mitochondria of photoreceptors [105, 119]. The absence of *ARMS2* transcripts and protein in murine macrophages RAW 264.7 confirmed the specificity of our results as *ARMS2* is expressed only in humans and higher primates (Figure 8B). Most of the endogenous *ARMS2* was localized in the cytoplasm of human monocytes as shown by different *ARMS2* antibodies, including a

newly generated monoclonal antibody to the ARMS2 C-terminus (Figure 10A), two different polyclonal antisera to recombinant ARMS2, and a purchased ARMS2 antiserum (data not shown). ARMS2 showed a similar distribution with all different antibodies used recognizing distinct epitopes (Figure 10A), confirming ARMS2 presence in the cytoplasm. The different ARMS2 subcellular distribution from each study might be attributed to the differences of fixation and permeabilization of the cells for detection of normal or overexpressed ARMS2. Another possibility is that the regulation of ARMS2 expression and transport are largely dependent on distinct types of cells and tissues or that a trigger is necessary for expression of ARMS2.

Current theories imply that age-related diseases are associated with accumulation of damaged proteins and DNA induced by ROS imbalance [131]. Therefore, we hypothesized that an oxidative microenvironment may stimulate ARMS2 production in monocytes. Indeed, upon oxidative stress with increased amounts of H₂O₂ (0.1-1 mM), monocytes elevate ARMS2 expression as detected by western blot analysis using polyclonal antiserum. The induction is prominent starting with 0.1 mM H₂O₂ by densitometry of western blot bands (Figure 9). These increased ARMS2 expression levels confirm that oxidative stress enhances ARMS2 production in monocytes. Upregulation of ARMS2 upon oxidative stress as it is observed implies that ARMS2 plays a role in oxidative stress response in AMD development. To confirm the detected signals are specific from ARMS2, ARMS2 was pulled down from THP-1 cell lysate using immunoprecipitation combined with mass spectrometry by immobilizing monoclonal ARMS2 antibodies to a column. Several ARMS2 peptides were identified from digested extracts, thus demonstrating for the first time the presence of the ARMS2 protein in human monocytes. Five independent precipitation experiments revealed almost complete coverage of the ARMS2 protein (Table 2). From this we concluded that ARMS2 is present in low concentration without stimulation. In conclusion, ARMS2 is expressed in human microglia and monocytes, and the protein is predominantly found in the cytoplasm of cells. ARMS2 protein levels increased upon oxidative stress in monocytes.

4.2 AMD patients carrying the ARMS2 risk haplotype lack the ARMS2 protein in monocytes

The AMD associated variants at 10q26 overlap *PLEKHA1*, *HTRA1* and *ARMS2* genes. All of these genes have a plausible biological relationship to AMD [129, 132, 133]. An increased level of *HTRA1* is suggested to play a role in the pathogenesis of AMD [132]. Currently, a single-nucleotide polymorphism represented by polymorphism rs10490924 linked with an indel mutation del443ins54 in the *ARMS2* gene shows higher association with AMD than the other two genes [105]. Polymorphism rs10490924 generates a replacement of alanine by serine in the protein at position 69 (A69S), making it a susceptible candidate. In addition, the indel mutation at the 3' UTR which is thought to destabilize mRNA is in strong linkage disequilibrium (LD) with A69S. The indel affects *ARMS2* mRNA stability, subsequently resulting in lower *ARMS2* transcripts and protein levels as previously demonstrated in *ARMS2* genotyped placenta [105]. Another polymorphism rs2736911 (R38X), which is more frequent in individuals from the Chinese population, results in a premature stop codon at

position 38 and correlates with a truncated version of *ARMS2* transcripts due to mRNA decay or no transcripts [134]. As the polymorphism rs10490924 plus indel increase the risk for AMD, suggested that AMD patients carrying the risk haplotype show *ARMS2* protein deficiency in blood-derived monocytes. To assess the impact of variants on *ARMS2* protein expression level, patients with the wet form of AMD were genotyped according the presence of rs10490924 plus indel and rs2736911. In total, out of 56 AMD patients who were sequenced for *ARMS2* polymorphisms, 52 patients harbored *ARMS2* gene modifications (either A69S plus indel or R38X), 4 patients did not carry *ARMS2* polymorphisms (Figure 11). These data revealed a correlation of the functional consequences of *ARMS2* risk allele with AMD. However, a large number of patient samples will be necessary to study the effects of the polymorphism in *ARMS2*.

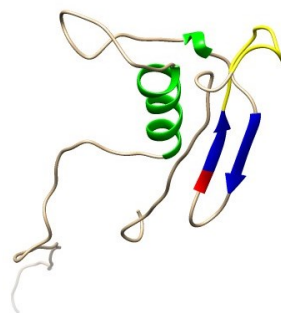
ARMS2 protein expression was analyzed in their isolated blood monocytes by LSM microscopy. There were significant differences in expression levels among the *ARMS2* haplotypes. In fact, *ARMS2* was detected in monocytes of AMD patients with non-risk alleles or one risk allele, but not in monocytes of homozygous carriers of the A69S risk genotype or the one patient we identified with the stop mutation (R38X). This is in agreement with previous findings that the indel decreases *ARMS2* protein in monocytes and microglia of the human retina section. Previous reports by Fritsche *et al.* also reported the *ARMS2* protein deficiency in placenta cells derived from the homozygous carriers of the risk haplotype [104]. Thus, the indel influences *ARMS2* protein levels *in vivo* and *in vitro*. Theoretically, the R38X variation leads to a premature stop in protein synthesis, so that a truncated *ARMS2* protein or no protein at all is produced. Interestingly, the R38X and A69S variants were not found on the same haplotype as described in a previous work by Minor *et al.* [105], nor from our cohort (104 AMD patients and 7 controls). A single AMD patient was observed homozygous of *ARMS2* R38X in our cohort, who also showed no expression of *ARMS2* in monocytes (Figure 12). Apparently, both polymorphisms rs10490924 and rs2736911 lead to *ARMS2* protein deficiency. However, the genetic association of rs2736911 (R38X) with AMD is considered to be weak because previous studies reported that rs2736911 was not statistically significant in AMD patients [105, 135]. The R38X allele is associated with normal *HTRA1* expression which is protective for AMD [136]. It is still unclear why this variant is found more in Asia than Europe or North America and whether it plays a more prominent role in China. Nevertheless, it is necessary to understand the biological consequences of R38X and A69S for the etiology of AMD. In conclusion, monocytes derived from AMD patients homozygous of the *ARMS2* risk haplotype lack the *ARMS2* protein.

4.3 *ARMS2* interacts with complement activator properdin and heparan sulfate

ARMS2 interacts with complement activator properdin and heparan sulfate, which mediates the binding of *ARMS2* to apoptotic cells [119]. The interaction of *ARMS2* with properdin describes the first biological function of *ARMS2*. In order to better understand the function of *ARMS2*, we expressed *ARMS2* in *Pichia pastoris* using optimized conditions and purified the recombinant protein by affinity chromatography. The interaction with properdin was

confirmed by ELISA and further characterized by measuring real time interaction using biolayer interferometry. Recombinant ARMS2 is a glycosylated protein which forms homodimers as identified by western blot analysis and mass spectrometry (Figure 15, 16, Table 3, 4). Deglycosylation of recombinant ARMS2 did not affect binding activities of ARMS2 to heparan sulfate or properdin (data not shown). The interaction affinity between ARMS2 and immobilized properdin was 500 nM. The ARMS2 binding motif was located to the sequence FFSPAGTQRRF within the C-terminus of ARMS2 using PepSpots arrays (Figure 18B). This motif is likely surface exposed and thus accessible for ligand binding indicated by the protein structure prediction (yellow structure, Figure 29). Specificity of interaction is demonstrated by no significant interaction of ARMS2 with DNA or LDL (Figure 17C,17D). Thus, ARMS2 likely acts as an enhancer of complement opsonization on apoptotic cells in recruiting the activator properdin (Figure 30).

On the genetic level, polymorphism rs10490924 and indel are in strong linkage disequilibrium so it was unclear which polymorphism is the biologically relevant one to AMD. To clarify this, ARMS2 S69 without the indel variation was recombinantly expressed in *P. pastoris* and purified under the same conditions as ARMS2 A69 (Figure 20). In general, the function of ARMS2 S69 was similar to that of ARMS2 A69 as it bound to properdin, heparan sulfate and ARPE-19 cells (Figure 21). The amino acid exchange did not affect the protein's mobility and activities. These results demonstrate that A69S does not change ARMS2 biological functions *in vitro*. Thus, the amino acid exchange at position 69 most likely is not the relevant functional variation associated with AMD. The indel variation in the *ARMS2* gene was previously described to lead to unstable *ARMS2* mRNA. As we saw no ARMS2 expression in monocytes from patients with this variation, the indel variation is most likely the AMD relevant modification. However, the introduction of R38X, which leads to a truncated ARMS2, does not confer risk of AMD. There may be additional events within the polymorphism R38X that occur to protect the disorder. Hence, ARMS2 interacts with properdin via its C-terminus and binds to the cell surface via heparan sulfate.



**RLYPGPMVTEAEGKGGPEMASLSSSVVPVSFISTLRESVLDPGVGGEGASDKQRSKLSLSHSMI
PAAKIHTELCLPAFFSPAGTQRRFQQPQHHLTSLIIHTAAR**

Figure 29. Hypothetical three-dimensional structure of the ARMS2 molecule.

The structure was calculated by RaptorX and modified using Chimera 1.11.2. Ribbons are shown in white and helical structures in green. Beta sheets are marked in blue and disulfide bond in red. The interaction domain with properdin FFSPAGTQRRF is shown in yellow. The ARMS2 amino acid

sequence is shown below.

Although it can be confirmed from current findings that there is a causal relationship between dysregulated complement activation and the development of AMD, the role of complement activation in late forms of AMD remains unclear. In this regard, the role of ARMS2 in complement activation was analyzed. We previously showed that ARMS2 binds to modified human RPE cell line, ARPE-19 cells or apoptotic T cells, but not to primary RPE or naïve T cells [119]. On this basis, this study confirmed that surface-bound ARMS2 serves as an anchor for properdin, thus enhancing C3b opsonization on ARPE-19 cell surfaces (Figure 19, 23). This surface regulatory ability of ARMS2 enhances opsonization, but also needs regulation to prevent unwanted over-activation of complement. The complement system plays a role in the clearance of dying cells through opsonization and the promotion of phagocytosis. Thus, deposition of C3b recruited by ARMS2 on the modified surface assists the removal of debris by human phagocytes. No effect on complement activation in fluid phase by ARMS2 insures that the cascade is restricted to the surface and prevents unwanted inflammation. Therefore, ARMS2 deficiency likely enhances accumulation of cell debris, which results in abnormal complement activation (Figure 30). Altogether, ARMS2 is a surface acting protein that increases C3b deposition via properdin, which enhances the opsonization and phagocytosis of dying cells by phagocytes.

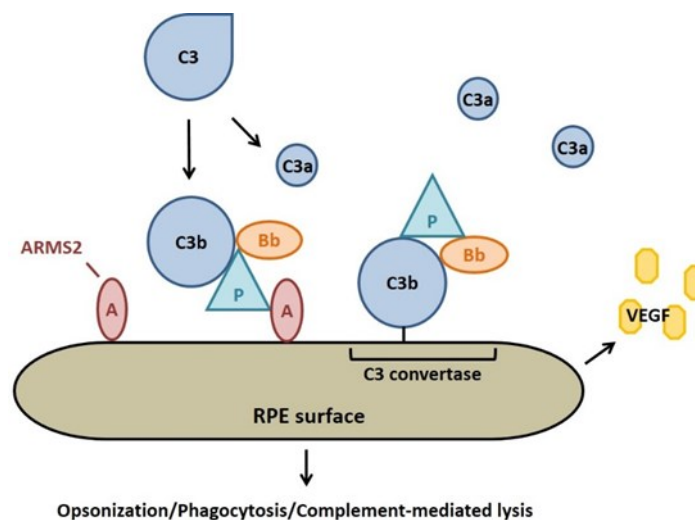


Figure 30. Complement activation on RPE cell surfaces.

Surface-bound ARMS2 enhances C3b opsonization via interaction with properdin. Complement activation increases VEGF secretion of ARPE-19 cells.

4.4 Oxidative stress promotes complement activation and VEGF secretion in ARPE-19 cells

Oxidative stress on RPE cells is an important risk factor in AMD [125]. The RPE layer is a monolayer of epithelial cells that forms the outer layer of the retina and performs multiple functions [57]. So far, the initial events that trigger immune complement activation in RPE cells remains unclear. Determining the effects of oxidative stress on ARPE-19 cells showed that ARPE-19 cells are very susceptible to oxidative stress-mediated cytolysis in a dose-dependent manner (Figure 22A). The cells suffered even more when, in addition to oxidative stress, complement was activated on their surface. This is demonstrated by increased C3b deposition on the cell surface, and dramatically reduced viability of the ARPE-19 cell monolayer (Figure 22C, 23A). Exposure of ARPE-19 cells to NHS alone resulted in weak cytolysis, and less damage of the cells (Figure 22B). This is likely due to complement regulators like CD46 on the cell surface [137]. When cells are challenged by oxidative stress, the surface remodels accelerate C3b opsonization, which mediates clearance of dying cells by phagocytosis. Likewise, the upregulation of ARMS2 in monocytes upon oxidative stress activates complement on the surface. Thus, high oxidative stress in the retina as detected in AMD patients leads to complement activation and enhanced stress on the RPE.

Once activated, the alternative pathway of complement amplifies very fast on foreign surfaces like microbes and on modified self surfaces like apoptotic cells. Human cells and tissues are protected from complement injury by membrane bound and fluid phase regulators [19]. FH is an essential complement regulator that plays a critical role in the homeostasis of the complement system in protecting host cells and tissues [55]. The contribution of FH to complement inhibition is more evident on cells treated with H₂O₂, as determined by a relative increase in the ability of FH to control C3 deposition on the stressed cell surface (Figure 24). This is explained by the enhanced binding of FH to oxidatively damaged cells (Data not shown). Oxidative stress modifies the lipid structures. FH exhibits increased affinity for oxidized phospholipids than native ones, thus preventing their inflammatory activity [138, 139]. Polymorphism in the factor H gene is strongly associated with the risk of developing AMD. The disease-associated polymorphism corresponds to a tyrosine/histidine exchange at amino acid position 402. Functional analysis has demonstrated that the Y402H protein product shows reduced binding to LDL conjugated with malondialdehyde (MDA) or malondialdehyde-acetaldehyde (MAA), thus exhibiting a significantly increased level of complement activation and inflammation [37, 42]. Oxidative stress on ARPE-19 cells creates cell damage and a surface for complement activation which is controlled by FH (Figure 23). Since the FH variant H402 is less effective in complement inhibition and oxidative stress protection on surfaces, it results in more activation of complement on the surface of stressed cells as compared to the FH variant Y402, which may contribute to AMD risk (Figure 30). RPE cells express other complement regulators like CD46 [137], and it is unclear why the retina is the specific site of complement injury carrying FH polymorphism. One possible explanation is that the retina has to neutralize a high amount of oxidative stress, so the regulation is largely relying on FH for protection. In contrast, oxidative

stress was also described to reduce the interaction of FH to the cell surface [102]. It may also be possible that FH interacts with the oxidatively stressed cells through additional domains which would affect the efficiency of binding.

In addition to cell damage, the activation of complement represents an additional stress on the cells and results in enhanced VEGF secretion. VEGF subsequently induces blood vessel formation. Oxidative stress alone (2 mM) induced a 1-fold upregulation of VEGF (Figure 25C) as well as activated complement when cells were exposed to 5-20% NHS (Figure 25B, 25D). Oxidative stress together with complement activation, on the other hand, increased VEGF release by ~3 fold (Figure 25B, 25C). Likewise, surface-bound ARMS2 strongly induces VEGF secretion via complement activation but not ARMS2 alone. That activated complement fragments mediate VEGF production is confirmed by suppressed C3b deposition and VEGF secretion upon heat-inactivation of complement (Figure 25D). However, C3a, C3b and C5a as priming agents did not significantly induce VEGF release, nor did complement inhibitors such as FH and eculizumab block VEGF secretion after incubation for 24h (Data not shown), indicating that more complex conditions lead to VEGF production. Recently it has been described that C3a and C5a individually (8h) or together (3d) induce VEGF in RPE cells in vitro [69, 140]. The incubation time varies in different studies and which further components participate are still unclear. Therefore, it is unlikely that the individual complement activation products provide sufficient signals to trigger VEGF secretion. The findings demonstrate that complement activation is involved in immune surveillance but also plays a role in angiogenesis. Oxidative stress together with NHS sensitizes ARPE-19 cells which is documented by enhanced C3b deposition and VEGF secretion. FH is a strong negative regulator of complement activation on damaged cell surfaces. Thus, the dysfunction of the RPE in AMD is likely not only due to the cytotoxicity mediated by oxidative stress and complement activation, but also related to cellular components and an abnormal VEGF secretion which is reported to disrupt the epithelial tight junctions of the retinal blood barrier.

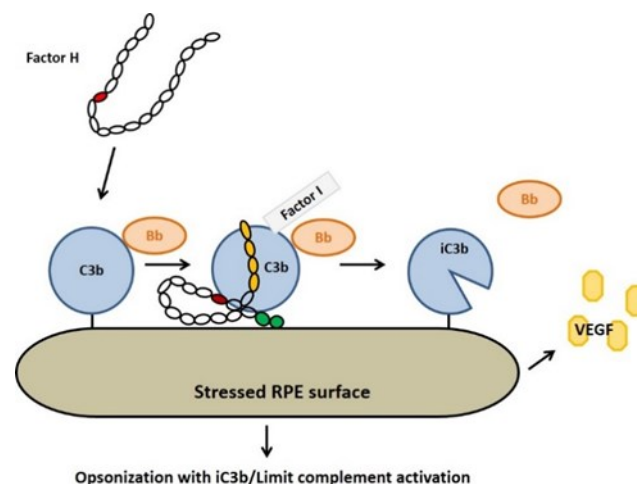


Figure 31. Factor H modulates complement activation on stressed cell surfaces.

Oxidative stress enhances complement activation on surfaces which is inhibited by FH.

A number of complement proteins were found in the deposits (drusen) in the retina [66, 67, 69]. However, the source of complement components in the retina is not completely clear. In this study local synthesis of complement C3, but not C5 is observed in ARPE-19 cells and in the human retina (Figure 27, 28). External complement proteins could be excluded as cells were serum starved prior to oxidative stress treatment for 24 h before analysis. Interestingly, upon oxidative stress (0.1-2 mM H₂O₂), intracellular C3 expression is upregulated and C3 activation occurs intracellularly to generate C3a and C3b, in contrast to C5 which was not found in ARPE-19 cells (Figure 27, 28). Recently, intracellular C3 and C5 were described in T cells. Local C3 activation within T cells is processed by T cell-expressed protease cathepsin L [27]. C3b is then released and involved in immune response by T cells. If and how C3b from ARPE-19 cells changes the immune response of ARPE-19 cells will be studied next. Unexpectedly, C5a receptor (C5aR) is present on the surface of ARPE-19 cells (data not shown) even though human ARPE-19 cells lack C5. It indicates that RPE cells may be in contact with bioactive C5a and have the capacity to react on terminal complement activation. Incubation of primary RPE cells with NHS resulted in upregulation of C5aR, but not C3aR [141]. Thus, C5aR might recognize extracellular complement activation and trigger further inflammatory reactions. Also activated C3a and C3b might interact with their corresponding receptors to initiate the downstream pathway intracellularly. We propose that intracellular activation is cell or tissue specific.

Local FH expression in ARPE-19 cells is elevated in response to oxidative stress (0.5 and 2 mM H₂O₂) as detected by western blot analysis (Figure 26). This phenomenon can be relevant when oxidative stress and enhanced C3b generation needs to be controlled on the RPE cells and to promote protection in this pro-inflammatory microenvironment. Normally human plasma is not present in the retina, which would explain why the retinal cells produce FH. Although FH is abundant in NHS, serum-derived extracellular FH is no longer able to provide sufficient inhibition on the stressed cell surface (Figure 24B). It has been reported that FHL-1 is the predominant regulatory protein in human retina rather than FH [47]. However, in this study FHL-1 was not detected in ARPE-19 cells upon oxidative stress by western blot analysis (Figure 26). This suggests that FHL-1, composed out of 7 SCR domains and thus smaller in size than FH, passively diffuses through Bruch's membrane from the choroid to function as regulator. Thus, the source of FHL-1 needs to be further investigated and intracellular complement activation should be followed regarding complement activation and regulation in AMD.

Taken together, the results show an intracellular pathway of C3 activation and FH generation triggered by oxidative stress in ARPE-19 cells which might function during the process of AMD. In addition, changes in complement proteins may have specific local effects, such as impairment of complement activation control at RPE. The mechanism links complement activation and RPE damage, and may contribute to the disease. Thus, both extracellular and intracellular complement activation are involved in AMD, although the identification of their distinct functions need to be unraveled in the future.

Conclusion

In summary, this study identified endogenous ARMS2 expression in human iPS-derived microglia and blood-derived monocytes, which is localized in the cytoplasm of cells. Recombinant ARMS2 binds properdin, highlighting the function of ARMS2 as an activator of the complement alternative pathway on the surface to which ARMS2 binds (such as modified, damaged or apoptotic cells). The amino acid exchange from A to S at position 69 in ARMS2 does not influence ARMS2 expression at the protein level or change its biological functions. Therefore, the indel mutation which is in strong LD with the polymorphism coding S69 and which causes unstable *ARMS2* mRNA is expected to be the contributing factor in AMD. Indeed, AMD patients with *ARMS2* risk alleles show ARMS2 protein deficiency. ARMS2 deficiency impairs opsonization and phagocytosis of dying cells. The data also show that an oxidative microenvironment triggered complement activation, and triggered VEGF secretion in ARPE-19 cells. An inefficient control by FH during complement over-activation was described to contribute to the development of AMD. RPE cells locally contribute to complement activation and regulation as they produced intracellular complement components including C3 and FH. This study links hallmark events of AMD pathogenesis including *ARMS2* variants, complement activation, oxidative stress, RPE damage and VEGF. However, the trigger for VEGF production, the difference between serum-derived and intracellular complement components, specifically in regulation of complement and inflammation, which contributes to AMD, need to be further characterized.

References

1. Hoffmann J, Akira S. Innate immunity. *Curr Opin Immunol*. 2013; 25 (1):1-3.
2. Dranoff G. Cytokines in cancer pathogenesis and cancer therapy. *Nat Rev Cancer*. 2004; 4:11-22.
3. Okun E, Griffioen KJ, Lathia JD, Tang SC, Mattson MP, Arumugam TV. Toll-like receptors in neurodegeneration. *Brain Res Rev*. 2009; 59 (2):278-92.
4. Kelly A, Houston SA, Sherwood E, Casulli J, Travis MA. Regulation of Innate and Adaptive Immunity by TGF β . *Adv Immunol*. 2017; 134:137-233.
5. Navegantes KC, de Souza Gomes R, Pereira PAT, Czaikoski PG, Azevedo CHM, Monteiro MC. Immune modulation of some autoimmune diseases: the critical role of macrophages and neutrophils in the innate and adaptive immunity. *J Transl Med*. 2017; 15 (1):36.
6. Nichols BA, Bainton DF, Farquhar MG. Differentiation of monocytes. Origin, nature, and fate of their azurophil granules. *J Cell Biol*. 1971; 50 (2):498-515.
7. Ziegler-Heitbrock L, Ancuta P, Crowe S, Dalod M, Grau V, Hart DN, Leenen PJ, Liu YJ, MacPherson G, Randolph GJ, Scherberich J, Schmitz J, Shortman K, Sozzani S, Strobl H, Zembala M, Austyn JM, Lutz MB. Nomenclature of monocytes and dendritic cells in blood. *Blood*. 2010;116 (16):e74-80.
8. Auffray C, Fogg D, Garfa M, Elain G, Join-Lambert O, Kayal S, Sarnacki S, Cumano A, Lauvau G, Geissmann F. Monitoring of blood vessels and tissues by a population of monocytes with patrolling behavior. *Science*. 2007; 317 (5838):666-70.
9. Shi C, Pamer EG. Monocyte recruitment during infection and inflammation. *Nat Rev Immunol*. 2011; 11 (11):762-74.
10. Hoyer BF, Radbruch A. Protective and pathogenic memory plasma cells. *Immunol Lett*. 2017; pii: S0165-2478(17)30112-8.
11. Willinger T, Freeman T, Hasegawa H, McMichael AJ, Callan MF. Molecular signatures distinguish human central memory from effector memory CD8 T cell subsets. *J Immunol*. 2005; 175 (9):5895-903.
12. Shin H, Iwasaki A. Tissue-resident memory T cells. *Immunol Rev*. 2013; 255 (1):165-81.
13. Ballabh P, Braun A, Nedergaard M. The blood-brain barrier: an overview: structure, regulation, and clinical implications. *Neurobiol Dis*. 2004; 16(1):1-13.
14. Graeber MB, Streit WJ. Microglia: immune network in the CNS. *Brain Pathol*. 1990; 1 (1):2-5.
15. Hanisch UK. Microglia as a source and target of cytokines. *Glia*. 2002; 40 (2):140-55.
16. Fan Y, Xie L, Chung CY. Signaling pathways controlling microglia chemotaxis. *Mol Cells*. 2017; 40 (3):163-168.
17. Nimmerjahn A, Kirchhoff F, Helmchen F. Resting microglial cells are highly dynamic surveillants of brain parenchyma in vivo. *Science*. 2005; 308 (5726):1314-8.
18. Kolev M, Le Friec G, Kemper C. Complement--tapping into new sites and effector systems. *Nat Rev Immunol*. 2014;14 (12):811-20.

19. Zipfel PF, Skerka C. Complement regulators and inhibitory proteins. *Nat Rev Immunol*. 2009; 9 (10):729-40.
20. Merle NS, Church SE, Fremeaux-Bacchi V, Roumenina LT. Complement system part I - molecular mechanisms of activation and regulation. *Front Immunol*. 2015; 6:262.
21. Merle NS, Noe R, Halbwachs-Mecarelli L, Fremeaux-Bacchi V, Roumenina LT. Complement System Part II: Role in Immunity. *Front Immunol*. 2015; 6:257.
22. Nemerow GR, Yamamoto KI, Lint TF. Restriction of complement-mediated membrane damage by the eighth component of complement: a dual role for C8 in the complement attack sequence. *J Immunol*. 1979; 123 (3):1245-52.
23. Huang Y, Qiao F, Abagyan R, Hazard S, Tomlinson S. Defining the CD59-C9 binding interaction. *J Biol Chem*. 2006; 281 (37):27398-404.
24. Klos A, Tenner AJ, Johswich KO, Ager RR, Reis ES, Köhl J. The role of the anaphylatoxins in health and disease. *Mol Immunol*. 2009; 46 (14):2753-66.
25. Wu F, Zou Q, Ding X, Shi D, Zhu X, Hu W, Liu L, Zhou H. Complement component C3a plays a critical role in endothelial activation and leukocyte recruitment into the brain. *J Neuroinflammation*. 2016; 13:23.
26. Yu J, Wiita P, Kawaguchi R, Honda J, Jorgensen A, Zhang K, Fischetti VA, Sun H. Biochemical analysis of a common human polymorphism associated with age-related macular degeneration. *Biochemistry*. 2007; 46 (28):8451-61.
27. Liszewski MK, Kolev M, Le Friec G, Leung M, Bertram PG, Fara AF, Subias M, Pickering MC, Drouet C, Meri S, Arstila TP, Pekkarinen PT, Ma M, Cope A, Reinheckel T, Rodriguez de Cordoba S, Afzali B, Atkinson JP, Kemper C. Intracellular complement activation sustains T cell homeostasis and mediates effector differentiation. *Immunity*. 2013; 39 (6):1143-57.
28. Barnum SR. Complement biosynthesis in the central nervous system. *Crit Rev Oral Biol Med*. 1995;6 (2):132-46.
29. Veerhuis R1, Nielsen HM, Tenner AJ. Complement in the brain. *Mol Immunol*. 2011; 48 (14):1592-603.
30. Kemper C, Atkinson JP, Hourcade DE. Properdin: emerging roles of a pattern-recognition molecule. *Annu Rev Immunol*. 2010; 28:131-55.
31. Cortes C, Ohtola JA, Saggiu G, Ferreira VP. Local release of properdin in the cellular microenvironment: role in pattern recognition and amplification of the alternative pathway of complement. *Front Immunol*. 2013; 3:412.
32. Sun Z, Reid KB, Perkins SJ. The dimeric and trimeric solution structures of the multidomain complement protein properdin by X-ray scattering, analytical ultracentrifugation and constrained modelling. *J Mol Biol*. 2004; 343 (5):1327-43.
33. Alcorlo M, Tortajada A, Rodríguez de Córdoba S, Llorca O. Structural basis for the stabilization of the complement alternative pathway C3 convertase by properdin. *Proc Natl Acad Sci U S A*. 2013; 110 (33):13504-9.

34. Kemper C, Mitchell LM, Zhang L, Hourcade DE. The complement protein properdin binds apoptotic T cells and promotes complement activation and phagocytosis. *Proc Natl Acad Sci U S A*. 2008; 105 (26):9023-8.
35. Herbert AP, Kavanagh D, Johansson C, Morgan HP, Blaum BS, Hannan JP, Barlow PN, Uhrin D. Structural and functional characterization of the product of disease-related factor H gene conversion. *Biochemistry*. 2012; 51 (9):1874-84.
36. Loeven MA, Rops AL, Berden JH, Daha MR, Rabelink TJ, van der Vlag J. The role of heparan sulfate as determining pathogenic factor in complement factor H-associated diseases. *Mol Immunol*. 2015; 63 (2):203-8.
37. Weismann D, Hartvigsen K, Lauer N, Bennett KL, Scholl HP, Charbel Issa P, Cano M, Brandstätter H, Tsimikas S, Skerka C, Superti-Furga G, Handa JT, Zipfel PF, Witztum JL, Binder CJ. Complement factor H binds malondialdehyde epitopes and protects from oxidative stress. *Nature*. 2011; 478 (7367):76-81.
38. Molins B, Fuentes-Prior P, Adán A, Antón R, Arostegui JI, Yagüe J, Dick AD. Complement factor H binding of monomeric C-reactive protein downregulates proinflammatory activity and is impaired with at risk polymorphic CFH variants. *Sci Rep*. 2016; 6:22889.
39. Ji SR, Wu Y, Zhu L, Potempa LA, Sheng FL, Lu W, Zhao J. Cell membranes and liposomes dissociate C-reactive protein (CRP) to form a new, biologically active structural intermediate: mCRP(m). *FASEB J*. 2007;21 (1):284-94.
40. Clark SJ, Bishop PN, Day AJ. Complement factor H and age-related macular degeneration: the role of glycosaminoglycan recognition in disease pathology. *Biochem Soc Trans*. 2010; 38 (5):1342-8.
41. Kelly U, Yu L, Kumar P, Ding JD, Jiang H, Hageman GS, Arshavsky VY, Frank MM, Hauser MA, Rickman CB. Heparan sulfate, including that in Bruch's membrane, inhibits the complement alternative pathway: implications for age-related macular degeneration. *J Immunol*. 2010; 185 (9):5486-94.
42. Lauer N, Mihlan M, Hartmann A, Schlötzer-Schrehardt U, Keilhauer C, Scholl HP, Charbel Issa P, Holz F, Weber BH, Skerka C, Zipfel PF. Complement regulation at necrotic cell lesions is impaired by the age-related macular degeneration-associated factor-H His402 risk variant. *J Immunol*. 2011; 187 (8):4374-83.
43. Ji SR, Wu Y, Zhu L, Potempa LA, Sheng FL, Lu W, Zhao J. Cell membranes and liposomes dissociate C-reactive protein (CRP) to form a new, biologically active structural intermediate: mCRP(m). *FASEB J*. 2007; 21 (1):284-94.
44. Molins B, Fuentes-Prior P, Adán A, Antón R, Arostegui JI, Yagüe J, Dick AD. Complement factor H binding of monomeric C-reactive protein downregulates proinflammatory activity and is impaired with at risk polymorphic CFH variants. *Sci Rep*. 2016; 6:22889.
45. Shaw PX, Zhang L, Zhang M, Du H, Zhao L, Lee C, Grob S, Lim SL, Hughes G, Lee J, Bedell M, Nelson MH, Lu F, Krupa M, Luo J, Ouyang H, Tu Z, Su Z, Zhu J, Wei X, Feng Z, Duan Y, Yang Z, Ferreyra H, Bartsch DU, Kozak I, Zhang L, Lin F, Sun H, Feng H, Zhang K. Complement factor H genotypes impact risk of age-related macular degeneration by interaction with oxidized phospholipids. *Proc Natl Acad Sci U S A*. 2012;109 (34):13757-62.

46. Zipfel PF, Skerka C. FHL-1/reconectin: a human complement and immune regulator with cell-adhesive function. *Immunol Today*. 1999; 20 (3):135-40.
47. Clark SJ, Schmidt CQ, White AM, Hakobyan S, Morgan BP, Bishop PN. Identification of factor H-like protein 1 as the predominant complement regulator in Bruch's membrane: implications for age-related macular degeneration. *J Immunol*. 2014; 193 (10):4962-70.
48. Bajic G, Degn SE, Thiel S, Andersen GR. Complement activation, regulation, and molecular basis for complement-related diseases. *EMBO J*. 2015; 34 (22):2735-57.
49. Skerka C, Chen Q, Fremeaux-Bacchi V, Roumenina LT. Complement factor H related proteins (CFHRs). *Mol Immunol*. 2013; 56 (3):170-80.
50. Leffler J, Bengtsson AA, Blom AM. The complement system in systemic lupus erythematosus: an update. *Ann Rheum Dis*. 2014; 73 (9):1601-6.
51. Fakhouri F, Frémeaux-Bacchi V, Noël LH, Cook HT, Pickering MC. C3 glomerulopathy: a new classification. *Nat Rev Nephrol*. 2010;6 (8):494-9.
52. Cho MS, Vasquez HG, Rupaimoole R, Pradeep S, Wu S, Zand B, Han HD, Rodriguez-Aguayo C, Bottsford-Miller J, Huang J, Miyake T, Choi HJ, Dalton HJ, Ivan C, Baggerly K, Lopez-Berestein G, Sood AK, Afshar-Kharghan V. Autocrine effects of tumor-derived complement. *Cell Rep*. 2014; 6 (6):1085-95.
53. Makou E, Herbert AP, Barlow PN. Functional anatomy of complement factor H. *Biochemistry*. 2013; 52 (23):3949-62.
54. Noris M, Remuzzi G. Atypical hemolytic-uremic syndrome. *N Engl J Med*. 2009; 361 (17):1676-87.
55. Ambati J, Atkinson JP, Gelfand BD. Immunology of age-related macular degeneration. *Nat Rev Immunol*. 2013; 13 (6):438-51.
56. Grossniklaus HE, Geisert EE, Nickerson JM. Introduction to the Retina. *Prog Mol Biol Transl Sci*. 2015; 134:383-96.
57. Strauss O. The retinal pigment epithelium in visual function. *Physiol Rev*. 2005 Jul;85(3):845-81.
58. Benhar I, Reemst K, Kalchenko V, Schwartz M. The retinal pigment epithelium as a gateway for monocyte trafficking into the eye. *EMBO J*. 2016; 35 (11):1219-35.
59. Bill A, Sperber G, Ujiie K. Physiology of the choroidal vascular bed. *Int Ophthalmol*. 1983; 6 (2):101-7.
60. Campochiaro PA. Molecular pathogenesis of retinal and choroidal vascular diseases. *Prog Retin Eye Res*. 2015; 49:67-81.
61. Bird AC, Bressler NM, Bressler SB, Chisholm IH, Coscas G, Davis MD, de Jong PT, Klaver CC, Klein BE, Klein R, et al. An international classification and grading system for age-related maculopathy and age-related macular degeneration. The International ARM Epidemiological Study Group. *Surv Ophthalmol*. 1995; 39 (5):367-74.
62. Coleman HR, Chan CC, Ferris FL 3rd, Chew EY. Age-related macular degeneration. *Lancet*. 2008; 372 (9652):1835-45.

63. Hageman GS, Luthert PJ, Victor Chong NH, Johnson LV, Anderson DH, Mullins RF. An integrated hypothesis that considers drusen as biomarkers of immune-mediated processes at the RPE-Bruch's membrane interface in aging and age-related macular degeneration. *Prog Retin Eye Res.* 2001; 20 (6):705-32.
64. Smith W, Assink J, Klein R, Mitchell P, Klaver CC, Klein BE, Hofman A, Jensen S, Wang JJ, de Jong PT. Risk factors for age-related macular degeneration: Pooled findings from three continents. *Ophthalmology.* 2001; 108 (4):697-704.
65. Allikmets R, Dean M. Bringing age-related macular degeneration into focus. *Nat Genet.* 2008; 40 (7):820-1.
66. Weber BH, Charbel Issa P, Pauly D, Herrmann P, Grassmann F, Holz FG. The role of the complement system in age-related macular degeneration. *Dtsch Arztebl Int.* 2014; 111 (8):133-8.
67. Johnson LV, Leitner WP, Staples MK, Anderson DH. Complement activation and inflammatory processes in Drusen formation and age related macular degeneration. *Exp Eye Res.* 2001; 73 (6):887-96.
68. Cao S, Ko A, Partanen M, Pakzad-Vaezi K, Merkur AB, Albiani DA, Kirker AW, Wang A, Cui JZ, Forooghian F, Matsubara JA. Relationship between systemic cytokines and complement factor H Y402H polymorphism in patients with dry age-related macular degeneration. *Am J Ophthalmol.* 2013; 156 (6):1176-83.
69. Nozaki M, Raisler BJ, Sakurai E, Sarma JV, Barnum SR, Lambris JD, Chen Y, Zhang K, Ambati BK, Baffi JZ, Ambati J. Drusen complement components C3a and C5a promote choroidal neovascularization. *Proc Natl Acad Sci U S A.* 2006; 103 (7):2328-33.
70. Tan PL, Bowes Rickman C, Katsanis N. AMD and the alternative complement pathway: genetics and functional implications. *Hum Genomics.* 2016; 10 (1):23.
71. Kubista KE, Tosakulwong N, Wu Y, Ryu E, Roeder JL, Hecker LA, Baratz KH, Brown WL, Edwards AO. Copy number variation in the complement factor H-related genes and age-related macular degeneration. *Mol Vis.* 2011; 17:2080-92.
72. Kelly U, Yu L, Kumar P, Ding JD, Jiang H, Hageman GS, Arshavsky VY, Frank MM, Hauser MA, Rickman CB. Heparan sulfate, including that in Bruch's membrane, inhibits the complement alternative pathway: implications for age-related macular degeneration. *J Immunol.* 2010; 185 (9):5486-94.
73. Langford-Smith A, Keenan TD, Clark SJ, Bishop PN, Day AJ. The role of complement in age-related macular degeneration: heparan sulphate, a ZIP code for complement factor H? *J Innate Immun.* 2014; 6 (4):407-16.
74. Clark SJ, Perveen R, Hakobyan S, Morgan BP, Sim RB, Bishop PN, Day AJ. Impaired binding of the age-related macular degeneration-associated complement factor H 402H allotype to Bruch's membrane in human retina. *J Biol Chem.* 2010; 285 (39):30192-202.
75. Lauer N, Mihlan M, Hartmann A, Schlötzer-Schrehardt U, Keilhauer C, Scholl HP, Charbel Issa P, Holz F, Weber BH, Skerka C, Zipfel PF. Complement regulation at necrotic cell lesions is impaired by the age-related macular degeneration-associated factor-H His402 risk variant. *J Immunol.* 2011; 187 (8):4374-83.

76. Molins B, Fuentes-Prior P, Adán A, Antón R, Arostegui JI, Yagüe J, Dick AD. Complement factor H binding of monomeric C-reactive protein downregulates proinflammatory activity and is impaired with at risk polymorphic CFH variants. *Sci Rep.* 2016; 6:22889.
77. Shaw PX, Zhang L, Zhang M, Du H, Zhao L, Lee C, Grob S, Lim SL, Hughes G, Lee J, Bedell M, Nelson MH, Lu F, Krupa M, Luo J, Ouyang H, Tu Z, Su Z, Zhu J, Wei X, Feng Z, Duan Y, Yang Z, Ferreyra H, Bartsch DU, Kozak I, Zhang L, Lin F, Sun H, Feng H, Zhang K. Complement factor H genotypes impact risk of age-related macular degeneration by interaction with oxidized phospholipids. *Proc Natl Acad Sci U S A.* 2012; 109 (34):13757-62.
78. Wang JC, Cao S, Wang A, To E, Law G, Gao J, Zhang D, Cui JZ, Matsubara JA. CFH Y402H polymorphism is associated with elevated vitreal GM-CSF and choroidal macrophages in the postmortem human eye. *Mol Vis.* 2015; 21:264-72.
79. Toomey CB, Kelly U, Saban DR, Bowes Rickman C. Regulation of age-related macular degeneration-like pathology by complement factor H. *Proc Natl Acad Sci U S A.* 2015; 112(23):E3040-9.
80. Capoluongo E, Concolino P, Piccardi M, Marangoni D, Mello E, Minnella AM, Savastano C, Fadda A, Zuppi C, Bisti S, Falsini B. Retinal function and CFH-ARMS2 polymorphisms analysis: a pilot study in Italian AMD patients. *Neurobiol Aging.* 2012; 33 (8):1852.e5-12.
81. Calippe B, Augustin S, Beguier F, Charles-Messance H, Poupel L, Conart JB, Hu SJ, Lavalette S, Fauvet A, Rayes J, Levy O, Raoul W, Fitting C, Denèfle T, Pickering MC, Harris C, Jorieux S, Sullivan PM, Sahel JA, Karoyan P, Sapieha P, Guillonneau X, Gautier EL, Sennlaub F. Complement Factor H Inhibits CD47-Mediated Resolution of Inflammation. *Immunity.* 2017; 46 (2):261-272.
82. Fritsche LG, Lauer N, Hartmann A, Stippa S, Keilhauer CN, Oppermann M, Pandey MK, Köhl J, Zipfel PF, Weber BH, Skerka C. An imbalance of human complement regulatory proteins CFHR1, CFHR3 and factor H influences risk for age-related macular degeneration (AMD). *Hum Mol Genet.* 2010 ;19 (23):4694-704.
83. Eberhardt HU, Buhlmann D, Hortschansky P, Chen Q, Böhm S, Kemper MJ, Wallich R, Hartmann A, Hallström T, Zipfel PF, Skerka C. Human factor H-related protein 2 (CFHR2) regulates complement activation. *PLoS One.* 2013; 8 (11):e78617.
84. Zipfel PF, Edey M, Heinen S, Józsi M, Richter H, Misselwitz J, Hoppe B, Routledge D, Strain L, Hughes AE, Goodship JA, Licht C, Goodship TH, Skerka C. Deletion of complement factor H-related genes CFHR1 and CFHR3 is associated with atypical hemolytic uremic syndrome. *PLoS Genet.* 2007; 3 (3):e41.
85. Calippe B, Guillonneau X, Sennlaub F. Complement factor H and related proteins in age-related macular degeneration. *C R Biol.* 2014; 337 (3):178-84.
86. Heinen S, Hartmann A, Lauer N, Wiehl U, Dahse HM, Schirmer S, Gropp K, Enghardt T, Wallich R, Hälbich S, Mihlan M, Schlötzer-Schrehardt U, Zipfel PF, Skerka C. Factor H-related protein 1 (CFHR-1) inhibits complement C5 convertase activity and terminal complex formation. *Blood.* 2009; 114 (12):2439-47.

87. Chen LJ, Liu DT, Tam PO, Chan WM, Liu K, Chong KK, Lam DS, Pang CP. Association of complement factor H polymorphisms with exudative age-related macular degeneration. *Mol Vis*. 2006; 12:1536-42.
88. Eberhardt HU, Buhlmann D, Hortschansky P, Chen Q, Böhm S, Kemper MJ, Wallich R, Hartmann A, Hallström T, Zipfel PF, Skerka C. Human factor H-related protein 2 (CFHR2) regulates complement activation. *PLoS One*. 2013; 8 (11):e78617.
89. Bergeron-Sawitzke J, Gold B, Olsh A, Schlotterbeck S, Lemon K, Visvanathan K, Allikmets R, Dean M. Multilocus analysis of age-related macular degeneration. *Eur J Hum Genet*. 2009; 17 (9):1190-9.
90. van Lookeren Campagne M, Strauss EC, Yaspan BL. Age-related macular degeneration: Complement in action. *Immunobiology*. 2016; 221 (6):733-9.
91. Zeng HY, Zhu XA, Zhang C, Yang LP, Wu LM, Tso MO. Identification of sequential events and factors associated with microglial activation, migration, and cytotoxicity in retinal degeneration in rd mice. *Invest Ophthalmol Vis Sci*. 2005; 46 (8):2992-9.
92. Karlstetter M, Ebert S, Langmann T. Microglia in the healthy and degenerating retina: insights from novel mouse models. *Immunobiology*. 2010; 215 (9-10):685-91.
93. Miyagi H, Kanemoto S, Saito A, Asada R, Iwamoto H, Izumi S, Kido M, Gomi F, Nishida K, Kiuchi Y, Imaizumi K. Transcriptional regulation of VEGFA by the endoplasmic reticulum stress transducer OASIS in ARPE-19 cells. *PLoS One*. 2013; 8 (1): e55155.
94. Marazita MC, Dugour A, Marquioni-Ramella MD, Figueroa JM, Suburo AM. Oxidative stress-induced premature senescence dysregulates VEGF and CFH expression in retinal pigment epithelial cells: Implications for Age-related Macular Degeneration. *Redox Biol*. 2016; 7:78-87.
95. Zeng S, Whitmore SS, Sohn EH, Riker MJ, Wiley LA, Scheetz TE, Stone EM, Tucker BA, Mullins RF. Molecular response of chorioretinal endothelial cells to complement injury: implications for macular degeneration. *J Pathol*. 2016; 238 (3):446-56.
96. Fulda S, Gorman AM, Hori O, Samali A. Cellular stress responses: cell survival and cell death. *Int J Cell Biol*. 2010; 2010: 214074.
97. Uday B, Dipak D, Ranajit B K. Reactive oxygen species: Oxidative damage and pathogenesis. *Curr Sci*. 1990; 77:658–666.
98. Yu DY, Cringle SJ. Oxygen distribution and consumption within the retina in vascularised and avascular retinas and in animal models of retinal disease. *Prog Retin Eye Res*. 2001; 20 (2):175-208.
99. Lee JB, Kim SH, Lee SC, Kim HG, Ahn HG, Li Z, Yoon KC. Blue light-induced oxidative stress in human corneal epithelial cells: protective effects of ethanolextracts of various medicinal plant mixtures. *Invest Ophthalmol Vis Sci*. 2014; 55 (7):4119-27.
100. Jaadane I, Villalpando Rodriguez GE, Boulenguez P, Chahory S, Carré S, Savoldelli M, Jonet L, Behar-Cohen F, Martinsons C, Torriglia A. Effects of white light-emitting diode (LED) exposure on retinal pigment epithelium in vivo. *J Cell Mol Med*. 2017.

101. Uttara B, Singh AV, Zamboni P, Mahajan RT. Oxidative stress and neurodegenerative diseases: a review of upstream and downstream antioxidant therapeutic options. *Curr Neuropharmacol*. 2009; 7 (1):65-74.
102. Thurman JM, Renner B, Kunchithapautham K, Ferreira VP, Pangburn MK, Ablonczy Z, Tomlinson S, Holers VM, Rohrer B. Oxidative stress renders retinal pigment epithelial cells susceptible to complement-mediated injury. *J Biol Chem*. 2009; 284 (25):16939-47.
103. Fritsche LG, Chen W, Schu M, Yaspan BL, Yu Y, Thorleifsson G, Zack DJ, Arakawa S, Cipriani V, Ripke S, Igo RP Jr, Buitendijk GH, Sim X, Weeks DE, Guymer RH, Merriam JE, Francis PJ, Hannum G, Agarwal A, Armbrecht AM, Audo I, Aung T, Barile GR, Benchaboune M, Bird AC, Bishop PN, Branham KE, Brooks M, Brucker AJ, Cade WH, Cain MS, Campochiaro PA, Chan CC, Cheng CY, Chew EY, Chin KA, Chowers I, Clayton DG, Cojocaru R, Conley YP, Cornes BK, Daly MJ, Dhillon B, Edwards AO, Evangelou E, Fagerness J, Ferreyra HA, Friedman JS, Geirsdottir A, George RJ, Gieger C, Gupta N, Hagstrom SA, Harding SP, Haritoglou C, Heckenlively JR, Holz FG, Hughes G, Ioannidis JP, Ishibashi T, Joseph P, Jun G, Kamatani Y, Katsanis N, Keilhauer C, Khan JC, Kim IK, Kiyohara Y, Klein BE, Klein R, Kovach JL, Kozak I, Lee CJ, Lee KE, Lichtner P, Lotery AJ, Meitinger T, Mitchell P, Mohand-Saïd S, Moore AT, Morgan DJ, Morrison MA, Myers CE, Naj AC, Nakamura Y, Okada Y, Orlin A, Ortube MC, Othman MI, Pappas C, Park KH, Pauer GJ, Peachey NS, Poch O, Priya RR, Reynolds R, Richardson AJ, Ripp R, Rudolph G, Ryu E, Sahel JA, Schaumberg DA, Scholl HP, Schwartz SG, Scott WK, Shahid H, Sigurdsson H, Silvestri G, Sivakumaran TA, Smith RT, Sobrin L, Souied EH, Stambolian DE, Stefansson H, Sturgill-Short GM, Takahashi A, Tosakulwong N, Truitt BJ, Tsironi EE, Uitterlinden AG, van Duijn CM, Vijaya L, Vingerling JR, Vithana EN, Webster AR, Wichmann HE, Winkler TW, Wong TY, Wright AF, Zelenika D, Zhang M, Zhao L, Zhang K, Klein ML, Hageman GS, Lathrop GM, Stefansson K, Allikmets R, Baird PN, Gorin MB, Wang JJ, Klaver CC, Seddon JM, Pericak-Vance MA, Iyengar SK, Yates JR, Swaroop A, Weber BH, Kubo M, Deangelis MM, Léveillard T, Thorsteinsdottir U, Haines JL, Farrer LA, Heid IM, Abecasis GR; AMD Gene Consortium. Seven new loci associated with age-related macular degeneration. *Nat Genet*. 2013; 45 (4):433-9, 439e1-2.
104. Fritsche LG, Loenhardt T, Janssen A, Fisher SA, Rivera A, Keilhauer CN, Weber BH. Age-related macular degeneration is associated with an unstable ARMS2 (LOC387715) mRNA. *Nat Genet*. 2008; 40 (7):892-6.
105. Minor EA, Court BL, Dubovy S, Wang G. AMD-associated variants at the chromosome 10q26 locus and the stability of ARMS2 transcripts. *Invest Ophthalmol Vis Sci*. 2013; 54 (8):5913-17.
106. Dewan A, Liu M, Hartman S, Zhang SS, Liu DT, Zhao C, Tam PO, Chan WM, Lam DS, Snyder M, Barnstable C, Pang CP, Hoh J. HTRA1 promoter polymorphism in wet age-related macular degeneration. *Science*. 2006; 314 (5801):989-92.
107. Yang Z, Camp NJ, Sun H, Tong Z, Gibbs D, Cameron DJ, Chen H, Zhao Y, Pearson E, Li X, Chien J, Dewan A, Harmon J, Bernstein PS, Shridhar V, Zabriskie NA, Hoh J, Howes K, Zhang K. A variant of the HTRA1 gene increases susceptibility to age-related macular degeneration. *Science*. 2006; 314 (5801):992-3.
108. Nakayama M, Iejima D, Akahori M, Kamei J, Goto A, Iwata T. Overexpression of HtrA1 and exposure to mainstream cigarette smoke leads to choroidal neovascularization and subretinal deposits in aged mice. *Invest Ophthalmol Vis Sci*. 2014; 55 (10):6514-23.

109. Kortvely E, Hauck SM, Duetsch G, Gloeckner CJ, Kremmer E, Alge-Priglinger CS, Deeg CA, Ueffing M. ARMS2 is a constituent of the extracellular matrix providing a link between familial and sporadic age-related macular degenerations. *Invest Ophthalmol Vis Sci.* 2010; 51 (1):79-88.
110. Wang G, Spencer KL, Scott WK, Whitehead P, Court BL, Ayala-Haedo J, Mayo P, Schwartz SG, Kovach JL, Gallins P, Polk M, Agarwal A, Postel EA, Haines JL, Pericak-Vance MA. Analysis of the indel at the ARMS2 3'UTR in age-related macular degeneration. *Hum Genet.* 2010; 127 (5):595-602.
111. Jones A, Kumar S, Zhang N, Tong Z, Yang JH, Watt C, Anderson J, Amrita, Fillerup H, McCloskey M, Luo L, Yang Z, Ambati B, Marc R, Oka C, Zhang K, Fu Y. Increased expression of multifunctional serine protease, HTRA1, in retinal pigment epithelium induces polypoidal choroidal vasculopathy in mice. *Proc Natl Acad Sci U S A.* 2011; 108 (35):14578-83.
112. Rivera A, Fisher SA, Fritsche LG, Keilhauer CN, Lichtner P, Meitinger T, Weber BH. Hypothetical LOC387715 is a second major susceptibility gene for age-related macular degeneration, contributing independently of complement factor H to disease risk. *Hum Mol Genet.* 2005; 14 (21):3227-36.
113. Kanda A, Stambolian D, Chen W, Curcio CA, Abecasis GR, Swaroop A. Age-related macular degeneration-associated variants at chromosome 10q26 do not significantly alter ARMS2 and HTRA1 transcript levels in the human retina. *Mol Vis.* 2010; 16:1317-23.
114. Teper SJ, Nowińska A, Wylęgała E. A69S and R38X ARMS2 and Y402H CFH gene polymorphisms as risk factors for neovascular age-related macular degeneration in Poland - a brief report. *Med Sci Monit.* 2012; 18 (2):PR1-3.
115. Wang G. Chromosome 10q26 locus and age-related macular degeneration: a progress update. *Exp Eye Res.* 2014; 119:1-7.
116. Kanda A, Chen W, Othman M, Branham KE, Brooks M, Khanna R, He S, Lyons R, Abecasis GR, Swaroop A. A variant of mitochondrial protein LOC387715/ARMS2, not HTRA1, is strongly associated with age-related macular degeneration. *Proc Natl Acad Sci U S A.* 2007; 104 (41):16227-32.
117. Mohanty K, Dada R, Dada T. Neurodegenerative Eye Disorders: Role of Mitochondrial Dynamics and Genomics. *Asia Pac J Ophthalmol (Phila).* 2016; 5(4):293-9.
118. Wang G, Spencer KL, Court BL, Olson LM, Scott WK, Haines JL, Pericak-Vance MA. Localization of age-related macular degeneration-associated ARMS2 in cytosol, not mitochondria. *Invest Ophthalmol Vis Sci.* 2009; 50 (7):3084-90.
119. Micklisch S, Lin Y, Jacob S, Karlstetter M, Dannhausen K, Dasari P, von der Heide M, Dahse HM, Schmözl L, Grassmann F, Alene M, Fauser S, Neumann H, Lorkowski S, Pauly D, Weber BH, Jousen AM, Langmann T, Zipfel PF, Skerka C. Age-related macular degeneration associated polymorphism rs10490924 in ARMS2 results in deficiency of a complement activator. *J Neuroinflammation.* 2017; 14 (1):4.
120. Xu YT, Wang Y, Chen P, Xu HF. Age-related maculopathy susceptibility 2 participates in the phagocytosis functions of the retinal pigment epithelium. *Int J Ophthalmol.* 2012; 5 (2):125-32.

121. Wang G, Scott WK, Whitehead P, Court BL, Kovach JL, Schwartz SG, Agarwal A, Dubovy S, Haines JL, Pericak-Vance MA. A novel ARMS2 splice variant is identified in human retina. *Exp Eye Res.* 2012; 94 (1):187-91.
122. Froger A, Hall JE. Transformation of plasmid DNA into E. coli using the heat shock method. *J Vis Exp.* 2007; (6) :253.
123. McLeod DS, Bhutto I, Edwards MM, Silver RE, Seddon JM, Luttly GA. Distribution and quantification of choroidal macrophages in human eyes with age-related macular degeneration. *Invest Ophthalmol Vis Sci.* 2016; 57 (14):5843-5855.
124. Killingsworth MC, Sarks JP, Sarks SH. Macrophages related to Bruch's membrane in age-related macular degeneration. *Eye (Lond).* 1990; 4 (4):613-21.
125. Cai J, Nelson KC, Wu M, Sternberg P Jr, Jones DP. Oxidative damage and protection of the RPE. *Prog Retin Eye Res.* 2000; 19 (2):205-21.
126. Edwards AO, Ritter R 3rd, Abel KJ, Manning A, Panhuysen C, Farrer LA. Complement factor H polymorphism and age-related macular degeneration. *Science.* 2005; 308 (5720):421-4.
127. Haines JL, Hauser MA, Schmidt S, Scott WK, Olson LM, Gallins P, Spencer KL, Kwan SY, Nouredine M, Gilbert JR, Schnetz-Boutaud N, Agarwal A, Postel EA, Pericak-Vance MA. Complement factor H variant increases the risk of age-related macular degeneration. *Science.* 2005; 308 (5720):419-21.
128. Klein RJ, Zeiss C, Chew EY, Tsai JY, Sackler RS, Haynes C, Henning AK, SanGiovanni JP, Mane SM, Mayne ST, Bracken MB, Ferris FL, Ott J, Barnstable C, Hoh J. Complement factor H polymorphism in age-related macular degeneration. *Science.* 2005; 308 (5720):385-9.
129. Rivera A, Fisher SA, Fritsche LG, Keilhauer CN, Lichtner P, Meitinger T, Weber BH. Hypothetical LOC387715 is a second major susceptibility gene for age-related macular degeneration, contributing independently of complement factor H to disease risk. *Hum Mol Genet.* 2005; 14 (21):3227-36.
130. Francis PJ, Appukuttan B, Simmons E, Landauer N, Stoddard J, Hamon S, Ott J, Ferguson B, Klein M, Stout JT, Neuringer M. Rhesus monkeys and humans share common susceptibility genes for age-related macular disease. *Hum Mol Genet.* 2008; 17 (17):2673-80.
131. Jones DP. Redox theory of aging. *Redox Biol.* 2015; 5:71-9.
132. Yang Z, Camp NJ, Sun H, Tong Z, Gibbs D, Cameron DJ, Chen H, Zhao Y, Pearson E, Li X, Chien J, Dewan A, Harmon J, Bernstein PS, Shridhar V, Zabriskie NA, Hoh J, Howes K, Zhang K. A variant of the HTRA1 gene increases susceptibility to age-related macular degeneration. *Science.* 2006; 314 (5801):992-3.
133. Jakobsdottir J, Conley YP, Weeks DE, Mah TS, Ferrell RE, Gorin MB. Susceptibility genes for age-related maculopathy on chromosome 10q26. *Am J Hum Genet.* 2005; 77 (3):389-407.
134. Yang Z, Tong Z, Chen Y, Zeng J, Lu F, Sun X, Zhao C, Wang K, Davey L, Chen H, London N, Muramatsu D, Salasar F, Carmona R, Kasuga D, Wang X, Bedell M, Dixie M, Zhao P, Yang R, Gibbs D, Liu X, Li Y, Li C, Li Y, Campochiaro B, Constantine R, Zack DJ, Campochiaro P, Fu Y, Li DY,

- Katsanis N, Zhang K. Genetic and functional dissection of HTRA1 and LOC387715 in age-related macular degeneration. *PLoS Genet.* 2010; 6 (2):e1000836.
135. Wang G, Scott WK, Agarwal A, Haines JL, Pericak-Vance MA. Coding variants in ARMS2 and the risk of age-related macular degeneration. *JAMA Ophthalmol.* 2013; 131 (6):804-5.
136. Yang Z, Tong Z, Chen Y, Zeng J, Lu F, Sun X, Zhao C, Wang K, Davey L, Chen H, London N, Muramatsu D, Salasar F, Carmona R, Kasuga D, Wang X, Bedell M, Dixie M, Zhao P, Yang R, Gibbs D, Liu X, Li Y, Li C, Li Y, Campochiaro B, Constantine R, Zack DJ, Campochiaro P, Fu Y, Li DY, Katsanis N, Zhang K. Genetic and functional dissection of HTRA1 and LOC387715 in age-related macular degeneration. *PLoS Genet.* 2010; 6 (2):e1000836.
137. Bora NS, Gobleman CL, Atkinson JP, Pepose JS, Kaplan HJ. Differential expression of the complement regulatory proteins in the human eye. *Invest Ophthalmol Vis Sci.* 1993; 34 (13):3579-84.
138. Shaw PX, Stiles T, Douglas C, Ho D, Fan W, Du H, Xiao X. Oxidative stress, innate immunity, and age-related macular degeneration. *AIMS Mol Sci.* 2016; 3(2):196-221.
139. Shaw PX, Zhang L, Zhang M, Du H, Zhao L, Lee C, Grob S, Lim SL, Hughes G, Lee J, Bedell M, Nelson MH, Lu F, Krupa M, Luo J, Ouyang H, Tu Z, Su Z, Zhu J, Wei X, Feng Z, Duan Y, Yang Z, Ferreyra H, Bartsch DU, Kozak I, Zhang L, Lin F, Sun H, Feng H, Zhang K. Complement factor H genotypes impact risk of age-related macular degeneration by interaction with oxidized phospholipids. *Proc Natl Acad Sci U S A.* 2012; 109 (34):13757-62.
140. Busch C, Annamalai B, Abdusalamova K, Reichhart N, Huber C, Lin Y, Jo EAH, Zipfel PF, Skerka C, Wildner G, Diedrichs-Möhring M, Rohrer B, Strauß O. Anaphylatoxins Activate Ca²⁺, Akt/PI3-Kinase, and FOXO1/FoxP3 in the retinal pigment epithelium. *Front Immunol.* 2017; 8:703.
141. Brandstetter C, Holz FG, Krohne TU. Complement Component C5a Primes Retinal Pigment Epithelial Cells for Inflammasome Activation by Lipofuscin-mediated Photooxidative Damage. *J Biol Chem.* 2015; 290 (52):31189-98.

Acknowledgments

I would like to first thank my supervisor Prof. Dr. Christine Skerka for the opportunity to work in this excellent group. I am grateful for her strong support of my ideas and research directions, scientific guidance and encouragement.

To Prof. Dr. Peter. F. Zipfel, I thank for his insightful comments and guidance of my research.

I am thankful for the advice and help from my second supervisor Prof. Dr. Ilse Denise Jacobsen.

I would like to thank my fellow doctoral students for their stimulating discussion and friendship.

In addition, I would like to express my gratitude to my fellow labmates of this department for their help and cooperation.

Special thanks go to my close friends for their support, company and experience in Germany.

Last but not the least, I would like to thank my parents for their love and supporting spiritually throughout my doctoral study.

Declaration of honor

I hereby declare on my honor that the present work has been independently prepared and I am the sole author of the current dissertation.

I declare that I only used those resources that are referenced in the work. All parts of this work that were taken from publications or outside communications are individually marked.

I declare that support during the work including significant supervision is indicated accordingly.

I also declare that the dissertation has not been presented to any other examination authority.

I am aware of legal consequences of a false declaration of honor.

Yuchen Lin

20.09.2017

Jena, Germany

Publications

Yuchen Lin, Shaobo Xiao, Yuqing Zeng, Tao Song, Songlin Zeng, Huanchun Chen, and Liurong Fang. Complete Genome Sequence of Porcine *Kobuvirus* Strain WUH1. *J Virol.* 2012; 86(12):7010. doi: 10.1128/JVI.00725-12.

Sven Micklisch†, **Yuchen Lin**†, Saskia Jacob, Marcus Karlstetter, Katharina Dannhausen, Prasad Dasari, Monika von der Heide, Hans-Martin Dahse, Lisa Schmölz, Felix Grassmann, Medhanie Alene, Sascha Fauser, Harald Neumann, Stefan Lorkowski, Diana Pauly, Bernhard H. Weber, Antonia M. Jousen, Thomas Langmann, Peter F. Zipfel, and Christine Skerka. †**Equal contributors**. Age-related macular degeneration associated polymorphism rs10490924 in ARMS2 results in deficiency of a complement activator. *J Neuroinflammation.* 2017; 14(1):4. doi: 10.1186/s12974-016-0776-3.

Marcus Karlstetter, Jens Kopatz, Alexander Aslanidis, Anahita Shahraz, Albert Caramo, Bettina Linnartz-Gerlach, **Yuchen Lin**, Anika Lückoff, Sascha Fauser, Katharina Düker, Janine Claude, Yiner Wang, Johannes Ackermann, Tobias Schmidt, Veit Hornung, Christine Skerka, Thomas Langmann*, and Harald Neumann*. *equal contribution. Polysialic acid blocks mononuclear phagocyte reactivity, inhibits complement activation and protects from vascular damage in the retina. *EMBO Mol Med.* 2017; 9(2):154-166.

Catharina Busch, Balasubramaniam Annamalai, Khava Abdusalamova, Christian Huber, **Yuchen Lin**, Emerald A.H. Jo, Peter F. Zipfel, Christine Skerka, Gerhild Wildner, Maria Diedrichs-Möhning, Bärbel Rohrer, and Olaf Strauss. Anaphylatoxins activate Ca²⁺, Akt/PI3-kinase, and FOXO1/FoxP3 in the retinal pigment epithelium. *Front Immunol.* 2017; 8:703. doi: 10.3389/fimmu.2017.00703. eCollection 2017.

Yuchen Lin, Peter F. Zipfel and Christine Skerka. Nicotinamide as a treatment option of Age-Related Macular Degeneration. *J Stem Cell Ther Transplant.* 2017; 1: 063-065. DOI: 10.29328/journal.jsctt.1001006.

Catharina Busch, Saskia Jacob, **Yuchen Lin**, Monika van der Heid, Daniel Pilger, Peter F. Zipfel, Olaf Strauss, Christine Skerka, and Antonia M. Jousen. Single-nucleotide polymorphisms in CFH and ARMS2 genes affect the response to intravitreal anti-VEGF therapy in patients with neovascular AMD (submitted).

Luciana M. Pujol-Lereis, Gerhard Liebisch, Tina Schick, **Yuchen Lin**, Caroline Brandl, Felix Graßmann, Koji Uchida, Peter F. Zipfel, Sascha Fauser, Christine Skerka, and Bernhard H.F. Weber. Altered serum ceramide levels in age-related macular degeneration links the disease with sphingolipid metabolism, autophagy and complement regulators (submitted).

Honors and Awards

Graduate National Scholarship in 2012.

Honor of Excellent Graduate Student of Huazhong Agricultural University in 2012.

Young Researcher Award of International symposium on AMD in 2015.

Research presentations

Oral presentations

Age-related macular degenerative susceptibility 2 (ARMS2) is expressed in monocytes and microglial cells, 10th PRO RETINA conference on retina degeneration, 2015.03.27-03.28, Potsdam, Germany.

Age-related macular degenerative susceptibility 2 (ARMS2) is expressed in monocytes, ILRS symposium, 2015.05.05, Jena, Germany.

Recombinant and endogenous expression of Age-related macular degenerative susceptibility 2 (ARMS2), Young researcher vision camp, 2015.06.12-06.15, Leibertingen, Germany.

Age-related macular degenerative susceptibility 2 (ARMS2) interacts with human properdin, VI. International symposium on AMD, 2015.09.11-09.12, Baden-Baden, Germany.

Age-related macular degenerative susceptibility 2 (ARMS2) interacts with human properdin, 113th DOG (German Society of Ophthalmology) Congress, 2015.09.29-10.02, Berlin, Germany.

Poster presentations

ARMS2 activates complement on stressed ARPE-19 cells and triggers VEGF secretion which is controlled by factor H, 11th PRO RETINA conference on retina degeneration, 2016.04.08-04.09, Potsdam, Germany.

ARMS2 activates complement on stressed ARPE-19 cells and triggers VEGF secretion which is restricted by factor H, Joint symposium ILRS and RTG 1870, 2016.05.02-05.04, Wittenberg, Germany.

Factor H controls VEGF secretion in ARPE-19 cells, 46th Annual Meeting German Society for Immunology (DGfI), 2016.09.27-09.30, Hamburg, Germany.

Low molecular weight polysialic acid inhibits complement activation, 12th PRO RETINA conference on retina degeneration, 2017.04.07-04.08, Potsdam, Germany.